TECHNISCHE UNIVERSITÄT MÜNCHEN

Helmholtz Zentrum München
Institut für Bioinformatik und Systembiologie

Master's Thesis
in Biochemie

Computational modeling of human mitochondrial beta-oxidation

Ferdinand Stückler

Aufgabensteller:	Prof. Fabian Theis, Prof. Hans-Werner Mewes
Betreuer:	Jan Krumsiek
Abgabedatum:	5.2.2010

Ich versichere, dass ich diese Master's Thesis selbständig verfasst und nur die angegebenen Quellen und Hilfsmittel verwendet habe.

5.2.2010 _____

Ferdinand Stückler

Abstract

Beta-oxidation, the catabolic breakdown of fatty acids, is an important physiological process which provides energy to the cell. In a recurring sequence of four enzymatic catalyzed reactions, the fatty acid chain is shortened by two carbon atoms during each round of the degradation cascade. In this work we developed a model for the beta-oxidation pathway by combining biochemical and physiological knowledge with methods of mathematical modeling. For reducing the model complexity, we introduced simplifications which are based on biological features of the oxidation cascade. In contrast to other approaches, our model does not rely on kinetic parameters that were derived from in-vitro measurements of purified enzymes. Instead, we estimated rate constants for fundamental steps in the beta-oxidation pathway based on metabolite concentrations of 15 male subjects during a fasting period of 24 hours. The compounds were quantified using electrospray ionization tandem mass spectrometry. For some reactions, estimated kinetic rates were highly different between subjects. Comparing these rate constants with physiological parameters such as body mass index, triglyceride blood levels or ratios of total fat in the body showed a relationship between rate profiles and individual phenotypes. We further developed a model to estimate substrate specificities and regulatory effects for enzymes which catalyze the first reaction in the beta-oxidation cascade. This estimation is based on reaction rate profiles obtained from steady state metabolite concentrations. Investigation of enzyme regulation time courses for all subjects revealed a concerted regulation of beta-oxidation enzymes with differing substrate specificity and a relationship between individual body mass index and activation of enzymes which metabolize short fatty acids. Our results show that modeling metabolic pathways by combining biological knowledge with steady state metabolite concentrations provides a promising approach to obtain deeper insights into the interplay between individual genotype, environment, nutrition and metabolism.

Zusammenfassung

Unter dem Begriff beta-Oxidation versteht man den biochemischen Abbaumechanismus von Fettsäuren, bei dem Energie für Stoffwechselvorgänge erzeugt wird. In jedem Reaktionszyklus wird durch eine sich wiederholende Abfolge von vier Enzymreaktionen eine Fettsäurekette schrittweise um zwei Kohlenstoffatome verkürzt. Wir haben mit Hilfe mathematischer Modellierung und unter Berücksichtigung von biochemischem und physiologischem Wissen ein Modell für den Fettsäureabbau konzipiert, das in dieser Arbeit vorgestellt wird. Durch Vereinfachungen, die auf biochemischem und physiologischem Wissen beruhen, wurde der Grad der Komplexität des Modells verringert. Unser Modell benötigt im Gegensatz zu anderen Modellen keine zusätzlichen kinetischen Parameter, die durch in-vitro Messungen an aufgereinigten Enzymen bestimmt wurden. Stattdessen schätzen wir kinetische Raten für beta-Oxidationsreaktionen anhand von gemessenen Metabolitkonzentrationen. Diese wurden in einer Studie mit 15 männliche Testpersonen im Verlauf einer 24 Stunden dauernden Fastenphase mit Hilfe von Tandem-Massenspektrometrie bestimmt. Die geschätzten Raten einiger Reaktionsschritte unterscheiden sich zwischen verschiedenen Probanden in hohem Maße. Bei diesen Reaktionen ergibt sich auch ein signifikanter Zusammenhang zwischen Reaktionsraten und physiologischem Eigenschaften wie body mass index, Triglyceridkonzentration im Blut oder Körperfettanteil. Des weiteren stellen wir eine Methode vor, die es ermöglicht, die Substratspezifität und Regulation von bestimmten Enzymen des beta-Oxidationszyklus zu bestimmen. Diese Vorhersage von Enzymeigenschaften erfolgt an Hand von Reaktionsraten, die aus dem Profil der Metabolitkonzentrationen gewonnen wurden. Die Zeitverläufe der Enzymregulation weisen auf eine abgestimmte Aktivierung von Enzymen mit unterschiedlicher Substratspezifität hin. Zudem besteht ein signifikanter Zusammenhang zwischen dem body mass index der Studienteilnehmer und der Regulation von Enzymen, die am Abbau von kurzen Fettsäureketten beteiligt sind. Unsere Ergebnisse zeigen, dass die mathematische Beschreibung von Stoffwechselwegen unter Einbeziehung von biologischem Wissen und steady-state Konzentrationen von Metaboliten ein vielversprechender Ansatz ist, um das Zusammenspiel von individuellem Genotyp, Umweltfaktoren, Ernährung und Metabolismus genauer zu untersuchen.

Acknowledgements

Thanks to Jan Krumsiek and Fabian Theis for being great supervisors and showing me the exciting areas of biology outside the lab, to Karsten Suhre and the metabolomics group for the experiments, valuable feedback and my green working environment, and to Prof. Hans-Werner Mewes for providing the possibility to write this thesis. Thanks to Daniel Schmidl and the whole CMB group for all explanations, for their patience and an inspiring working atmosphere.

Special thanks to Melli, my family and WG7 for support and abundance of patience throughout the whole thesis.

Contents

1 Introduction **1**

1.1 Fatty Acids in the human body 4

1.1.1 Physiological functions of fatty acids 5

1.1.2 Uptake and transport of dietary fatty acids 6

1.2 Beta-oxidation of fatty acids 7

1.2.1 Transport into the mitochondrial matrix 7

1.2.2 Degradation of fatty acids in the beta-oxidation pathway 8

2 Methods **13**

2.1 Metabolomics 13

2.1.1 Analytical techniques 14

2.1.2 Database resources 17

2.2 HuMet Study 18

2.3 Mathemetical modeling 19

2.3.1 Modeling biochemical systems by ordinary differential equations 19

2.3.2 Kinetic laws for enzymatic modeling 20

2.3.3 Matrix notation of multiple enzymatic reactions 22

2.3.4 Analysis of metabolic reactions for steady state conditions 24

3 Model development for the beta-oxidation pathway **27**

3.1 Existing models 27

3.2 Model development 28

3.2.1 Assumptions for reducing complexity 30

3.2.2 Link between model and experimental data 36
3.3 Conclusion 38

4 Modeling mitochondrial beta-oxidation 39
4.1 Analysis of metabolite concentration profiles 39
4.2 Relative rate calculation 43
4.2.1 Comparison of interindividual rates for specific reaction steps 44
4.2.2 Comparison of rate profiles with physiological parameters 46
4.2.3 Comparison of individual rate constant time-courses 48
4.3 Non-negative factorization of reaction rate matrices 52
4.3.1 Mathematical model for combined enzymatic activities 53
4.3.2 Non-negative factorization applied on the HuMet dataset 54
4.4 Concluding discussion 61

5 Summary and Outlook 63

Appendices 66

A Metabolites measured using tandem mass spectrometry 67

B Phenotypic parameters 73

Chapter 1

Introduction

Mitochondrial *beta-oxidation* of fatty acids is an important physiological process which provides a major source of energy to the cell. In a recurring sequence of four reactions, acyl-CoA, an activated form of a fatty acid molecule, is degraded. During each round of the beta-oxidation pathway, two carbon atoms are sequentially removed from the acyl chain. Energy-rich electron carrier molecules and acyl-CoA are formed, which enter the citric acid cycle and the oxidative phosphorylation pathway. As a result, adenosine triphosphate molecules are generated providing energy for multiple cellular and physiological processes such as synthesis of biomolecules, growth and cell division [6].

Fat is an efficient energy source and constitutes the major fuel reserve in the human body [24]. During specific physiological conditions such as fasting, catabolic stress and sustained exercise, oxidation of fatty acids becomes especially important for the providing of energy. The metabolic stages of the beta-oxidation cascade were elucidated 40-50 years ago and detailed knowledge about involved enzymes and pathway related diseases has been obtained since then [21]. For many inheritable disorders, pathway-specific enzymes show molecular defects, which may pertubate the homeostasis of lipid metabolism. Impaired degradation of fatty acid molecules therefore can cause severe symptoms such as brain damage, multiple organ failure, coma and death [66]. Many studies have investigated these inherited disorders, but there remains uncertainty regarding the relationship between observed clinical phenotypes and known genetic mutations [5]. Therefore, deeper insights into metabolic processes are required for the understanding of beta-oxidation related diseases.

Imbalanced fat metabolism is also a risk factor for the pathogenesis of systemic diseases. The crucial role of lipids in the physiology of cells, tissues and organs has been shown in many studies. The disruption of metabolic pathways can cause many human diseases including cancer, neurodegenerative and infectious diseases [82]. Fat accumulation in obese individuals, for instance, contributes to the development of cardiovascular diseases and insulin resistance [46, 70]. Since malfunction of fatty acid metabolism is a major contributor to the pathogenesis of many diseases, a better understanding of the interplay between metabolic processes and control mechanisms of beta-oxidation reactions is required.

A promising approach for the investigation of this interaction is the field of metabolomics, the system-wide and large-scale analysis of the total metabolite pool. Compared to genomics or

proteomics, metabolomics is the best indicator for an organism's phenotype, since real endpoints of cellular processes are measured [8, 39]. Modern high-throughput methods allow for the simultaneous quantification of hundreds of metabolites for a large numbers of individuals. The samples of biological fluids (e.g. blood and urine) for these measurements can be collected fairly easily. Metabolites can be seen as biomarker molecules, carrying information about the sites and the mechanism of biological events and diseases [62].

The combination of established knowledge about biochemical pathways with the development of computational models allows for the investigation of multidimensional data for large sample sizes created by modern high-throughput methods and may reveal more detailed knowledge about features of the biological system. By comparing large metabolite collections, links between different biochemical processes with many coupled reactions can be studied on a whole. This system-wide approach can provide valuable insights, since many diseases have multiple factors and result from the complex interplay between individual genotype, metabolism, environment and nutrition [19].

In this work we develope a knowledge based modeling method which incorporates steady state metabolite concentrations for the estimation of effective rates of metabolic reactions (see Figure 1.1). Aim of this approach is to gain deeper insights into metabolic processes by considering biochemical pathway information when investigating metabolomics data. In order to reduce the model complexity simplifications are introduced based on biological features of the metabolism. The estimation of reaction specific rate parameters then allows for a better description of the metabolomics data. Effective reaction rates can be compared with physiological parameters and provide more information about metabolic processes than metabolite concentration alone. The combination of biological knowledge with mathematical modeling and metabolomics data hence can contribute to a better understanding of metabolic processes.

The following sections of this chapter give a detailed description of the fatty acid metabolism. We explain physiological functions of fatty acid molecules and transport mechanism for the mobilization of stored fatty acids, as well as all biochemical reactions of the beta-oxidation pathway. At the beginning of Chapter 2, analytical techniques for the quantification of metabolites are presented. Furthermore, we describe the database resources that were applied and give details about the design and the dataset of the metabolomics study which we investigated in this work. The chapter ends with a brief primer on the mathematical modeling of biochemical systems. In Chapter 3 a short overview about existing models for lipid metabolism is given. We present a modeling approach for the description of the beta-oxidation pathway and discuss all assumptions that we introduced to reduce the model complexity. In Chapter 4 we use our model to investigate metabolic profiles of subjects from the metabolomics study. First we describe the change of metabolite concentrations over time and how this change varies between individuals. Then we compare rate constants that were estimated using our model of the beta-oxidation pathway. For the estimated reaction rates we discuss interindividual variations and the relationship with physiological phenotypes. In addition, we describe how a non-negative factorization approach was used in order to estimate substrate specificity and regulation effects for enzymes which are involved in the beta-oxidation pathway. The final Chapter 5 summarizes the contributions of this work and provides future directions for the investigation of metabolic pathways.

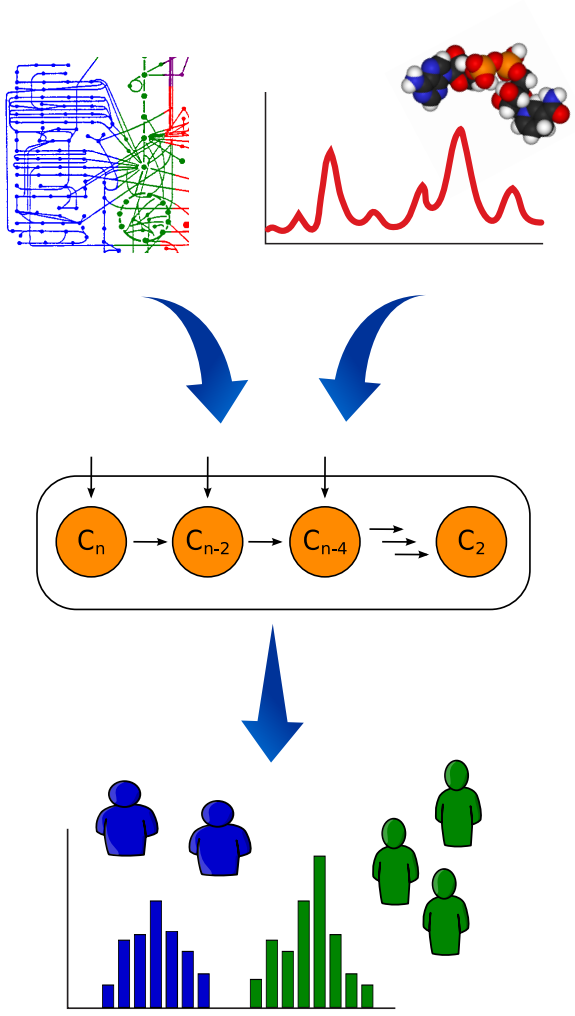

Figure 1.1: Sketch of our knowledge based modeling approach for the investigation of human mitochondrial beta-oxidation. For developing a model of the metabolic pathway we combined biochemical and physiological knowledge about fatty acid metabolism with methods of mathematical modeling. We used our model to describe blood metabolite profiles of fatty acids under fasting conditions which were measured in a metabolomics study. This approach allows for the estimation of effective reaction rates based on steady state metabolite concentrations. Comparing these rate constants with physiological parameters such as body mass index and ratio of total fat in the body showed a relationship between rate profiles and individual phenotypes, which cannot be seen for metabolite concentrations alone. Our approach can be extended to other pathways and allows for the investigation of enzymatic reactions based on metabolomics data.

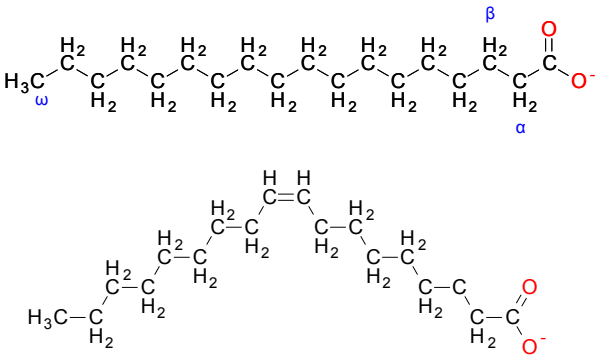

Figure 1.2: **Top:** Octadecanoic acid (C18:0) as an example for the general structure of ionized fatty acids. Fatty acid carbon atoms are numbered starting at the carboxyl terminus (red). Carbon atoms 2 and 3 are often referred to as α and β. The last carbon atom in the chain is called the ω-carbon. **Bottom:** Oleic acid (C18:1), an unsaturated fatty acid with a *cis* double bond between carbon 9 and 10, i.e. carbon 8 and 11 are on the same side.

1.1 Fatty Acids in the human body

Fatty acids consist of a long hydrocarbon chain with a terminal carboxylate group (see Figure 1.2). The hydrocarbon or *alkyl* chains can be of various lengths and can contain one or more double bonds between carbon atoms[1]. Unsaturated fatty acid chains have one or more double bonds in the chain, while saturated fatty acids have no double bonds in the alkyl chain. The systematic name for a fatty acid molecule is derived from the name of the hydrocarbon chain, for example *octadecanoic acid* for a saturated fatty acid with 18 carbon atoms. Trivial names instead of systematic names are often used to describe fatty acids, for instance *stearic acid* for the molecule *octadecanoic acid*. The abbreviated notation *Cn:d* is used to describe a fatty acid with n carbon atoms and d double bonds in the chain, for instance C18:0 for stearic acid[2]. At physiological pH, fatty acids are usually present in their ionized form with a negative charge at the carboxyl terminus.

Fatty acids in biological systems usually contain an even number of carbon atoms, primarily ranging from 14 to 24 carbons. The alkyl chain can either be saturated or contain one or more double bonds. In polyunsaturated molecules the double bonds are separated by at least one carbon atom. Most unsaturated fatty acids have double bonds with *cis* configuration, i.e. carbon atoms adjacent to the double bonds are on the same side (see Figure 1.2).

The most abundant fatty acids have 16 or 18 carbon atoms, for instance palmitic acid (C16:0), stearic acid (C18:0), oleic acid (C18:1) and linoleic acid (C18:2). The predominant even number of carbon atoms in the alkyl chain is a result of the synthesis of fatty acids, since building blocks are molecules with two carbon atoms. The length of the carbon chain and the degree of unsaturation define the chemical properties of fatty acids and, consequently, of the lipid metabolites into which they are incorporated. Long chain lengths and saturation lower the fluidity of molecules, while short chain length and unsaturation increase it. This is especially important for the fluidity of cellular membranes, which consist of compounds that contain fatty acids.

[1] Fundamental biological background in this chapter was extracted from two text books: [1, 6]

[2] In some cases the number of double bonds for saturated fatty acids is omitted, and only the chain length is used in abbreviated notation, for instance C18 instead of C18:0.

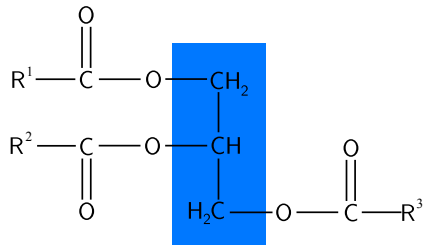

Figure 1.3: Structure of a triglyceride molecule. Three fatty acids with different chain lengths are esterified with a glycerol molecule (blue). Triglycerides are used to store highly concentrated metabolic energy and molecules are accumulated in the cytoplasm of adipose cells. R^1, R^2 and R^3 represent alkyl chain residues.

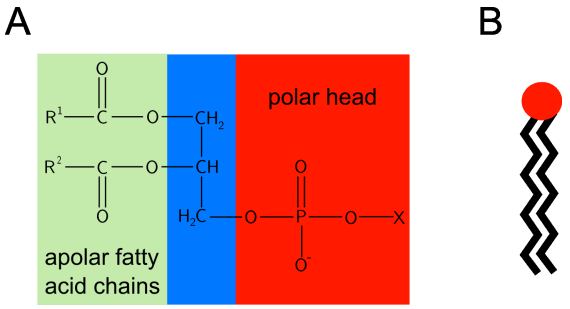

Figure 1.4: Schematic structure of a phospholipid. (A) Two apolar fatty acids (green) and a polar phosphate group with rest X (red) are attached to the glycerol backbone (blue). (B) Shorthand depiction with polar head group (red) and two fatty acid alkyl chains.

1.1.1 Physiological functions of fatty acids

Fatty acids have various functions in the metabolism. First, they are used as fuel molecules to store highly concentrated metabolic energy in the form of triacylglycerides, also referred to as triglycerides or triacylglyceroles. These compounds consist of a single glycerol molecule which is esterified with three fatty acids (see Figure 1.3). Compared to carbohydrates, triglycerides are more reduced and nearly anhydrous, which minimizes the amount of water that binds to the molecules. As a result, one gram of triglycerides stores 6.75 times as much energy as a gram of glycogen, which is the major storage form for carbohydrates. This compactness allows for a very efficient storage of energy. In the human body, carbohydrate stores provide energy to sustain physiological functions for about 24 hours, while fat or triacylglycerides reservoirs allow survival for several weeks. Most triglycerides are accumulated in the cytoplasm of specialized fat cells in the adipose tissue. For providing energy during rest or moderate exercise, fatty acids are mobilized from triglycerides and oxidized in the mitochondria.
Fatty acids are also building blocks of phospholipids and glycolipids, two of the main components of biological membranes (see Figure 1.4). Plasma membranes are physical boundaries which define the inside and outside of a cell. Inside the cell, membranes form barriers that separate organelles such as mitochondria and peroxisomes from the cytoplasm. Membrane molecules with long, apolar fatty acid alkyl chain tails interact with each other and form a bilayer (see

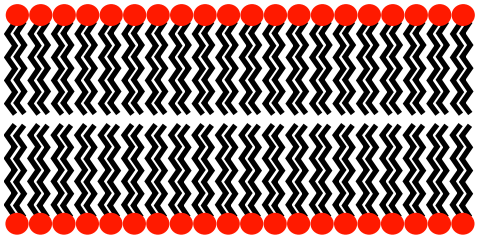

Figure 1.5: Schematic structure of a bilayer membrane. Hydrophobic long fatty acid alkyl chains (black) are inside the bilayer, polar head groups (red) interact with the aqueous environment. Plasma membranes are physical boundaries defining the inside and outside of a cell. Intracellular membranes separate organelles such as mitochondria and peroxisomes from the cytoplasma.

Figure 1.5). The polar head groups of this bilayer interact with the aqueous environment on both sides of the bilayer. The membranes are selectively permeable for specific molecules allowing for the establishment of concentration gradients, which is important for the production and storage of metabolic energy.
Fatty acids are also used to modify proteins and target them for membrane localization. The covalent attachment of long fatty acid chains serves as a hydrophobic membrane anchor and soluble proteins can dock onto the membrane. Furthermore fatty acid derivatives and membrane molecules are used as hormones and intracellular messengers for the signal transmission between cells.

1.1.2 Uptake and transport of dietary fatty acids

Most of the dietary fatty acids which the body ingests are bound in the form of triglycerides. These molecules cannot cross the membranes of cells and have to be broken down to fatty acids first. Triglycerides are converted to free fatty acids and monoacylglycerol, a glycerol molecule with one bound fatty acid. Lipase enzymes, which are secreted by the pancreas, catalyze this reaction. Free fatty acids and monoacylglycerols are then transported across the plasma membrane into the inside of intestinal cells, where they are in turn reassembled to triglycerides. Together with apolipoproteins, the triglycerides are packed into lipid transport particles and released into the lymph system and then into the blood. In peripheral tissues, primarily muscle and adipose tissue, the particles bind to membrane-bound lipases. For the transport across the plasma membrane, triglycerides are once again converted to free fatty acids and monoacylglycerols. In adipose cells, triglycerides are resynthesized inside the cell and stored. In muscle and other tissues, fatty acids are oxidized for providing energy by the beta-oxidation pathway, which is described in the following section.
Lipid energy reserves which are stored in adipose tissue have to be mobilized to release and transport fatty acids to peripheral tissues. If energy supply is needed, specific hormones activate lipases in adipose tissue, which catalyze the degradation of triglycerides into free fatty acids and glycerol. Released fatty acids bind to serum albumin molecules in the bloodstream and are hence transported to other tissues, where they are now accessible as fuel molecules for the production of metabolic energy.

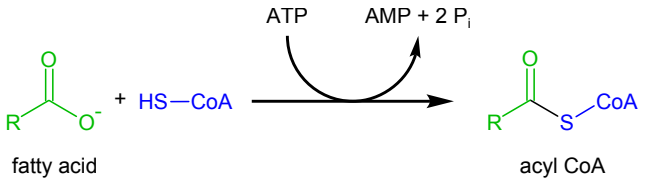

Figure 1.6: Activation of a fatty acid molecule through the formation of a thioester linkage with coenzyme A (CoA). This reaction takes place before fatty acid molecules enter the mitochondrial matrix. The hydrolization of ATP into AMP and two phosphate ions drives this reaction. Acyl CoA molecules are more reactive compared to free fatty acids, which is required for further degradation steps.

1.2 Beta-oxidation of fatty acids

After the uptake of fatty acids from the blood, these compounds are transported to the mitochondria, cellular compartments with two membranes which generate most of the cell's energy supply. Beta-oxidation reactions take place at the inside of this compartment which is called the mitochondrial matrix. Before fatty acid molecules enter the mitochondrial matrix, they are activated through the formation of a thioester linkage with coenzyme A (CoA). In this reaction, which takes place on the outer mitochondrial membrane and is catalyzed by acyl-CoA-synthetase, the fatty acid carboxyl group is bound to the sulfhydryl group of coenzyme A (see Figure 1.6). The linkage with coenzyme A makes free fatty acids more reactive for further conversion and degradation steps.

1.2.1 Transport into the mitochondrial matrix

The activation of fatty acids occurs on the outer mitochondrial membrane, but all beta-oxidation reactions take place in the mitochondrial matrix. Molecules with short and medium alkyl chain length can diffuse freely into the inside of the mitochondrium, but for long-chain fatty acids a special transport system is required. The acyl group of a fatty acid is split off the coenzyme A sulfur atom and conjugated with a carnitine, a zwitterionic transporter molecule. This reaction is catalyzed by carnitine acyltransferase I, which is localized at the outer mitochondrial membrane. The generated acyl carnitine is then shuttled across the inner membrane by a translocase. On the matrix side of the inner membrane, the acyl group is transferred back to coenzyme A and free carnitine is released. This reaction, which is catalyzed by carnitine acyltransferase II, is the reverse process of the conjugation reaction mediated by carnitine acyltransferase I. During the transport of acylcarnitine into the mitochondrial matrix, free carnitine is returned in exchange to the cytoplasmic side of the inner membrane (see Figure 1.7). The carnitine transport system is needed, because there is no transport mechanism for acyl CoA molecules across the mitochondrial membrane. Moreover, the modulation of the transport system allows for the regulation of general beta-oxidation activity. When synthesis instead of degradation of fatty acids is required, carnitine acyltransferase I is inhibited and less fatty acids are carried into the mitochondrium [67].

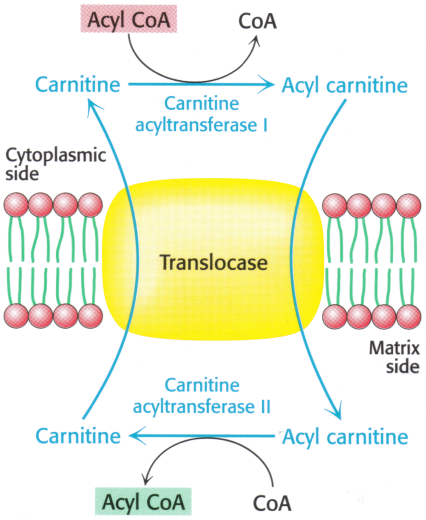

Figure 1.7: Carnitine carries activated fatty acids into the mitochondrial matrix. Acyl groups are conjugated with and removed from carnitines by carnitine acyltransferase I and II. The transport through the inner membrane is mediated by a translocase. During the transport of acylcarnitine into the mitochondrial matrix, free carnitine is returned in exchange to the cytoplasmic side of the inner matrix (reprinted from [6]).

1.2.2 Degradation of fatty acids in the beta-oxidation pathway

Activated fatty acids are degraded by a recurring sequence of four reactions: oxidation, hydration, a second oxidation and thiolysis. As a result, the fatty acid chain is shortened by two carbon atoms, and molecules with with a high energy potential are generated. This series of reactions is called the beta-oxidation pathway (see Figure 1.8).
In the first reaction of each cycle, acyl-CoA is oxidized by acyl-CoA dehydrogenase to enoyl CoA with a *trans* double bond between C-2 and C-3. By the transfer of high energy electrons, reduced flavin adenine dinucleotide ($FADH_2$) is generated. Theses electrons are then used in the oxidative phosphorylation pathway for the generation of energy transfer molecules adenosine triphosphate (ATP).
The next step is the hydration of the generated double bond by enoyl-CoA hydratase, which forms a hydroxyl group at carbon atom C-3. In the third step, hydroxyacyl CoA is oxidized to ketoacyl CoA by hydroxyacyl-CoA dehydrogenase and energy-rich electrons are transfered to nicotinamide adenine dinucleotide (NADH). These electrons are transfered to other molecules in the respiratory chain and finally used to produce ATP. In the final step of one beta-oxidation cycle, β-ketothiolase catalyzes the cleavage of ketoacyl CoA by the thiol group of a second coenzyme A molecule. As a result, the acyl CoA chain length is shortened by two carbon atoms and acetyl CoA is generated, which enters the citric acid cycle for the production of ATP.
The first reaction in one cycle is catalyzed by four dehydrogenase enzymes with varying chain-length specific activities, which are present in the mitochondrium: short-chain acyl-CoA dehydrogenase (SCAD), medium-chain acyl-CoA dehydrogenase (MCAD), long-chain acyl-CoA dehydrogenase (LCAD) and very-long-chain acyl-CoA dehydrogenase (VLCAD) [21]. The three

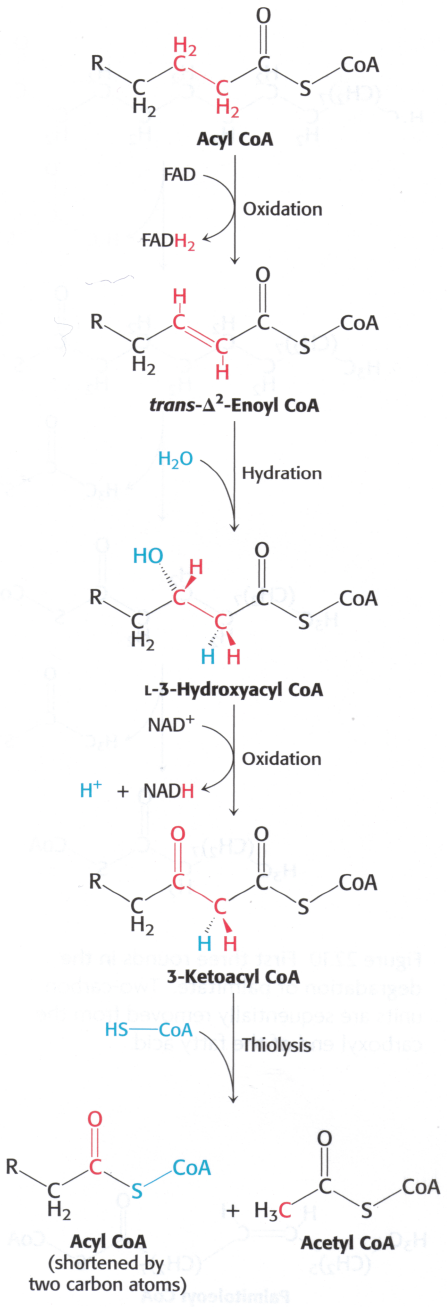

Figure 1.8: Reaction sequence for one beta-oxidation cycle. As a result, the acyl-CoA chain is shortened by two carbon atoms and one molecule each of $FADH_2$, NADH and acetyl CoA is formed. Reactions are catalyzed by enzymes acyl-CoA dehydrogenase, enoyl-CoA hydratase, hydroxyacyl-CoA dehydrogenase and β-ketothiolase. Shortened acyl-CoA chains undergo further beta-oxidation cycles until the whole fatty acid chain is degraded. Generated $FADH_2$, NADH and acetyl CoA are used in the citric acid cycle and the respiratory chain for the production of energy-rich ATP (reprinted from [6]).

remaining enzymes enoyl-CoA hydratase, hydroxyacyl-CoA dehydrogenase and β-ketothiolase do not show chain-length specificities.

The shortened acyl-CoA chain undergoes further beta-oxidation cycles until the whole fatty acid chain is degraded (see Figure 1.9). Saturated fatty acids with an even number of carbon atoms are completely degraded by this pathway. For the beta-oxidation of unsaturated fatty acids additional steps are required, that change the positions of the double bonds in the alkyl chain. The degradation of odd-numbered carbon chains is similar to the oxidation of fatty acids having an even number. However, instead of two molecules of acetyl CoA, one molecule of acetyl CoA and one molecule of propionyl CoA with three carbon units is generated in the final round. Propionyl CoA is converted into succinyl CoA, which enters the citric acid cycle for the production of ATP.

Fatty acids can also be degraded in other cellular compartments, which are called *peroxisomes*. Especially molecules with very long alkyl chains (greater than C22) are first shortened in peroxisomes before they enter the mitochondria for further beta-oxidation steps. The transport mechanism and degradation reactions are similar to the steps described for the mitochondrial beta-oxidation pathway, yet different enzymes with varying substrate specificities are involved. The peroxisomal beta-oxidation usually terminates for fatty acids with eight carbon atoms and therefore provides fatty acids which are better substrates for the mitochondrial beta-oxidation.
The synthesis of fatty acid molecules can be seen as the reversal of the degradation pathway, since most chemical reactions are carried out in the opposite direction. However, there are some important differences. While beta-oxidation takes place in the mitochondrial matrix, synthesis of fatty acids is carried out in the cytoplasm. During synthesis steps, fatty acid intermediates are linked to acyl carrier proteins instead of coenzyme A molecules. The synthesis of new fatty acids terminates after the formation of palmitic acid (C16), further elongation steps are carried out by other enzymes. These and other differences assure that generally synthesis and degradation are not active at the same time. Due to the antagonistic regulation of both pathways metabolic energy is saved since newly produced fatty acids are not instantly oxidized again.

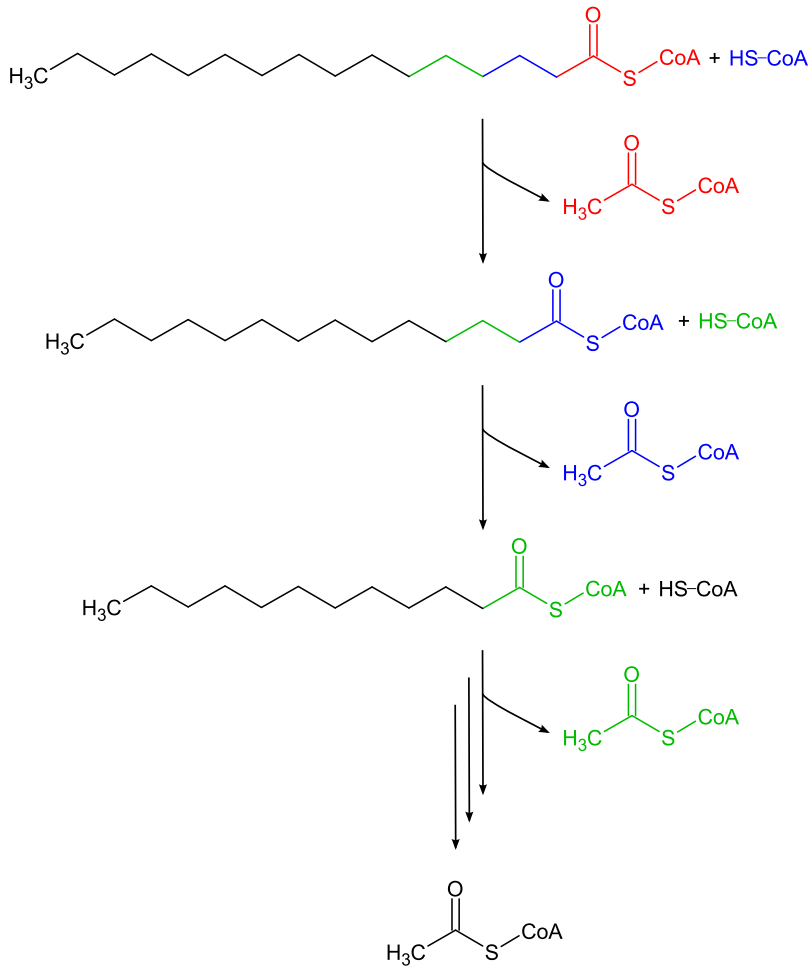

Figure 1.9: Beta-oxidation of palmitic acid (C16). During each beta-oxidation round, two carbon atoms are removed from the carboxyl end of the fatty acid and acetyl CoA is generated. In the final round, two molecules of acetyl CoA are generated. The complete degradation of palmitic acid requires seven reaction rounds and generates 7 molecules of $FADH_2$ and NADH and 8 molecules of acetyl CoA. These energy-rich molecules finally produce 106 molecules of ATP, a very high yield of energy compared to other metabolic reactions.

Chapter 2

Methods

This chapter introduces the methods that were applied for the acquisition of data and for the modeling of fatty acid beta-oxidation. First we will give a short overview about metabolomics, a new field in biological science. Common techniques for detecting and quantifying metabolites in samples will be explained. This includes both techniques for the separation of analytes and analytical methods such as mass spectrometry and nuclear magnetic resonance (NMR) spectroscopy. Then we will present the Human Metabolome Study (HuMet), a highly-controlled trial that was used to acquire the data we examined in this work. The rest of the chapter gives an introduction to modeling methods applied in this work.

2.1 Metabolomics

Metabolomics is a system-wide and large-scale approach to analyze the total metabolite pool in specific cells or tissues [80]. Metabolites, which are intermediates or products of metabolic processes, normally show a molecular weight below 300 g/mol [64]. Examples for such small molecules are sugars, lipids and amino acids, but also hormones, drugs and organic compounds from food. The collection of metabolites as a whole is then called *metabolome* [8, 63]. The set of metabolites found within a biological sample under specific conditions is also referred to as a *metabolic profile*. This characteristic composition of small molecules results from biochemical reactions and thus reflects distinct physiological states of the investigated cell or tissue [62].
Compared to other large-scale, biological approaches such as proteomics and genomics, the presence and level of metabolites is more closely linked to the phenotypic state of a cell [2, 29]. For instance, a short medical drug treatment might not modify the levels of mRNA and proteins, but it changes the concentrations of specific metabolites, for instance derivatives of drug metabolization. Analyzing products of metabolic reactions allows therefore for the measurement of true endpoints of biological processes, making the metabolome a valuable indicator of an organism's phenotype.

Currently, two major approaches are followed in metabolomics, namely *targeted* and *non-targeted metabolomics*. The first approach describes the quantitative measurements of a set of known metabolites with high accuracy. This is mostly combined with high-throughput methods allowing for the investigation of a large number of samples. The second approach, non-targeted

metabolomics, is often referred to as metabolic profiling [63]. In contrast to targeted approaches it is more focused on discovering unknown metabolites and the development of new techniques of metabolite detection. Typically, the degree of resolution, the accuracy of quantification and the sample throughput is much lower than in the case of targeted metabolomics [62].
Over the last few years, metabolomics has made enormous progress in terms of expertise and technology, comparable to the development steps of genomics and proteomics a decade ago. Metabolomics has emerged from its scientific niche existence to a widely-used application in biological and medical sciences [8, 64]. Improvements have been made especially concerning data acquisition and integration. Various scientific studies have been published highlighting the potential and benefits of this new technology [8, 32, 62]. The following section will give a short introduction into laboratory techniques used in metabolomics for both analyte separation and identification, and into currently available metabolomic databases.

2.1.1 Analytical techniques

Analytical platforms in metabolomics are often based on spectroscopic methods such as nuclear magnetic resonance spectroscopy (NMR) or mass spectrometry (MS). These analytical techniques are generally combined with chromatographic separation techniques such as gas chromatography (GC) or liquid chromatography (LC) [32, 61]. Since metabolite concentration levels in the cell can be down to picomolar range [20], separation techniques are important in order to enhance the capabilities of metabolite detection and to increase the analytic resolution level.

Chromatographic separation techniques

Chromatographic methods are used to separate individual chemical compounds from complex mixtures. The mixture is solved in a *mobile phase* and passes through a *stationary phase*. For the separation procedure the stationary phase is fixed in place (often in a column). Typically applied stationary phases are silica gels with long hydrophobic or hydrophilic carbon chains, depending on the chemical characteristics of the sample. The mobile phase comprises a solvent and the sample which has to be separated. For gaseous mobile phases the method is called gas chromatography, for liquid mobile phases liquid chromatography. During the chromatographic process the mobile phase propels the sample through the column where the sample interacts with the stationary phase. Individual components in the sample are differently retained by the stationary phase. Molecules with high affinity for the stationary phase stay longer in the chromatographic column compared to molecules with lower affinity. The different migration speed through the column therefore provides a separation of chemical compounds in complex mixtures (see Figure 2.1). *High performance liquid chromatography* (HPLC) is a special form of liquid column chromatography commonly applied in metabolomics. Here a pump provides a higher pressure (compared to gravity in the case of normal columns) in order to move the mobile phase and therein solved analytes through a more densely packed column [52]. Compared to ordinary chromatographic applications, this provides a better compound separation on columns with shorter length, enabling for highly selective and efficient sample preparations [82].

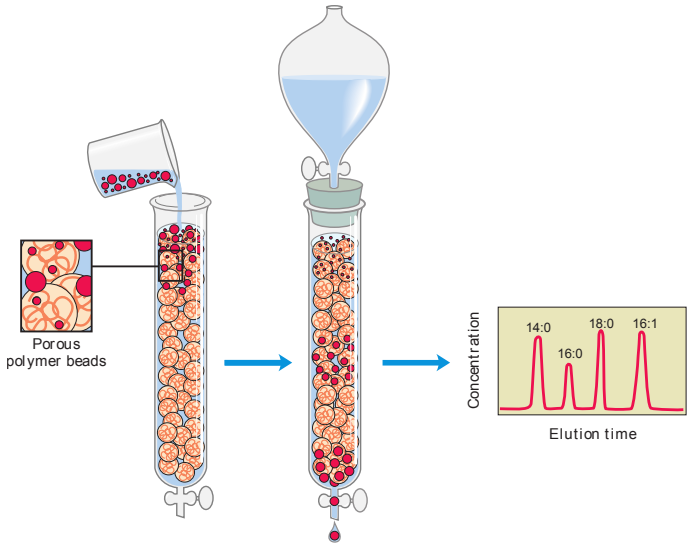

Figure 2.1: Chromatographic separation of analytes. Sample molecules interact with the stationary phase consisting of porous polymer beads. Molecules with high affinity for the stationary phase stay longer in the chromatographic column compared to molecules with lower affinity. This provides separation of chemical compounds in complex mixtures (adapted from [60]).

Analytical methods

After having separated individual chemical compounds, metabolites have to be identified and their concentrations have to be determined. The two leading detection technologies in the field of metabolomics are NMR-spectroscopy and mass spectrometry.

NMR-spectroscopy

For the case of *NMR-spectroscopy* molecules are identified by exploiting the quantum mechanical magnetic properties of an atomic nucleus. In a constant, strong magnetic field NMR-active isotopes with correct magnetic properties (e.g. ^{1}H or ^{13}C) absorb energy from an applied electromagnetic pulse. The absorbed energy is radiated back out at a specific resonance frequency. The energy level of such an emission depends, amongst other features, on the chemical environment of a NMR-active atomic nucleus. The chemical environment is determined for instance by the number of other surrounding homo- or heterogeneous atomic nuclei and by the covalent character of the chemical bound between atomic nuclei. By using these information it is possible to determine the chemical structure of compounds which then allows for the identification and quantification of metabolites found in the sample [52].
All biological metabolites consist of hydrogen atoms, therefore most NMR detection methods in metabolomics are based on the detection of these NMR-sensitive nuclei. In a biological sample such as cells, tissues or blood, all hydrogen-containing molecules above the detection limit thus will show a ^{1}H-NMR spectrum. The detected NMR spectrum of a biological sample is then a superposition of all spectra of metabolites that can be found in the sample [62].

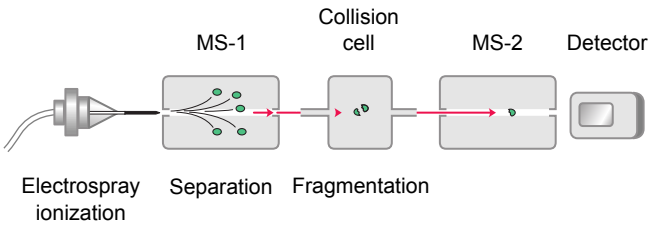

Figure 2.2: Schematic representation of electrospray ionization tandem mass spectrometry. Ionized metabolized are separated in the first mass analyzer (MS-1). Single metabolites are isolated and further fractionized. The fragments and their precursor molecule are then investigated in the second mass analyzer (MS-2). The detector quantifies the different ionized molecules (adapted from [60]).

A benefit of NMR-spectroscopy is that it can typically be applied without any preceding chromatographic separation of chemical compounds. However, NMR-based techniques are often less sensitive compared to mass spectrometry-based techniques. In addition, it can be very difficult to interpret NMR spectra and identify metabolites of complex mixtures [20, 62].

Mass spectrometry

Mass spectrometry, another detection technology, is even more widely used in metabolomics. Normally it is coupled with chromatographic methods for efficient separation of analytes. Gas chromatography interfaced with mass spectrometry (GC-MS) is a very popular combination due to its high-resolution characteristics. However, the required chemical derivatization of many biomolecules and the inability to detect many large and polar metabolites is a major drawback of this technique. Liquid chromatography coupled with mass spectrometry (LC-MS) is not subject to these restriction and a broad range of molecules can be measured. However, the resolution of LC-MS is lower compared to GC-MS.
In mass spectrometry measurements metabolites are identified according to their molecular mass. The general detection principle is generating charged molecules or molecule fragments by ionization and subsequent measurement of their mass-to-charge ratios (m/z) [52]. A metabolite thus can be identified by its molecular mass and by the pattern of its molecular fragmentation. However, this implies that two molecules with identical mass and fragmentation pattern cannot be distinguished in general by this method. In this case, the two analytes have to be separated first by other methods.

A mass spectrometer consists of three components: first an ion source, where chemical compounds are ionized; second an analyzer, which sorts and separates the charged molecules according to their m/z-ratio; and third a detector, which monitors different ionized molecules for quantification. The most common ionization methods for metabolites are Electrospray Ionization (ESI) [83, 86] and Matrix Assisted Laser Desorption Ionization (MALDI) [31]. Both methods can be used for biomolecules and large organic molecules which are fragile and often generate too many fragments when ionized by other techniques.
The MALDI technique is a *soft ionization method* using bombardment of laser light with sample molecules for analyte ionization. Sample molecules are embedded in a matrix which transforms the laser beam energy into excitation energy for analytes resulting in metabolite ionization and vaporization. This indirect excitation helps to protect the analytes from being destroyed by direct laser light.

For Electrospray Ionization the liquid sample together with a solvent is pumped through a very narrow steel capillary. A high voltage applied to the tip of the capillary generates a strong electric field which disperses the emerging liquid into a fine aerosol of highly charged droplets. A flow of warm nitrogen gas heats up the droplets leading to solvent evaporation and decreasing size of the droplets. During this process charged analyte ions are released from the droplet and channeled into the analyzer [52].

The mass analyzer, the second component of a mass spectrometer, sorts and separates ionized analytes according to their m/z-ratio. A variety of mass analyzers exists, the most common are magnetic sector field, quadrupoles, time-of-flight (TOF) analyzers, quadrupole ion traps, Fourier transform ion cyclotron resonance (FT-ICR) and Orbitrap. All methods are based on the fact that charged molecules are differently accelerated depending on their molecular mass and the number of elementary charges, which enables for the separation of these molecules. In tandem mass spectrometry (MS/MS) two or more analyzer elements are coupled in a row allowing for multiple steps of mass separations with fragmentation stages occurring in between. A single fragment of each analyte is isolated and in turn fractionized. The second fragments and their precursor molecule are then investigated. This provides further information about the chemical structure of compounds and helps to identify metabolites with similar chemical characteristics and molecular masses. Figure 2.2 illustrates the design of a tandem mass spectrometer.

The mass detector is the last element of a mass spectrometer. It monitors the charge or current induced by passing ions. The measured signal intensity of an ionized analyte is proportional to its relative abundance in the sample. The type of detector depends on the features of the applied analyzer. A typical detector is an electron multiplier. Here ion bombardment on an emissive material induces the emission of more than one electron. The emitted particles are accelerated by an electrical potential and again induce emission of electrons. Repeating these steps a number of times results in a strong amplification of the original signal of one single ion. Both analyzer and detector in a mass spectrometer are maintained under high vacuum to avoid collision of analyte molecules with air molecules.

2.1.2 Database resources

With the advance of analytical methods the number of identified metabolites has increased rapidly. For structuring this magnitude of data, several metabolomics databases have been established. The latest EcoCyc database release 13.6, for example, lists 1326 compounds of identified metabolites for the prokaryotic model organism *Escherichia coli* [40], while the most recent database version for human metabolites (HMDB v2.5) contains 6586 compounds [84]. It is to be mentioned that these numbers do not reflect the real size of the specific metabolome, but only the number of metabolites that can be detected with up to date methods. Particular plants are expected to show a metabolite pool of more than 200,000 chemical compounds [64].

The databases we used in our studies on beta-oxidation of fatty acids can be divided into three groups: pathway databases, metabolite databases and enzyme information databases (see Figure 2.3). The first group consists of databases that store metabolic pathway information for various organisms. They are mostly manually curated and contain experimentally validated information. From the Kyoto Encyclopedia of Genes and Genomes (KEGG) database [38] we deduced the topology of our metabolic pathways as well as involved metabolites and enzymes. For further information about metabolic pathways we used the MetaCyc Encyclopedia of Metabolic Pathways (MetaCyc) [14]. Resources from the second group, metabolite databases, were used

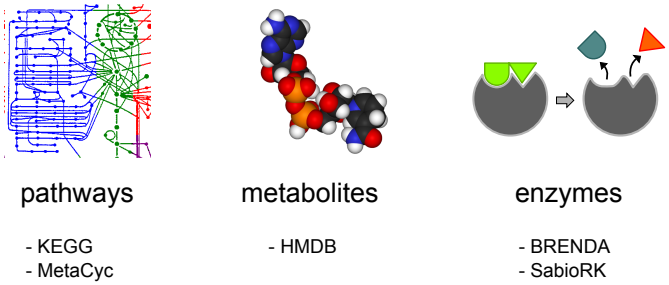

Figure 2.3: Overview about the database resources which were used in this work. Information about the topology of metabolic pathways, involved metabolites and catalyzing enzymes were taken form KEGG and MetaCyc database. Biochemical properties of compounds and their connections to diseases were inferred from the Human Metabolite Database (HMDB). Information about substrate specificity and kinetic constants for enzymes were taken from BRENDA and SabioRK.

in order to retrieve detailed information about metabolites that have been analytically detected and quantified in our dataset. Knowledge about biochemical properties of metabolites and connections to diseases was mainly inferred from Human Metabolite Database (HMDB) [84]. The last group of databases stores information about kinetic and functional enzyme properties. For enzymes involved in the beta-oxidation pathway, kinetic parameters and information about substrate specificity and regulation were taken from two enzyme information databases, BRENDA [16] and SabioRK [85].

2.2 HuMet Study

The Human Metabolome (HuMet) Study[1] was conducted in 2009 in order to investigate metabolomic profiles in healthy, male individuals under highly-controlled and well-defined conditions. The aim of the study was to define a basal metabolomic state for healthy probands as well as intra- and interindividual variations from this state. In addition, the effect of several defined physiological and nutritional interventions to the metabolomic profile was studied. The interventions included for example fasting, lipid-rich diet and physical exercise. Metabolites were identified and quantified using different analyte separation techniques combined with mass spectrometry and NMR spectroscopy.

For the HuMet study, 15 young volunteers with an age range of 22 - 33 years were recruited. All individuals were metabolically healthy and had a body mass index (BMI) between 20 - 25 kg/m^2. The probands underwent different nutritional interventions (fasting, lipid rich and/or sugar rich diet) and physiological interventions (ergometry and low temperature stress test). The study was performed in two blocks each consisting of two days with a period of 14 days between the blocks. During block I, probands had a well-defined meal and afterwards fasted for 36 hours. After the fasting period, volunteers received a standardized Fresubin drink for breakfast and lunch.
On the first day of block II, probands underwent an oral glucose tolerance test (OGT) with 75 gram of glucose in the morning and 30 minutes of bike ergometry in the afternoon. For lunch and dinner they received a standardized Fresubin drink. On day two in the morning, volunteers

[1] http://www.humet-tum.de/

were subjected to a oral lipid tolerance test (OLT) with diets containing long chain triglyceride fat emulsions. At the end of the second day, probands underwent a low temperature stress test. Over the course of the study 56 blood samples, 25 urine samples and 32 breath condensate samples were collected for each proband. Samples were normally taken every two to four hours; for nutritional and physical interventions as ergometry and nutritional tolerance test, sampling was done at more frequent intervals of 15 to 30 minutes.

In this work we examined blood metabolite levels from all 15 probands participating in the HuMet study with a focus on the fasting period of block I. During this period 10 blood samples at different time points were taken for each proband. In each sample 41 different acylcarnitine concentrations were detected using AbsoluteIDQ kits from Biocrates life sciences GmbH, Austria. Targeted metabolite profiles were measured by electrospray ionization (ESI) tandem mass spectrometry (MS/MS) as described in Section 2.1.1. Quality control of metabolite quantification was achieved by reference to appropriate internal standards. The technique was described previously [33] and in detail by patent US 2007/0004044[2]. The detection kit allows for the quantification of 41 acylcarnitines, which are fatty acid derivatives, 14 amino acids and one sugar compound. In addition, 15 sphingolipids and 92 glycerophospholipids are measured, both components of cellular membranes. For our studies we focused on the metabolite profile of acylcarnitines, which are transport forms of fatty acids in the beta-oxidation pathway. A list of all quantified metabolites is given in Appendix A.

2.3 Mathemetical modeling

In natural sciences theoretical models are widely used to describe complex processes or relationships in a mathematically concise framework. This is also the case for biological sciences, especially in the field of systems biology. Models are used as an abstract representation of objects such as processes or relationships between different entities and summarize established knowledge about a system in a coherent mathematical representation. This allows for the explanation of features of objects, the understanding of the internal nature and dynamics of involved processes, and the prediction of the behaviour of a system under simulated conditions [42].
The subsequent part gives a short introduction in modeling methods we applied in this work. First we will introduce ordinary differential equations (ODE) as a tool to describe biochemical reactions. Then we will give an overview about existing kinetic models for enzymatic biochemical reactions. Furthermore, we will describe a matrix notation that helps to deal with systems of linear equations representing multiple enzymatic reactions.

2.3.1 Modeling biochemical systems by ordinary differential equations

A common way of modeling the dynamics of biochemical reactions is the usage of *ordinary differential equations* (ODE). A *differential equation* in general describes the rate of change of a variable x over time. An ordinary differential equation is a relation which contains functions of only one variable. The order of an ODE is the order of the highest derivative in this relation. ODEs have been used for biological modeling in ecology for a long time. Examples are Verhulst equation and Lotka-Volterra equations which describe population growth dynamics [58]. In a biochemical sense, the variable x can stand for instance for the concentration of a molecule

[2]accessible online at http://www.freepatentsonline.com/20070004044.html

that is metabolized by a specific enzyme. Simple and straightforward examples for ODEs are exponential growth and decay:

$$\frac{\mathrm{d}x}{\mathrm{d}t} = \dot{x} = kx, \quad x(0) = x_0 \tag{2.1}$$

For a negative rate parameter k ($k < 0$) variable x is decreasing over time in a decay process, while for positive k ($k > 0$) x is going to increase. Note that $\dot{x}$ is a common notation to abbreviate time derivative $\mathrm{d}x/\mathrm{d}t$. Equation (2.1) can be used, for example, to model growth processes of microorganism such as viruses or bacteria or to represent radioactive decay of unstable isotopes. In both cases, growth or decay rates are proportional to the current value of variable x. If we understand the underlying principles of such a process and are able to describe it with an ODE, we can make predictions about future values. For doing so we need to solve the differential equation. Solving equation (2.1) analytically gives

$$x(t) = x_0 e^{kt} \tag{2.2}$$

where x_0 describes the initial value of variable x at time point $t = 0$. That is, if we know the rate coefficient k and the concentration of a molecule at a given time point t, we can describe the change of concentration over time and predict concentration values for the molecule.

For simple cases as shown above, solutions can be found analytically. However, many models in biology consist of more complex differential equations that are not linear. In this case it is not possible to find exact analytical solutions, but we can approximate the solutions using numerical methods [17]. In this work we used the variable order multistep solver *ode15s* for differential equations implemented in MATLAB (version 7.6.0, The MathWorks, Inc., Natick, MA) [74].

2.3.2 Kinetic laws for enzymatic modeling

We have seen that biochemical reactions can be described by ordinary differential equations. The *production rate* of a biochemical reaction, i.e. the change of substrate concentrations per time, is generally determined by different factors: concentrations of the substrates, concentration of the catalyzing enzyme, concentrations of possible activating or inhibiting modifiers, and other parameters [42]. The latter arise from biochemical properties of the enzyme and its substrates, for example how tightly the substrate can bind to the catalytic center of the enzyme and how many chemical reactions are required to transform substrates to product molecules. Kinetic rate laws then describe the relationship between all factors mentioned above and their impact on the reaction rate. In the following part we will introduce mass action kinetics and Michaelis-Menten kinetics, two rate laws commonly used to describe enzymatic reactions.

Mass action kinetics

The law of *mass action* is a general way of describing chemical reactions. It was formulated by Guldberg and Waage in the nineteenth century [30]. The law states that the reaction rate is proportional to the probability of collision of the reactants. This probability in turn depends on the product of the concentrations of the participating molecules to the power of the *stoichiometric coefficients*, i.e. how many molecules of one species enter the reaction. The general law of mass

action for a reaction which transforms m substrates with concentrations X_i $(i = 1, ..., m)$ into a products with concentrations P_j $(j = 1, ..., a)$ is

$$v := v_+ - v_- = k_+ \prod_{i=1}^{m} X_i^{n_i} - k_- \prod_{j=1}^{a} P_j^{n_j}, \tag{2.3}$$

where n_i and n_j denote the respective molecularities of X_i and P_j in this reaction [42]. Net rate v is the difference between forward (v_+) and backward (v_-) reaction rates with respective kinetic constants or proportionality factors k_+ and k_-.
Given the simple, irreversible reaction

$$2A + B \xrightarrow{k} C \tag{2.4}$$

as an example, the mass action reaction rate reads

$$v_C := \frac{\mathrm{d}C}{\mathrm{d}t} = \dot{C} = kA^2B^1 = kA^2B, \tag{2.5}$$

where rate constant k is a proportionality factor and the stoichiometric coefficients of A and B are 2 and 1, respectively. The kinetics of a simple decay reaction as

$$D \xrightarrow{k} \varnothing \tag{2.6}$$

can also be represented by the equation

$$v_D = \frac{\mathrm{d}D}{\mathrm{d}t} = -kD \tag{2.7}$$

which is the same differential equation as (2.1).

For a metabolic network which consists of m substances and r reactions, the dynamics for each species X_i can be described by

$$\frac{\mathrm{d}X_i}{\mathrm{d}t} := \sum_{j=1}^{r} s_{ij} v_j \quad \text{for} \quad i = 1, ..., m, \tag{2.8}$$

with rate v_j for the jth reaction. The quantities s_{ij} are the stoichiometric coefficients of the ith metabolite in the jth reaction and represent the *stoichiometry matrix*

$$\mathbf{S} := \{s_{ij}\} \quad \text{for} \quad i = 1, ..., m \quad \text{and} \quad j = 1, ..., r, \tag{2.9}$$

where each column belongs to a reaction and each row to a compound. Negative stoichiometric coefficients in one column represent educts and positive coefficients products of one specific reaction. For compounds which are not involved in the specific reactions, entries in the reaction column are zero.

Several refinements on mass action kinetics have been proposed, for instance power law kinetics and approximate kinetic formats, which take more thermodynamical aspects of chemical reactions into account [18, 42].

Michaelis-Menten kinetics

Michaelis-Menten kinetics, another established and well known kinetic rate law, proposes a mechanism that approximately describes the kinetics of many enzymes [10, 55]. The standard model holds for one-substrate reactions without any effectors and no backward reaction. The reaction scheme looks as follows

$$E + S \underset{k_{-1}}{\overset{k_1}{\rightleftharpoons}} ES \xrightarrow{k_2} E + P \tag{2.10}$$

with enzyme E and substrate S forming an enzyme-substrate complex ES. After the substrate S is converted into product P, the complex dissociates and P is released. The reaction scheme (2.10) already shows some assumptions of the Michaelis-Menten model: product formation is irreversible, i.e. once P is produced, it cannot be converted back to substrate S anymore. The complex formation on the other hand is reversible. During the whole reaction the total concentration of enzyme E_T remains constant, meaning that enzyme molecules are neither consumed nor produced. The amount of total enzyme E_T is the sum of free enzymes E and enzyme molecules bound in the ES complex ($E_T = E + ES = const$ for all timepoints). Scheme (2.10) can be represented by a system of differential equations. For obtaining an analytical solution of this system a so-called *quasi-steady state* for the ES complex is assumed. During the course of reaction the concentration of ES then remains constant. This assumption only holds if the substrate concentration at the beginning of the reaction is much larger than the total enzyme concentration ($S(t = 0) \gg E_T$), which is the case for many enzymatic reactions[3]. Using these assumptions leads to the following relationship between substrate concentration S and production rate v, i.e. the change of concentration S per time t:

$$v_P := \frac{\mathrm{d}P}{\mathrm{d}t} = \frac{v_{max} S}{S + K_M} \tag{2.11}$$

This relationship is often referred to as *Michaelis-Menten equation*. The *Michaelis constant*

$$K_M = \frac{k_{-1} + k_2}{k_1} \tag{2.12}$$

with parameters k_1, k_{-1} and k_2 describes the substrate concentration that yields a half-maximal reaction rate $v_{max}/2$. The *maximal rate* $v_{max} = k_2 E_T$ is attained when all enzyme molecules are completely saturated with substrate molecules. Plotting the Michaelis-Menten equation shows a linear dependency between reaction rate and substrate concentration for very low substrate concentrations. For high amounts of substrate the curve approaches an asymptote at $v = v_{max}$ when all enzyme molecules are bound with substrate molecules. Figure 2.4 illustrates the features of the Michaelis-Menten rate law and the meaning of parameters v_{max} and K_M. In order to describe enzymatic reactions in more detail, models such as reversible Michaelis-Menten kinetics or convenience kinetics have been proposed [42, 50]. These models incorporate enzyme regulation by activators and inhibitors and allow for the representation of reactions with multiple substrates and products.

2.3.3 Matrix notation of multiple enzymatic reactions

Beta-oxidation of long fatty acids is carried out in several consecutive reactions with sequential removal of two carbon atoms from fatty acid chains (see Section 1.2.2). This metabolic pathway

[3]Further justifications for the above mentioned assumptions and a more detailed derivation of the Michaelis-Menten rate law can be found in many biochemical or biomathematical textbooks (for example [6, 58, 60]).

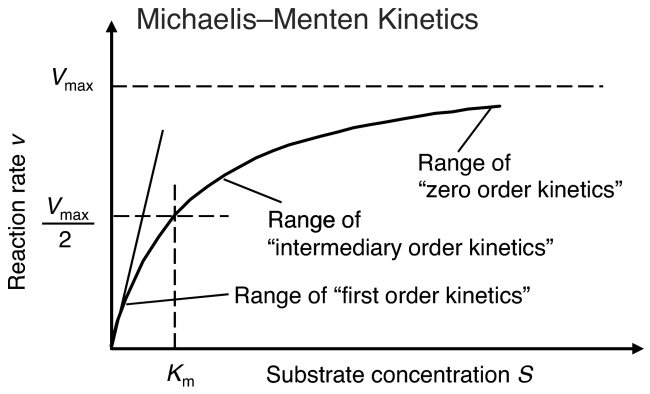

Figure 2.4: Michaelis-Menten plot showing the dependence of reaction rate v on substrate concentration S. v_{max} denotes the maximal reaction rate that is reached when all enzyme molecules are completely saturated with substrate molecules. For a substrate concentration of K_M, a half-maximal reaction rate $v_{max}/2$ is reached (reprinted from [42]).

can be described as a cascade of multiple enzymatic steps. Each step or elementary reactions in turn can be represented by kinetic rate laws like mass action or Michaelis-Menten. However, multiple enzymatic reactions are dependent on each other, therefore we obtain a system of coupled differential equations. This system can be represented in matrix notation. As an example, we take a simple reaction cascade with irreversible influx, outflux and enzymatic reactions:

$$\xrightarrow{k_i} A \xrightarrow{k_A} B \xrightarrow{k_B} C \xrightarrow{k_o} \tag{2.13}$$

Here k_i and k_o are parameters for influx and outflux reactions and k_A and k_B kinetic parameters for enzymatic reactions. Using mass action kinetics, scheme (2.13) can be written as a system of differential equations with A, B and C reflecting compound concentrations:

$$\begin{array}{rcrcr} \dot{A} & = & k_i & - & k_A \cdot A \\ \dot{B} & = & k_A \cdot A & - & k_B \cdot B \\ \dot{C} & = & k_B \cdot B & - & k_o \cdot C \end{array} \tag{2.14}$$

We can describe the stoichiometry of the reaction cascade (2.13) using the stoichiometry matrix $\mathbf{S}$ (see Section 2.3.2). Each row of the matrix belongs to a compound and each column to an elementary reaction (denoted as an arrow in the reaction scheme).

$$\mathbf{S} = \begin{pmatrix} 1 & -1 & 0 & 0 \\ 0 & 1 & -1 & 0 \\ 0 & 0 & 1 & -1 \end{pmatrix} \tag{2.15}$$

A negative entry s_{ij} in $\mathbf{S}$ states that compound X_i is an educt for reaction v_j. For a product of reaction v_j, the stoichiometric coefficient s_{ij} is positive. If compound X_i is not involved in the reaction v_j, then s_{ij} is zero. For a metabolic system with m substances $(X_1, ..., X_m)$ and r reactions $(v_1, ..., v_r)$ we can describe all substance concentrations by a concentration vector

$$\mathbf{C} = \{c_1, ..., c_m\}\,. \tag{2.16}$$

Metabolites which constantly flow from an external pool into the system are also considered in the concentration vector. Vector $\mathbf{k}$ contains elementary rate constants for all reactions $v_1, ..., v_r$. Using $\mathbf{S}$, $\mathbf{C}$ and $\mathbf{k}$, we can express the system of differential equations (2.14) in matrix notation

$$\mathbf{S} \cdot \mathrm{diag}(\mathbf{C}) \cdot \mathbf{k} = \begin{pmatrix} 1 & -1 & 0 & 0 \\ 0 & 1 & -1 & 0 \\ 0 & 0 & 1 & -1 \end{pmatrix} \begin{pmatrix} 1 & 0 & 0 & 0 \\ 0 & \mathbf{A} & 0 & 0 \\ 0 & 0 & \mathbf{B} & 0 \\ 0 & 0 & 0 & \mathbf{C} \end{pmatrix} \begin{pmatrix} k_i \\ k_A \\ k_B \\ k_o \end{pmatrix} \tag{2.17}$$

or by substituting $\mathbf{M} := \mathbf{S} \cdot \mathrm{diag}(\mathbf{C})$

$$\mathbf{M} \cdot \mathbf{k} = \begin{pmatrix} 1 & -\mathbf{A} & 0 & 0 \\ 0 & \mathbf{A} & -\mathbf{B} & 0 \\ 0 & 0 & \mathbf{B} & -\mathbf{B} \end{pmatrix} \begin{pmatrix} k_i \\ k_A \\ k_B \\ k_o \end{pmatrix} \tag{2.18}$$

Matrix $\mathbf{M}$ then contains information about both the stoichiometry of the reaction and the concentration of all reactants.

2.3.4 Analysis of metabolic reactions for steady state conditions

Under *steady-state* conditions, the concentrations of all compounds remain constant, i.e. the change in concentration over time is zero. Measured metabolite concentrations often reflect these conditions, as biochemical reactions are supposed to reach equilibrium in the order of milliseconds to seconds. If we know the topology of a biochemical pathway we can describe all reactions using the matrix notation proposed in the previous section. For a given set of metabolite concentrations we can estimate rate constants by setting

$$\mathbf{M} \cdot \mathbf{k} = \begin{pmatrix} 1 & -\mathbf{A} & 0 & 0 \\ 0 & \mathbf{A} & -\mathbf{B} & 0 \\ 0 & 0 & \mathbf{B} & -\mathbf{B} \end{pmatrix} \begin{pmatrix} k_i \\ k_A \\ k_B \\ k_o \end{pmatrix} = \mathbf{0} \tag{2.19}$$

The system of linear equations (2.19) is underdetermined as it has four unknown parameters but only three independent linear equations (rank of matrix $\mathbf{M}$ is 3). Therefore we cannot find an exact solution, but by defining one parameter ($k_o > 0$) we can calculate all remaining parameters (if we choose $k_o = 0$, then all parameters are zero):

$$\begin{aligned} k_i &= C \cdot k_o \\ k_A &= \tfrac{C}{A} \cdot k_o \\ k_B &= \tfrac{C}{B} \cdot k_o \end{aligned} \tag{2.20}$$

This solution vector for the cascade reaction (2.14) can be seen as a positive ray in the parameter space, since one parameter was freely chosen. We can also derive such a solution by calculating the null space using extreme pathway [72] or elementary flux mode analysis [73]. Both methods solve the system of linear equation with constraints that rate parameters have to be greather than or equal to zero, since negative kinetic rates do not make sense for biochemical reactions.

If more influx or outflux terms are added to the cascade reaction scheme (2.13), the system of linear equations becomes even more underdetermined. The null or solution space of such a system

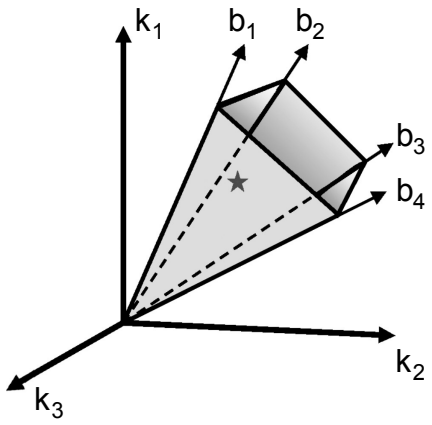

Figure 2.5: Schematic representation of a k-cone. Basis vectors b_1, b_2, b_3 and b_4 are solutions for a system with condition specific metabolite concentrations and span up a positive convex cone (marked with an asterisk) for the solution space. All positive linear combinations of basis vectors are solutions and lie within the 'filled' k-cone (adapted from [42]).

is spanned by several positive basis vectors, describing a positive convex cone in the parameter space [26]. All non-negative linear combinations of basis vectors then in turn are valid solutions and lie within the convex cone. Points inside the convex cone satisfy both physiochemical and condition-specific constraints and can be seen as kinetic states the system can attain (see Figure 2.5). Compared to flux analysis, these solutions additionally contain information about condition specific metabolite concentrations, which allows for the comparison of dynamical variations between intra- and interindividual metabolic profiles. In Chapter 4 we use this approach to investigate the rate constants of subjects in a metabolomics study.

Chapter 3

Model development for the fatty acid beta-oxidation pathway

In order to provide energy fatty acids are primarily metabolized in the beta-oxidation pathway. In repeating cycles, two carbon atoms are removed from fatty acid chains (see Section 1.2). This reaction sequence can be modeled as a cascade of coupled elementary reactions, similar to the example given in Section 2.3.3. In this chapter we will describe how we obtained a model for fatty acid beta-oxidation. First we will give an overview about existing models for lipid metabolism. Then we will show how we developed a simplified model for the beta-oxidation pathway and discuss all assumptions that have been made for reducing the complexity of the model. In addition, we will highlight the link between our model and measured metabolite concentrations of the HuMet dataset.

3.1 Existing models

Many metabolic pathways have been elucidated within the last century. For a variety of organisms, the core metabolic network is well known and provided in maps like the *Boehringer Chart* [56] or in databases as KEGG [38]. Moreover, details about involved compounds and catalyzing enzymes are accessible. Many mathematical models exist that describe metabolic reaction networks, for instance in bacteria [18], but also for human liver metabolism [12] and gluconeogenesis [15]. However, for mitochondrial beta-oxidation only few computational models are published. Two of them describe fatty acid metabolism in heart [43, 44, 45] and liver mitochondria [47] of rat cells. Both models do not incorporate pathway regulation features (e.g. the inhibition of fatty acid transporter proteins by starting compounds of fatty acid synthesis [67]) and lack detailed data about kinetic constants of enzymes that have been determined in the recent past.
For the description of the human beta-oxidation pathway two more recent mathematical model exist. Yugi and Tomita [87] proposed a computational model of mitochondrial metabolism on a whole organelle scale, which also includes beta-oxidation reaction steps that take place in the mitochondrium. The model has been developed within the E-Cell2 simulation framework [79]. Many rate equations and kinetic parameters are based on published in-vitro enzyme kinetic studies. However, a large fraction of the parameter set had to be estimated computationally.

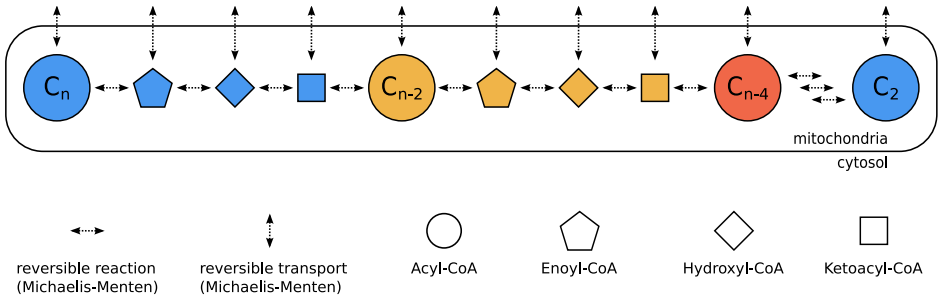

Figure 3.1: General model of the beta-oxidation cascade. Enzymatic steps are described with reversible Michaelis-Menten rate laws. All main metabolites and intermediate compounds are included in the model and compounds can be transported between mitochondrium and cytosol. Split off acetyl-CoA molecules and coenzymes are not shown in this simplified scheme.

Modre-Osprian *et al.* [57] developed a model for mitochondrial fatty acid beta-oxidation. It is based on the whole organelle model by Yugi and Tomita and explains biochemical reactions in more detail. Here kinetic parameters have likewise been taken from the literature. In the case that no kinetic data are available for human enzymes, experimental data from other organism such as rat or mouse have been incorporated. The model only considerates beta-oxidation of even, saturated fatty acid chains. It was applied to concentrations of acyl-carnitines measured in newborn screenings. Differences between existing models and our model will be discussed in Section 4.4.

3.2 Model development

The beta-oxidation reaction pathway as described in Section 1.2 consists of four elementary intermediate reactions which are catalyzed by different enzymes: oxidation, hydration, a second oxidation and thiolysis. The reactions are sequentially repeated and at the end of each reaction cycle two carbon atoms in the form of acetyl-CoA are removed. The general model (see Figure 3.1) consists of fatty acid compounds and their respective intermediate metabolites. Transport processes of molecules occur between the outside and inside of the mitochondria and all biochemical reactions are described with reversible Michaelis-Menten rate laws. Such a general model can be described in a huge system of ordinary differential equations with multiple kinetic parameters and variable metabolite concentrations. However, many kinetic constants are not known and it is extremely labor-intensive to measure them. Moreover, it is often very difficult to quantify concentrations of intermediate metabolites, since they are immediately converted to other metabolites. In our case we only detected main compounds of beta-oxidation pathway such as palmitoylcarnitine and stearoylcarnitine, transport forms of palmitic (C16) and stearic (C18) fatty acids. The mass spectrometry measurements we used did not allow for the detection of many fatty acids and their respective enoyl-, hydroxyacyl- or ketoacyl-forms, which are products of intermediate steps. Since it is not feasible to estimate many unknown parameters using a limited set of experimental data without introducing large indeterminacies, assumptions on the general model are needed in order to reduce its complexity. Figure 3.2 illustrates the flowchart for the development of the simplified beta-oxidation model. All assumptions will be discussed in the following part.

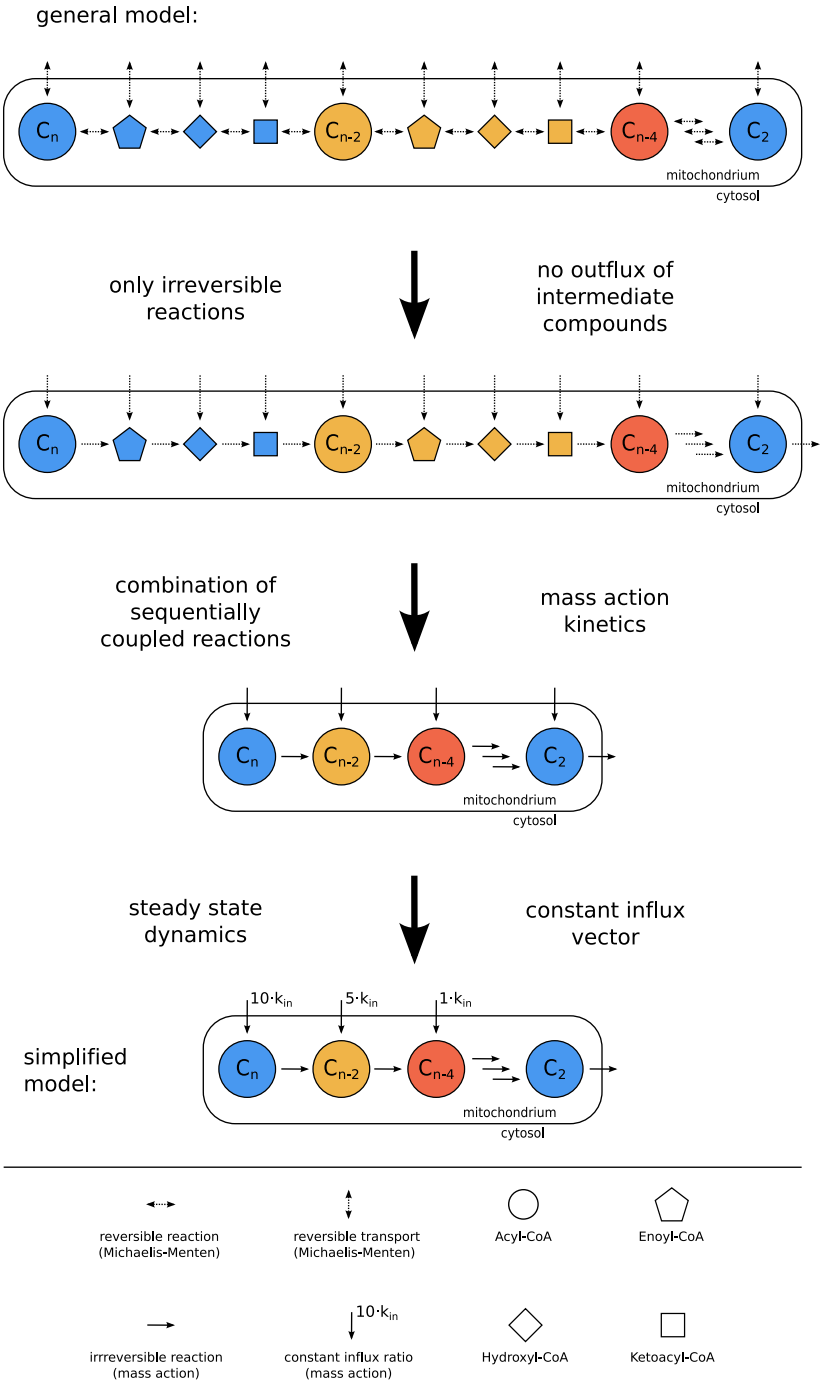

Figure 3.2: Flowchart for the development of the simplified beta-oxidation model. Physiological and biochemical knowledge about features of fatty acid catabolism were incorporated in order to reduce the model complexity. This facilitates the investigation of the solution space for the system of linear equations. Features of the proposed model are irreversibility of cascade reactions and simplification by leaving out unlikely intermediate outflux processes. Sequentially coupled reactions in the pathway are combined and treated with mass action rate laws under steady state dynamics. Substrate influx is set to a constant ratio that is proportional to the composition of specific fatty acids in human adipose tissue.

3.2.1 Assumptions for reducing complexity

In the following part we will propose a simplified model for the beta-oxidation pathway. The proposed model attempts to strike a balance between complexity and simplification. For designing this model we incorporated physiological and biochemical knowledge about features of fatty acid catabolism in order to reduce the complexity. All assumptions are based on this knowledge and were only applied if simplifications are in accordance with biological conditions.

Irreversible reactions

The first assumption about the fatty acid beta-oxidation pathway is that all biochemical reactions are treated as irreversible reactions. This means products of one reaction can only react back to its chemical precursor if such a back reaction is explicitly stated in the model. The first step of each beta-oxidation cycle, the dehydrogenation of acyl-CoA, is an irreversible reaction, since high amounts of energy are produced in this reaction. This energy is used in the respiratory chain to generate energy-rich transfer molecules [6]. If the first reaction in a metabolic cascade is irreversible (which is also referred to as the committed step), then all subsequent reactions can be treated as irreversible, too. Substrates which enter the pathway will ultimately end up in the pathway's final product. In the beta-oxidation cascade the product of one reaction is substrate to the next reaction in the chain. For example stearic acid (C18) is degraded to palmitic acid (C16), which in turn is again metabolized to myristic acid (C14) and so on. Acetyl-CoA (C2), that is split off the fatty acid chain during each beta-oxidation step, is channeled into the citric acid cycle for generation of energy-rich ATP molecules. Hence products of biochemical reactions are continuously removed. According to Le Chatelier's principle the change of concentration of one compound in an equilibrium reaction will shift the equilibrium to that reaction side which reduces the change in concentration [4]. Therefore ongoing removal of reaction products in the beta-oxidation cascade will shift the direction of reactions to the product side. The net flux in all reactions then points downwards the pathway and goes from long chain to short chain fatty acids. As a result we can treat all reversible reactions as irreversible.

No simultaneous fatty acid synthesis

For the fasting period we can also neglect effects of fatty acid synthesis, since the interplay between fatty acid catabolism and anabolism is highly regulated and spatially separated [1, 24]. The synthesis of fatty acids generally takes place in the cytosol, while beta-oxidation occurs in the mitochondrial matrix. In addition, molecules involved in one pathway can act as regulators on enzymes of the other pathway. For instance, malonyl-CoA, a starting compound for fatty acid synthesis, inhibits carnitine palmitoyltransferase I (CPTI) [67]. This enzyme catalyzes the transport of fatty acids into the inner part of the mitochondrium, where beta-oxidation takes place. For fatty acid synthesis malonyl-CoA is produced in high concentrations leading to suppression of degradation processes. Either fatty acid anabolism or catabolism is switched on, so the body saves energy and newly synthesized molecules are not instantly degraded again. The antagonistic regulation of both pathways therefore allows for neglecting effects of fatty acid synthesis on the concentration levels of quantified metabolites.

No outflux reactions for intermediate compounds

In contrast to the general model, our proposed model does not take outflux reactions for intermediate compounds into account. That is, only the last product of the reaction cascade can leave the system. A biological interpretation is that the purpose of mitochondrial beta-oxidation is to provide energy to the cell by entirely metabolizing fatty acids, but not to provide precursor molecules for subsequent anabolic reactions. In fact, there are fatty acids that require beta-oxidation steps as part of their synthesis, for example the production of long, polyunsaturated fatty acid docosahexaenoylic acid (C22:6) out of detracosahexaenoylic acid (C24:6). However, the oxidation steps take place outside the mitochondrium in the cytosol or in peroxisomes [75, 76]. Identical reactions exist for both catabolism and anabolism of fatty acids, but they are spatially separated and antagonistically regulated (see above).
Since we assume irreversible reactions and no outflux reactions, the only possible flux for an intermediate metabolite is in direction to fatty acids with shorter chain length. For instance, the enoyl-form of myristic acid (C14-enoyl), the product of a dehydrogenation reaction catalyzed by acyl-CoA-dehydrogenase (see Section 1.2), can only be converted to the hydroxy-form of myristic acid (C14-hydroxy), since no back reaction to C14-enoyl and no outflux out of the system is allowed. Consequently, shortened fatty acids are restricted to stay inside the mitochondrium and cannot flow into other compartments of the cell. Experimental results from Nada *et al.* [59] also suggested such an *intermediate channeling*. Here especially long chain intermediates of the degradation of labeled linoleic acid (C18:2) could not be detected.

Taken together, we can assume that once a fatty acid chain is transported into the mitochondrium, it will be completely metabolized. All intermediate metabolites stay within the closed reaction space of the mitochondrial matrix until they are broken down to acetyl-CoA molecules. Moreover, all intermediates in the cascade are substrates for further reactions and thus are constantly removed, as it was described above. Hence it can be concluded on the basis of these observations that outflux reactions for intermediate compounds can be neglected.

Mass action kinetics

Enzymatic reactions in pathway models are usually described by mass action or Michaelis-Menten rate laws (see 2.3.2). Applying Michaelis-Menten kinetics allows to describe enzymatic steps in more detail by including saturation effects and maximal conversion rates. However, compared to simple mass action kinetics, modeling of reactions with Michaelis-Menten requires at least one additional parameter per reaction. For the estimation of unknown parameters it is beneficial to reduce the indeterminacies of the system of linear equations. If the concentration of substrate S is small compared to K_M ($S \ll K_M$), the Michaelis-Menten equation (2.11) can be approximated by:

$$v = \frac{\mathrm{d}P}{\mathrm{d}t} = \frac{v_{max} S}{S + K_M} \approx \frac{v_{max}}{K_M} S \tag{3.1}$$

Combining the ratio of two parameters v_{max} and K_M into one parameter $k = v_{max}/K_M$ gives a linear relationship between product formation rate v and substrate concentration S (see also Figure 2.4):

$$v = k \cdot S \tag{3.2}$$

We can also derive this relationship by using mass action rate laws for describing enzymatic reactions.
Table 3.1 compares quantified metabolite concentrations of acylcarnitines with published K_M

values for different acyl CoA dehydrogenase enzymes. These enzymes catalyze the dehydrogenation of acyl-CoA, the first step of one beta-oxidation cycle, which is believed to be the rate-determining and committed step of the whole cycle [35, 36, 54].

Chain length	metabolite [μM]	K_M [μM]	S/K_M	Enzyme
4	0.17	12.9	0.0136	SCAD
6	0.07	33.9	0.0019	SCAD
8	0.17	8	0.0207	MCAD
10	0.28	9.1	0.0312	MCAD
12	0.11	7	0.0161	LCAD
14	0.05	10	0.0051	LCAD
16	0.13	14	0.0091	LCAD
18	0.05	8	0.0065	LCAD

Table 3.1: Comparison of acyl-CoA dehydrogenase K_M values with concentration mean of their respective substrate metabolites. All concentrations and constants are shown in μM. The ratio between S and K_M shows that substrates are very small compared to Michaelis constant. Therefore linear mass action kinetic laws can be assumed for the simplified model. K_M values were taken from [25, 27].

The comparison shows that concentrations for different acylcarnitines are very small compared to the K_M values of acyl CoA dehydrogenase enzymes. Therefore we can assume a linear rate law for the metabolization of fatty acids as depicted in equation (3.2). Figure 3.3 shows exemplarily the Michaelis-Menten curve for enzyme medium-chain acyl-CoA dehydrogenase (MCAD) with kinetic parameters K_M and v_{max} taken from [27]. The arrow denotes the highest measured concentration of all acylcarnitines with fatty acid chain length three or higher. Therefore we can deduce that all measured substrate concentrations fall into the linear range of the curve, which allows us to simplify the general model by using mass action kinetics instead of Michaelis-Menten rate laws. Our parameters then incorporate both K_M and v_{max} values, so they should not be seen as real kinetic parameters. Rather, calculated parameter values represent observed kinetic values, referred to as pseudoelementary rate constants by Famili *et al.* [26].

Combination of sequentially coupled reactions

A further assumption of our proposed model is that sequentially coupled reactions can be combined into an overall reaction. Experimental findings corroborate this hypothesis. Early studies on beta-oxidation of labeled fatty acids in intact mitochondria reported predominant proportions of saturated CoA and carnitine esters as intermediate metabolites [51, 77, 78]. Kler *et al.* [41] and Jackson *et al.* [36] also studied acyl-CoA ester and acylcarnitine intermediates formed during mitochondrial fatty acid beta-oxidation. The treatment of isolated mitochondria from human fibroblast with labeled palmitic acid (C16) resulted in the detection of saturated acyl-CoA and carnitine esters as products of the oxidation process. Intermediates such as enoyl-, hydroxyacyl- or ketoacyl-forms of fatty acids on the contrary could not be measured. Other experiments, which used isolated rat mitochondria instead of human mitochondria, detected acyl-CoA and carnitine ester intermediates during oxidation of fatty acids [22, 23]. However, only saturated CoA and carnitine esters were predominant, confirming previous results [51, 77, 78].
Additionally, the existence of a trifunctional protein complex with long-chain-enoyl-CoA hy-

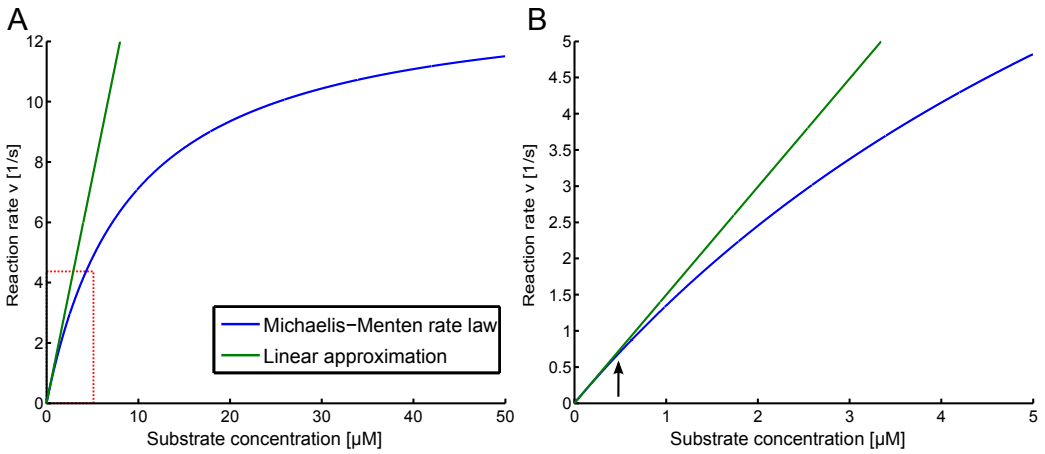

Figure 3.3: Michaelis-Menten curve for human medium-chain acyl CoA dehydrogenase (MCAD). Substrate concentration is plotted against reaction rate. The green line represents the linear approximation for small S compared to K_M with slope v_{max}/K_M. (A) Kinetics for parameters $K_M = 9.1\ \mu M$ and $v_{max} = 13.6\ s^{-1}$, taken from [27]. Both parameters are specific for substrate decanoyl-carnitine (C10). (B) Detail of the area in plot (A) which is surrounded by a red dashed line. The arrow denotes the highest measured concentration of all acylcarnitines with fatty acid chain length three or higher (decanoyl-carnitine (C10) concentration 0.627 μM). This concentration lies within the linear range of the curve, which allows us to assume mass action rate laws for our model.

dratase, hydroxyacyl-CoA dehydrogenase and long-chain oxothiolase activities has been reported [13, 53, 81]. The complex is closely associated with the inner mitochondrial membrane and catalyzes all enzymatic reactions in the beta-oxidation cycle except for the first dehydrogenation step. This trifunctional protein complex also provides evidence for the above mentioned intermediate channeling, which has been observed especially for beta-oxidation of long chain fatty acids [59].

A cascade with coupled, irreversible reactions and no outflux of intermediate products can be described by the following scheme (similar to (2.13) in Section 2.3.3:

$$\xrightarrow{k_i} A \xrightarrow{k_A} B \xrightarrow{k_B} C \xrightarrow{k_C} \tag{3.3}$$

where k_i is the constant influx rate and k_A, k_B and k_C are kinetic parameters for enzymatic reactions. Let us assume that we can measure the concentrations of metabolites A and C, but not of intermediate compound B. For steady state conditions and by using mass action kinetics we can describe the cascade by the system of linear equations

$$\begin{array}{rcrcrcl} \dot{A} & = & k_i & - & k_A \cdot A & = & 0 \\ \dot{B} & = & k_A \cdot A & - & k_B \cdot B & = & 0 \\ \dot{C} & = & k_B \cdot B & - & k_C \cdot C & = & 0 \end{array} \tag{3.4}$$

If we solve the system for the rate constants, we get

$$\begin{array}{rcl} k_A & = & \frac{k_i}{A} \\ k_B & = & \frac{k_i}{B} \\ k_C & = & \frac{k_i}{C} \end{array} \tag{3.5}$$

We can directly see from Equation (3.5) that if we know A, C and influx rate k_i, we can determine rate constants k_A and k_C without knowing the concentration of B. For steady state conditions, influx and outflux rates of the cascade define the rates of all intermediate reactions. If we assume that there is no outflux of intermediates in the beta-oxidation pathway, then we obtain effective parameters for all reactions with measurable substrate concentrations.

To sum up, experimental observations reporting the failure to detect intermediate compounds of beta-oxidation and the existence of a trifunctional protein complex suggest that intermediate channeling for reaction products (e.g. enoyl-, hydroxyacyl- or ketoacyl-forms of fatty acids) exists. It also indicates that intermediate metabolites do not exit the mitochondrium, which is another assumption of our model (see above). This means produced compounds are rapidly metabolized in subsequent reactions. In addition, metabolite profiles for intermediate compounds have not been quantified in the HuMet study. Since these missing observations do not allow for the estimation of rate constants for intermediate reactions, we assume that all four reactions that constitute one beta-oxidation round (dehydrogenation, hydration, oxidation, thiolysis) can be combined into an overall reaction with one effective parameter [7]. The net effect of such an reaction still is the same as for the four sequentially coupled reaction, namely removal of two carbon atoms from the fatty acid chain. Instead of dealing with four reactions for each round we now only have to estimate an effective parameter for one reaction, resulting in less underdetermined systems of linear equations.

Constant influx vector

Another assumption for reducing complexity is to introduce constant influx vectors for all main metabolites. This reduces the number of unknown parameters that have to be estimated. The general model contains individual influx reactions. Each metabolite in the pathway can be subject to two reactions: transport across the mitochondrial membrane and enzymatic removal of two carbon atoms. Each of these reactions is represented by mass action rate laws with one unknown rate parameter. If we set up the system of linear equations for this coupled reaction scheme, we will have n main metabolites, whose concentrations are quantified, and therefore n linear independent equations with $2n$ unknown kinetic parameters. Since the number of unknown parameters is twice the number of known variables, it is difficult to calculate or estimate a good solution. For this reason we either set only one, constant influx vector at the beginning of the cascade chain, or we define a fixed ratio of influx rates for specific main metabolites. The fixed ratio is derived from the fatty acid composition in human adipose tissue. This composition was determined in several studies [3, 9, 34, 37, 48, 65] and shows that only distinct species of long-chain fatty acids are stored, mainly palmitoylic (C16) and linoleic (C18:1) acid. During fasting, fatty acids have to be mobilized and transported from fat reservoir cells to for example muscle cells in order to provide energy. If we assume that transport processes are the same for all fatty acids, then their respective influx into the beta-oxidation cascade has to be proportional to the composition of adipose tissue (see Figure 3.4).
This assumption reduces the number of unknown parameters so that we will have n variables and $n+1$ parameters. Finding solutions for such a system of linear equations was described in Section 2.3.3. There it was shown that we cannot find an exact solution, but by fixing one parameter, we can calculate all remaining parameters. Choosing this method of parametrization allows us to compare solutions for the beta-oxidation pathway between individuals, without knowing exact kinetic rate values. Table 3.2 shows the composition of adipose tissue we have taken from the literature and incorporated into our model.

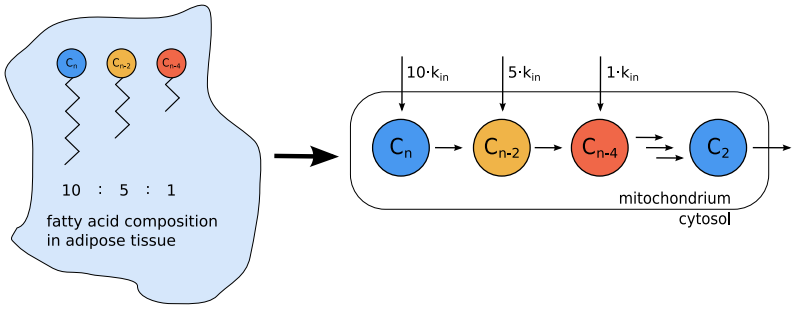

Figure 3.4: Fixed ratio of influx rate k_{in} for specific metabolites is assumed in our model. The ratio depends on the fatty acid composition in human adipose tissue. By assuming that transport reactions are similar for all fatty acids, then their respective influx into the beta-oxidation cascade has to be proportional to the composition of adipose tissue.

Saturated fatty acids	Tissue composition [%]
C18	12.31
C16	76.92
C14	9.23
C12	1.54

Table 3.2: Composition of human adipose tissue for saturated and unsaturated fatty acids. Numbers have been taken from the literature [37, 48] and depict the experimentally measured ratio of long fatty acids. The ratio is used for defining a fixed ratio of influx rates in the simplified model of the beta-oxidation pathway.

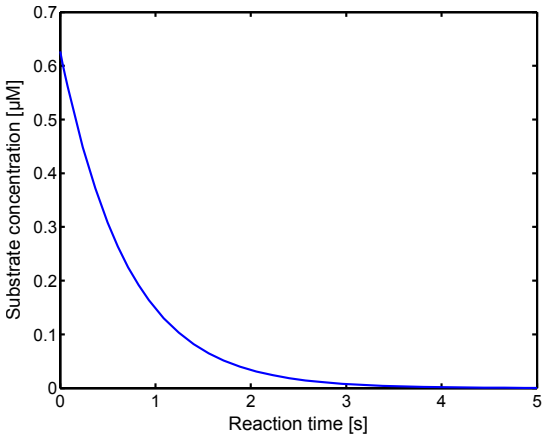

Figure 3.5: Metabolization of fatty acids by medium-chain acyl CoA dehydrogenase (MCAD) modeled with Michaelis-Menten kinetics. Initial substrate concentration of decanoyl-carnitine (C10) is 0.627 μM, the highest measured concentration of all acylcarnitines with fatty acid chain length three or higher. Kinetic parameters are $K_M = 9.1\ \mu M$ and $v_{max} = 13.6\ s^{-1}$, taken from [27]. Both parameters are specific for substrate decanoyl-carnitine (C10). After a few seconds all substrate molecules are consumed. This shows that the system attains new steady state conditions very rapidly.

Steady state dynamics

Steady state conditions are usually assumed for the modeling of metabolic pathways [11, 12, 15]. A stationary state in an organism's metabolism does not mean that dynamical processes are absent, but only that concentrations of metabolites do not change over time. This implies for a system like our cascade model that if the influx of substrates for one reaction increases, the flux of the substrates through the cascade increases as well. Otherwise there would be an accumulation of compounds, which violates steady state assumptions. Biochemical reactions in general are on a timescale of milliseconds to minutes [6] and a biological system rapidly attains a new steady state after perturbations.
Figure 3.5 illustrates the fast reaction kinetics for the conversion of fatty acid decanoyl-carnitine (C10) to its enoyl-form by medium-chain acyl CoA dehydrogenase (MCAD). The initial concentration is the highest measured concentration for all acylcarnitines with fatty acid chain length three or higher. After a few seconds all substrate molecules are consumed and product formation stops. While enzymatic metabolic reactions are on a timescale of milliseconds to minutes, blood samples in the HuMet study for measuring metabolite concentrations have been taken in general every two to four hours. Therefore, if we study the system on hour timescales, we can assume that the system of biochemical reactions is always in a stationary state. Such an assumption is often referred to as *adiabatic elimination* and can help so simplify mathematical problems [42].

3.2.2 Link between model and experimental data

Acyl-CoA molecules that are directed to beta-oxidation have to be converted to acylcarnitines for the transport across membranes between cytosol and mitochondrium. Inside the mitochondrium, acylcarnitines are in turn converted to acyl-CoA molecules, an activated form of fatty

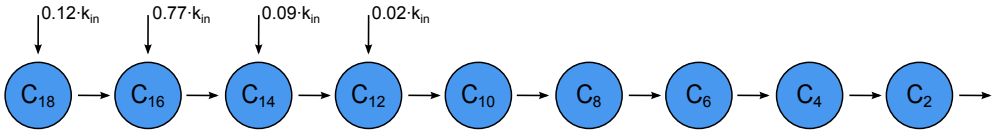

Figure 3.6: Scheme of the model for the beta-oxidation cascade which was used for the estimation of rate constants. Substrate influx is set to a constant ratio that is proportional to the composition of fatty acids in human adipose tissue, which is shown in table 3.2. Influx reactions are present for metabolites C18, C16, C14 and C12. The sum over all influx rates is 1.

acids, which is needed for further degradation steps (see Section 1.2). Since it is very difficult to measure intracellular and intramitochondrial *in-vivo* acyl-CoA concentrations for several individuals under changing conditions, the HuMet dataset contains measured acylcarnitine concentrations from blood samples. In our model, which describes intracellular reactions, we hence assume that the acylcarnitine pool of fatty acids measured in blood reflects the acyl-CoA pool in mitochondria and that concentration levels are approximately similar. This assumption is based on several observations which are discussed in the following.

First, it was shown in two genome-wide association studies (GWAS) that single-nucleotide polymorphism (SNPs) in genes for acyl CoA dehydrogenases SCAD, MCAD and LCAD associate with altered levels of acylcarnitines [28, 33]. Both studies used the same metabolite quantification methods as the HuMet study. SNPs in genomic regions of enzymes can have an indirect or direct impact on the biochemical characteristics of proteins such as expression or enzymatic activity. The set of identified acylcarnitines corresponds to respective substrate metabolites for SCAD, MCAD and LCAD, which catalyze the rate limiting step in beta-oxidation for short-, middle- and long-chain fatty acids. For instance, SNPs in SCAD associate with the acylcarnitine form of butyric fatty acid (C4), which strongly indicates that this transport metabolite is linked to beta-oxidation reactions.

Another evidence that the acylcarnitine pool maps fatty acids in catabolic reactions was reported by Jan Krumsiek by the investigation of partial correlation coefficients between metabolites (unpublished results). Partial correlations measure the degree of association between two variables, with the effect of all other variables removed [71]. Many acylcarnitine pairs, which are directly connected by beta-oxidation steps, show high partial correlation coefficients for their respective metabolite profile. For instance, metabolite profiles of octanoyl- (C8) and decanoylcarnitine (C10) are highly associated in terms of partial correlation. The observation of strong partial correlation between biochemical closely connected metabolites thus is another indicator for the link between acylcarnitine compounds and fatty acid substrates of beta-oxidation in mitochondria.

It has to be mentioned that especially small fatty acids can pass cellular membranes without the need of any transportation steps. Moreover, enzymes for beta-oxidation are not only located in mitochondria, but also in peroxisomes for oxidation of primarily long-chain fatty acids. Degradation cascades in both cellular compartments generally involve the same steps as in mitochondria. These considerations have to be kept in mind when simulating mitochondrial beta-oxidation reactions with concentrations of proxy molecules such as acylcarnitines.

3.3 Conclusion

All above mentioned simplifications were applied in order to reduce the model complexity and thus facilitate the investigation of the solution space for the system of linear equations. The proposed model tries to strike a balance between complexity and simplification. Compared to existing models, no *in-vitro* measured kinetic parameters were applied for *in-vivo* modeling of biochemical reactions. All simplification were only introduced if the biological context was not changed and justified by physiological and biochemical knowledge. Features of the model are irreversibility of cascade reactions and simplification by leaving out unlikely intermediate outflux processes. Sequentially coupled reactions in the pathway are combined and treated with mass action rate laws under steady state dynamics. Substrate influx is set to a constant ratio that is proportional to the composition of specific fatty acids in human adipose tissue. In Table 3.3 all assumptions and their effect on the reduction of the model complexity are summarized. Figure 3.6 shows a schematic illustration of the beta-oxidation pathway which is described by our model. For each metabolite C_n the rate constant k_{C_n} for the conversion from C_n to C_{n-2} can be estimated for a fixed rate k_{C_2} by

$$k_{C_n} = \frac{C_2}{C_n} \cdot k_{C_2}. \tag{3.6}$$

Using this mathematical model with incorporation of condition-specific metabolite concentrations allows to estimate observed kinetic rate constants rather than pure fluxes of metabolites. These kinetic values can be compared between individuals with respect to their dynamical variations.

assumptions incorporated into the model	number of parameters
no assumptions	32 n
+ irreversible/no outflux	16 n
+ combination of reactions	4 n
+ mass action kinetics	2 n
+ constant influx	n + 1

Table 3.3: Summary of all introduced assumptions. The number of parameters is shown which is needed to describe a pathway with n main metabolites and $3n$ intermediate compounds. Assumptions reduce the amount of parameters and allow for an estimation of rate constants. By fixing one parameter, we can calculate all remaining parameters. Choosing this method of parametrization allows us to compare solutions for the beta-oxidation pathway between individuals, without knowing exact kinetic rate values.

Chapter 4

Modeling mitochondrial beta-oxidation on the HuMet dataset

In the previous chapter we proposed a model which describes the beta-oxidation cascade for fatty acids. We incorporated assumptions that help to reduce model complexity and to compare metabolic states between individuals. The model for the beta-oxidation pathway allows to determine relative kinetic parameters and compare them between individuals. The estimation of these parameters is based on steady state metabolite concentrations, as shown in Section 2.3.3. In this chapter, we will now use our proposed model to describe metabolite profiles of probands from the HuMet study (see Section 2.2). For each of the 15 subjects, blood metabolite levels were measured under different physiological conditions. In the following we will focus on metabolite profiles quantified during a fasting period of 36 hours and subsequent uptake of lipid and energy-rich diet. We will first describe the change of concentrations of fatty acids[1] over time and how this change varies between probands. Then we will compare relative rate constants between individuals, which were estimated using our model. In addition we will describe a non-negative factorization approach that we used to estimate substrate specificity and regulation effects for enzymes of the beta-oxidation pathway.

4.1 Analysis of metabolite concentration profiles

We first analyzed metabolite profiles of concentration levels in order to obtain a basic overview about variation between subjects. The HuMet study was performed under highly controlled and well-defined conditions, as it was mentioned in Section 2.2. All participants were male and young with no known metabolic diseases. Nevertheless, metabolite concentrations measured in blood samples differ between individuals. Figure 4.1 illustrates the intra- and interindividual changes for acetylcarnitine (C2), the transport form of acetyl-CoA, which is a product of each

[1]Since we assume that blood acylcarnitine concentrations are linked to intracellular and intramitochondrial fatty acid and acyl-CoA concentrations (see Section 3.2.2), all terms will be used interchangeably to describe fatty acid molecules that are involved in mitochondrial beta-oxidation.

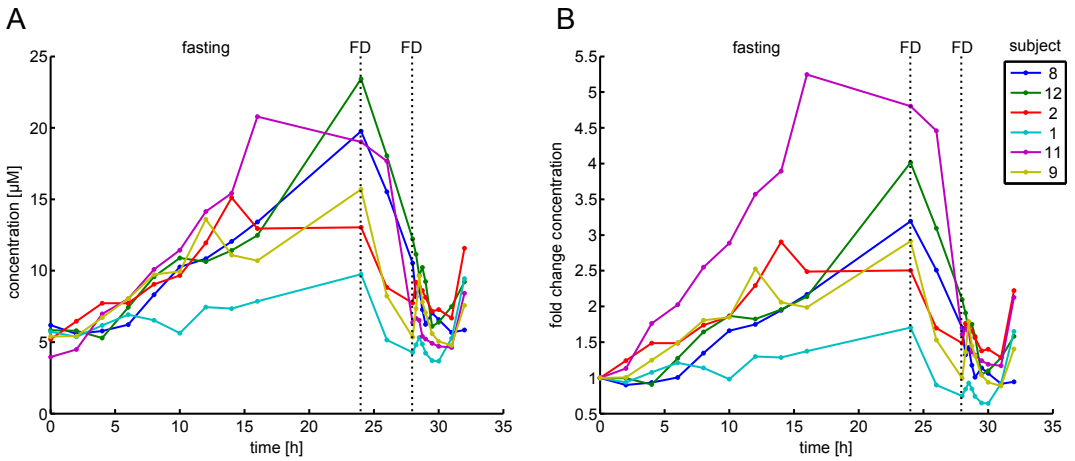

Figure 4.1: Concentration profile of acetylcarnitine (C2) for subjects with low (8, 12), medium (2, 1) and high BMI (11, 9) during the fasting period and subsequent uptake of energy and lipid rich diet (Fresubin drink, FD). (A) For all subjects, C2 concentrations increase during fasting and rapidly decline with nutrition uptake at time point 24 h. Uptake of the second Fresubin drink shorty increases C2 concentrations after 28 h. (B) Fold change of C2 concentration with respect to initial concentrations. Concentration profiles for subject 1 and 11 are distinct from the other probands.

beta-oxidation cycle. Concentration profiles for two probands with low, medium and high body mass index (BMI), respectively, are shown. At the beginning of the HuMet study all individuals show similar levels of C2. During the fasting period acetylcarnitine concentrations rise only slightly for some probands, while a strong increase can be observed for others. After the uptake of Fresubin diet as breakfast, concentrations then return to the initial level. This example shows the individual responses to physiological conditions, which depends on the proband's metabolism. During the fasting period, metabolite profiles evolve differently. Basal levels of metabolites show a narrow range (for instance 4-6 μM for C2). After the end of the fasting period, concentrations of C2 quickly drop and return to the initial levels. This might indicate a physiological regulation for the concentration of metabolites.

Figure 4.2 shows several acylcarnitine concentration profiles for two probands during the fasting period and after the uptake of Fresubin. The example illustrates, similarly to Figure 4.1, the variation of metabolite concentrations between subjects. For proband 6, the increase of long-chain fatty acids is stronger compared to proband 1, and reaches higher maximal concentration values, especially for palmitic acid (C16). This could be the result of less metabolization of C16 or a stronger mobilization of C16 molecules from fat reservoirs to for example muscle or liver cells. For both probands there is only a slight growth of stearic acid (C18) within the first 24 hours.
Figure 4.2 (C) and (D) shows the concentrations of short butyric fatty acid (C4) and free carnitine (C0). During the first part of the fasting period C4 concentration decreases for both probands. A physiological explanation for this is the preceding period of fasting over night, when no samples have been taken. After this period, short fatty acids have already been oxidized for energy production while there is a deferred supply with long fatty acid chains to the beta-oxidation cascade. Free carnitine concentrations decrease, since these molecules are required for the ransport of long fatty acids into the mitochondrium. The figures also show that

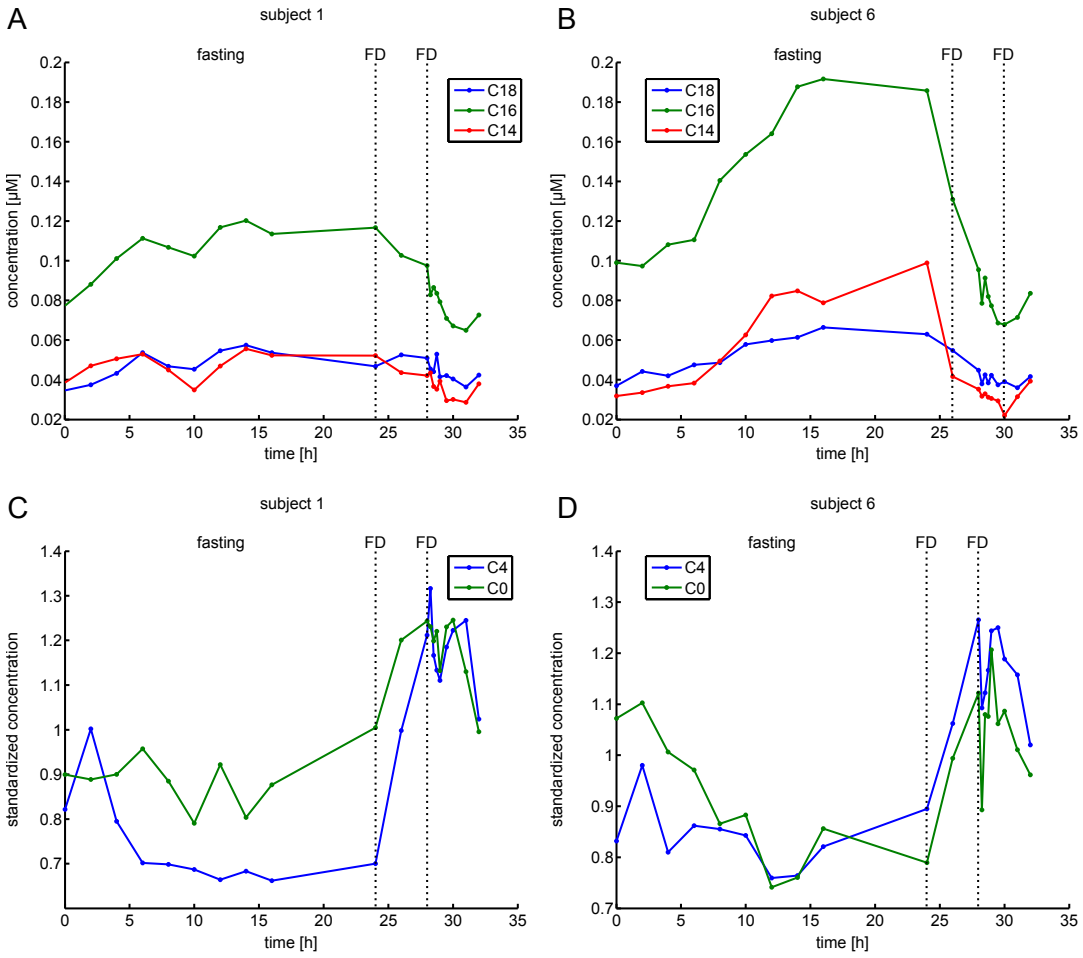

Figure 4.2: (A) and (B): Concentration of stearoyl- (C18), palmitoyl- (C16) and myristoyl-carnitine (C14) for proband 1 and proband 6. The increase of C16 and C18 concentrations is stronger for proband 6 compared to proband 1. (C) and (D): Concentration of butyric fatty acid (C4) and free carnitine (C0) for proband 1 and proband 6. C4 and C0 decrease for both subjects during the fasting period. After ingestion of lipid rich diet (Fresubin drink, FD) less fatty acids have to be mobilized for beta-oxidation reactions. As a result, free carnitine concentration increases.

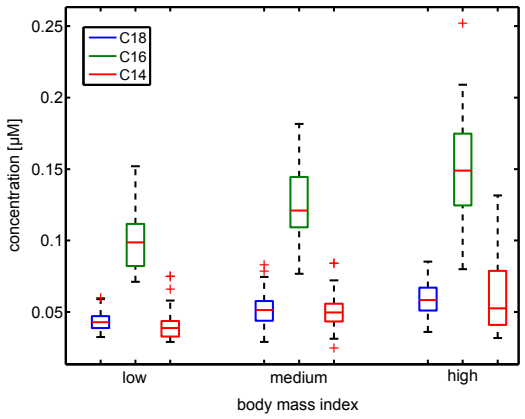

Figure 4.3: Box plot of metabolite concentrations during the fasting period for probands with low (20.4 - 21.0), medium (22.6 - 23.5) and high (24.9 - 25.5) BMI. Concentration profiles of C18 and C16 between probands with low and high BMI differ significantly.

the overall trend is the same for both probands. During fasting period long fatty acids increase due to a mobilization of lipid molecules from adipose tissue. After the uptake of energy and lipid rich diet, this mobilization stops. The body first metabolizes carbohydrates compounds, which are also ingredients of the Fresubin drink. This leads to low concentrations of long-chain fatty acids and high concentrations of transport molecules C0. After having consumed nutritional carbohydrates sources, beta-oxidation of exogenous and endogenous lipids starts again, which can be seen by the rise of long fatty acids after 30 hours in Figure 4.2. For developing our model we only considered beta-oxidation during fasting conditions and did not include reactions after the ingestion of lipid rich diet. For further studies we could also consider beta-oxidation of exogenous lipids for the estimation of reaction rates.

Figure 4.3 illustrates the variation of metabolite concentration between groups of subjects with low, medium and high BMI. For all probands, palmitic acid (C16) concentration is very high compared to stearic (C18) and myristic acid (C14). A physiological explanation might be that C16 is one of the main components of adipose tissue [37, 48]. Mobilization of stored lipids during fasting then results in a high concentration of palmitic acid. This observation indicates that the influx rates for C16 are higher than for C14 and C18. As described in Section 3.2.1, we have incorporated this feature into our model by using a fixed ratio of influx rates for long fatty acids, which is proportional to the composition of fat tissue. The box plot also shows the interindividual variations of metabolite concentrations. Probands with high BMI, for instance, have high concentrations of C14, C16 and C18 compared to probands with low BMI. For other metabolites of the beta-oxidation pathway no relationship between BMI and concentration was obtained. Gabi Kastenmueller from the metabolomics group of Karsten Suhre also reported that principal component analysis (PCA) of fatty acid concentrations during the fasting period revealed a relationship between metabolite profiles and BMI (unpublished results).

Figure 4.4 illustrates concentration profiles for groups of probands with low and high BMI. During the fasting period, mean metabolite concentrations of the low-BMI group are distinct from the high-BMI group. After the uptake of Fresubin, metabolite levels become more similar. These results suggest that there is a relationship between the BMI value and metabolite concentrations. However, this relationship does not hold for other metabolites. A significant difference between

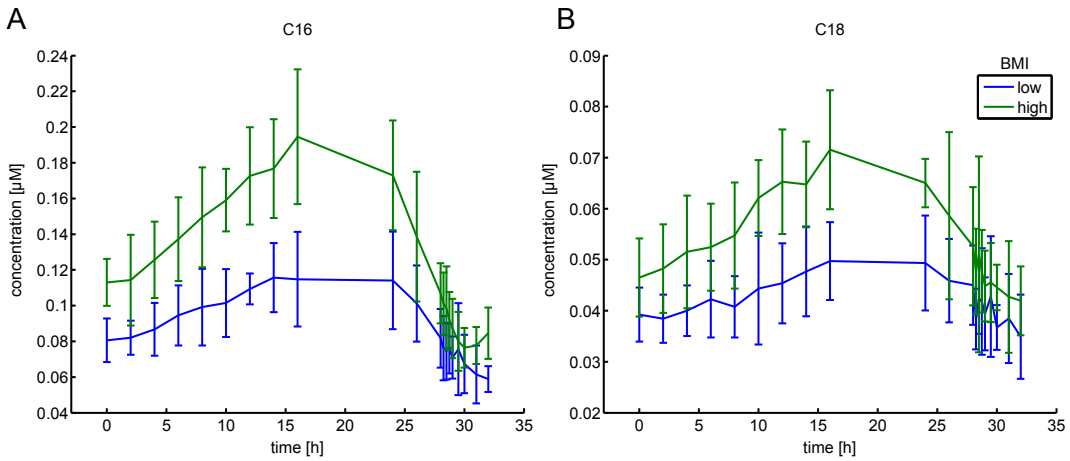

Figure 4.4: Concentration profile of palmitic (A) and stearic acid (B). The time course of mean concentration is plotted for probands with low (proband 8, 10, 12, 15) and high BMI (proband 6, 9, 11, 14, 16). Errorbars represent standard deviations of metabolite concentrations. During the fasting period (time 0 to 24 h) especially C16 concentration differs significantly between probands with low and high BMI. After the uptake of lipid-rich Fresubin drinks is at time points 24h and 28h metabolite levels become more similar.

groups of low and medium, as well as medium and high BMI was also not obtained. The interindividual variations could result from different metabolic activities and enzyme regulations, as well as from differing fatty acid composition in adipose tissue. We can exclude effects of varying diet, since all probands received the same meal before fasting. In the following part we will now apply our proposed model on the fatty acid concentration data measured during the fasting period in order to further investigate variations in metabolic profiles.

4.2 Relative rate calculation

In Chapter 3 we have developed a model of the beta-oxidation pathway, which incorporates metabolite concentrations and allows for the estimation of relative rates for reaction steps of the degradation cascade. Estimated rate constants are comparable since the outflux rate constant was held fixed (see Section 2.3.3). Figure 3.6 shows the scheme of the pathway model that we used for the estimation of rate constants. In the following part we will examine rate constant profiles estimated during the fasting period. We will investigate the relationship between rate constants and physiological parameters. Individual rate profiles for subject 1, 8 and 9 will be shown to illustrate the interindividual variations. The probands were chosen as an example for individual rate profiles of probands with low (subject 8) and high BMI (subject 9). Proband 1 with medium BMI was chosen in addition due to the low rate constants compared to other subjects.

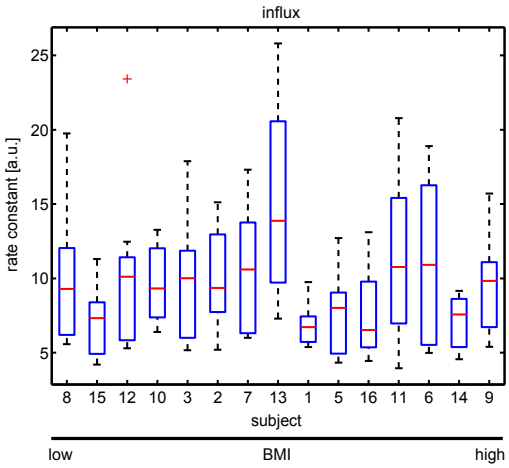

Figure 4.5: Box plot of estimated rates for influx reactions during the fasting period. For all probands, reaction rates are shown in arbitrary units (a.u.). The outflux parameter for the last step in our model was set to 1. Subjects are sorted with respect to increasing BMI. Variation of rate constants is high for subject 13 and low for subject 1.

4.2.1 Comparison of interindividual rates for specific reaction steps

Figures 4.6 and 4.5 illustrate individual rate constants for all steps in the beta-oxidation cascade.

The results clearly show that rate constant profiles vary between probands[2]. Rate constants for subject 13 are in a wide range for most reactions, compared to the profile of subject 1, which is in a narrow range. The metabolization from C14 to C12 has high rate constants compared to other reactions. This can result from high concentrations of C16, which is converted to C14 and therefore a substrate for the subsequent reaction. Compared to the other probands, reaction rates are generally small for subjects 1, 14, 15 and 16. This could be an indicator for comparatively low overall metabolic activity. Another reason could be that for this group less fatty acid oxidation is needed to provide energy, since other sources like carbohydrates have not been entirely consumed. Subject 13 in contrast shows a broad range of rate constants for all reactions. Potentially metabolic activity is less regulated resulting in a higher variability of rate constants. It is to be noted that metabolite concentration profiles for subject 13 were also distinct from the other probands, which could result from potential measurement errors.
Influx rates and conversion of small-chain fatty acids show more variation than reactions with long-chain substrates. The units for influx rates are not the same as for conversion reactions. Therefore we cannot compare absolute values. A higher variation of rate constants for the conversion from C4 to C2 can be observed for all subjects. At this point, molecules from other metabolic pathways (e.g. degradation of amino acid carbon backbones and fatty acids with uneven chain length) can enter the beta-oxidation cascade as C4 chains. The quantified concentrations of C4 and C2 hence are not exclusive products of preceding beta-oxidation steps. Our model does not incorporate the interplay with other metabolic pathways, since their specific intermediate

[2]Subject numbering was done in accordance with the dataset of the HuMet study and skips number 4. For future comparison with other results from this study we will stick to this scheme.

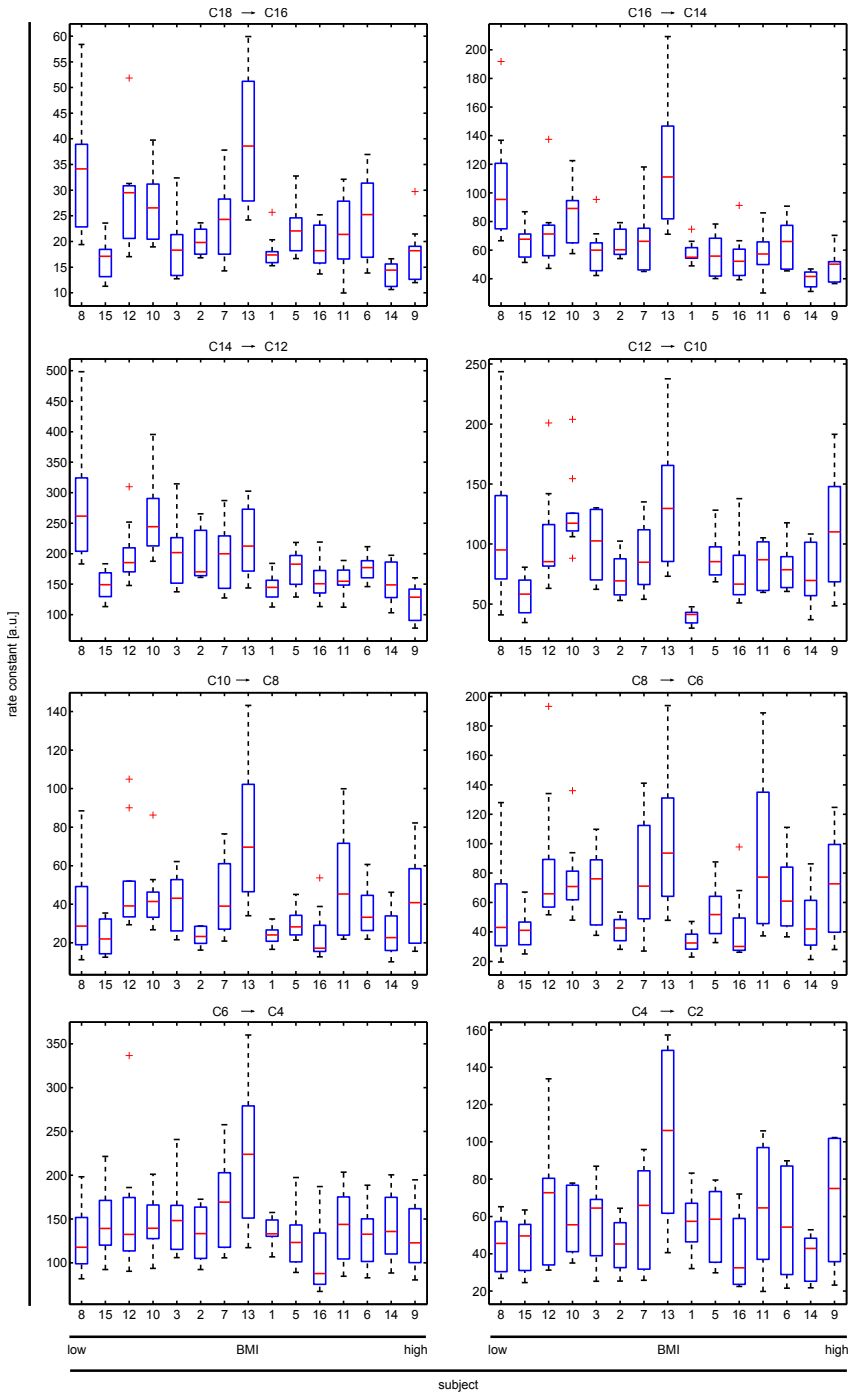

Figure 4.6: Box plots of relative rates for conversion reactions during the fasting period estimated by our model. For all probands, reaction rates for all steps in the beta-oxidation pathway are shown in arbitrary units (a.u.). The outflux parameter for the last step in our model was set to 1. Subjects are sorted with respect to increasing BMI. Rate constant profiles for conversion from C16 to C14 and C14 to C12 indicate a relationship between individual BMI and reaction rates.

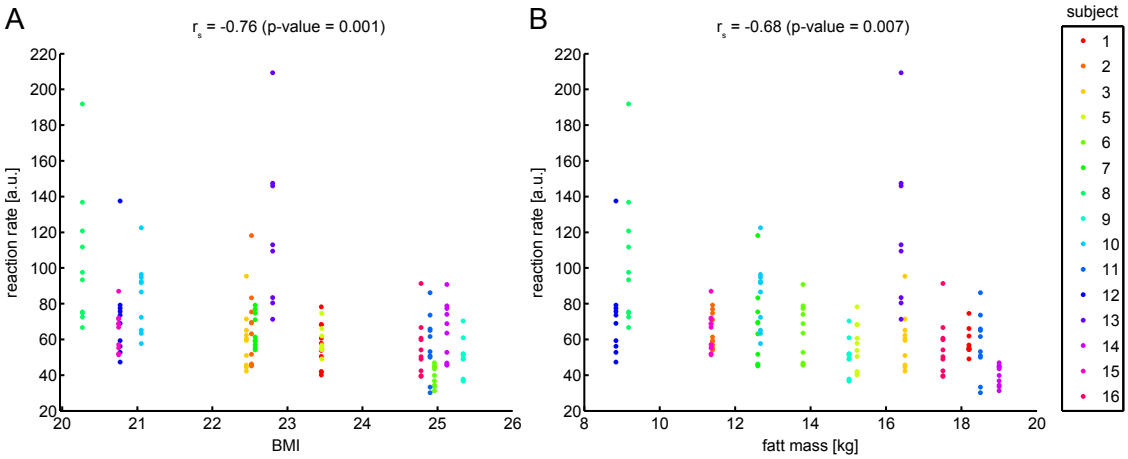

Figure 4.7: Rate constants for the conversion reaction from C16 to C14 are plotted against the subject's BMI (A) and fat mass (B). Spearman coefficient r_s shows significant negative correlation between the median of estimated rates and physiological parameters fat mass and BMI.

molecules have not been quantified in the HuMet study. Therefore it is difficult, for instance, to distinguish the impact of fatty acid metabolism on rate constants from effects of amino acid metabolism.
Degradation rates of long- and medium-chain fatty acids are in a narrow range for most subjects, which can result from a higher degree of metabolic regulation for these steps. Different metabolic activities as a response to fasting conditions can also be seen from the individual rate profiles. The rates for the conversion from palmitic acid (C16) to myristic acid (C14), for instance, are high for proband 8 (lowest BMI) compared to proband 9 (highest BMI). Decreasing rate constants with increasing BMI for reactions with substrates C18, C16 and C14 indicate a relationship between body mass index and reaction profiles. Rate constants for probands with low BMI are higher compared to probands with high BMI. Comparing the rates for these reactions with the concentration profile in Figure 4.3 reveals that, compared to probands with high BMI, probands in the group of low BMI have low concentrations of substrates C18, C16 and C14. The reaction rates in turn show a negative correlation. The higher the BMI, the lower rate constants are. A physiological explanation can be that for keeping metabolite concentrations low, fatty acid molecules, which are provided either by beta-oxidation of C18 or by transport from fat reservoir, have to be metabolized. This mobilization leads to increased reaction rates.

4.2.2 Comparison of rate profiles with physiological parameters

We further investigated the relationship between physiological parameters and rate constant profiles. For each reaction step in the pathway, we compared the median reaction rate constants of each proband with individual phenotypes, such as BMI, fat mass, fat fraction of the whole body and fat fraction of the trunk (see phenotype table in appendix B). Only for the conversion reactions from C16 to C14 and C14 to C12 significant Spearman rank correlation coefficients were obtained. Figures 4.7 and 4.8 illustrate the correlation between rate constants during the fasting period and individual BMI and fat mass.

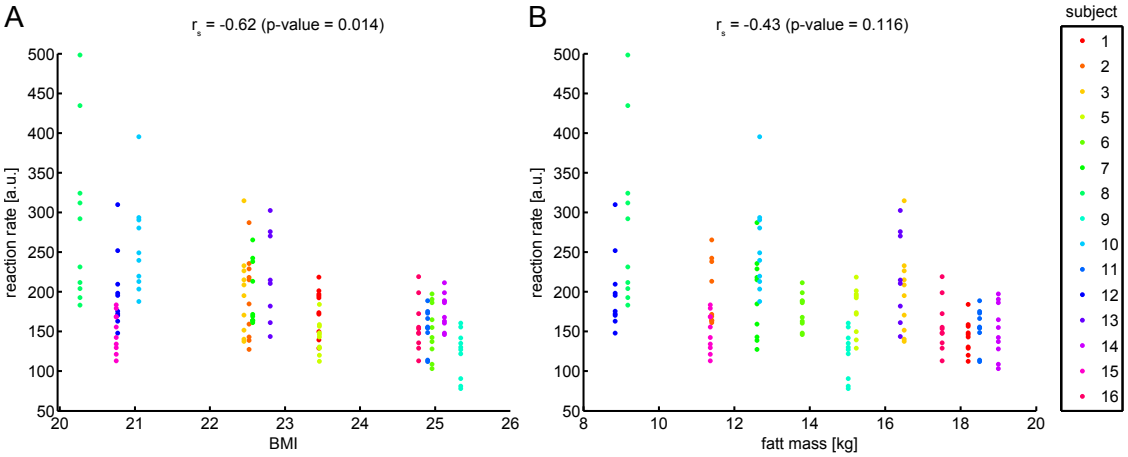

Figure 4.8: Rate constants for the conversion reaction from C14 to C12 are plotted against the subject's BMI (A) and fat mass (B). Spearman coefficient r_s shows significant negative correlation between individual BMI and the median of estimated rates. No significant relationship can be seen for the physiologcal parameter fat mass.

For the reaction C16 to C14, BMI, fat mass and fat fraction of the whole body show significant correlation with reaction rates (correlation coefficients 0.76, 0.68 and 0.60, respectively, with p-values less than 0.01). For the reaction from C14 to C12, only BMI was correlated with median reaction constants. We also investigated the correlation between metabolite concentrations and phenotype. The concentration of compounds C16 and C14, which are substrates for the above mentioned reactions, were significantly correlated with individual BMI values (coefficients 0.79 and 0.62 with p-values less than 0.05). However, no significant relationship between metabolite concentrations and other physiological parameters was found. A possible explanation can be that the fat composition and mobilization of stored fatty acids is different for subjects with respect to the body mass index. These differences then might lead to distinct rate profiles. Our observations suggest that rate constants estimated from the proposed model of beta-oxidation can describe the relationship between phenotype and metabolism in more detail compared to pure concentration profiles. In addition, we also found significant correlation between rate profiles and other phenotypic parameters such as erythrocytes, muscle mass, hematocrit and hemoglobin levels. For further studies these observations possibly can be used to gain more insight into the interplay between fatty acid degradation and other metabolic pathways.

In conclusion, the comparison of step specific rates between individuals has revealed variations of rate constants especially for the conversion steps of long-chain fatty acids. Different profiles were derived for probands with respect to BMI levels. To obtain more information about the metabolic pathway, we will look at the time-course of rate constants for specific probands in the following part.

4.2.3 Comparison of individual rate constant time-courses

Influx rate constants

In Figure 4.9, rate constant time-courses for all probands were compared using clustering methods. Furthermore, three time-courses of subjects are shown in Figure 4.10. The probands were chosen to illustrate individual rate profiles for probands with very low (subject 8) and high BMI (subject 9). Proband 1 is illustrated due to the generally low rate constants (see Figure 4.6). In our model, influx rates represent mobilization reactions for fatty acids and describe a constant supply with molecules from fat storage. The composition of beta-oxidation substrates, which enter the mitochondrium, was set according to the ratio of long-chain fatty acids found in adipose tissue. Therefore only C12, C14, C16 and C18 fatty acids flow into the system (cf. Section 3.2.1).
The influx rates for all individuals, with the strongest increase for proband 1 and only slight increase for proband 14. The example for probands with low, medium and high BMI shows that all probands have similar rates at the start of the fasting period but later evolve differently. At the beginning, when energy derived from carbohydrates is still available, mobilization of fatty acids is slow. Later on subjects have to adapt to the new situation and activate alternative metabolic pathways. With ongoing fasting time, influx rates also increase, since more and more energy is provided by beta-oxidation. The interindividual variations could be explained, for instance, by regulatory effects of fatty acid mobilization or by diverse compositions of fat tissues. Influx rates in Figure 4.10 cannot be linked to the individual BMI. For the influx reactions thus it is difficult to establish a link between this physiological parameter and metabolic activity.
It is also interesting to note that probands 6, 7, 10 and 15, which fall into one cluster group, show low ratios of total fat in the body (15.6 - 17.8 %) and similar blood levels of triglycerides (62 - 75 mg/dl). Triglycerides, which consist of three long fatty acids, are stored in adipose tissue and represent a major form of energy storage in the body [6]. For futher studies it will be interesting to investigate the relationship between these paramters and metabolic profiles.

Rate constants for the conversion from C12 to C10

Figures 4.11 and 4.12 compare time-courses for the conversion step of C12 to C10 fatty acid chains. From the clustergram and example time-courses we can see that rate constants vary between subjects. For one group of probands the maximum of the curve is at the end of the fasting period, while for others rates decline after 12 to 16 hours. Reduced supply with long-chain fatty acids and therefore less production of C12 fatty acids can explain the decreasing rates. The body has consumed available medium-chain CoA molecules and now first has to mobilize further resources, resulting in increasing influx rates as illustrated in Figure 4.10. Subjects 6, 7, 10 and 15 that showed similar influx rate profiles, do not fall into same clusters for the beta-oxidation step C12 to C10. Potentially fatty acid mobilization and degradation reactions are regulated differently, resulting in varying rate profiles.
The rate time-course for proband 1 is distinct from the other probands, since the conversion rate remains the same during the whole fasting period. Compared to the other probands, proband 1 shows the highest ratio of total fat in the body (23.9 %) and total fat in the trunk (22.3 %), as well as the highest level of blood triglycerides (125 mg/dl). This might indicate that under normal conditions, the person already mobilizes and catabolizes increased amounts of acyl-CoA molecules and the supply of new long-chain fatty acids does not have to increase strongly. This assumption would also explain the minor raise of influx rates shown in Figure 4.10. Another

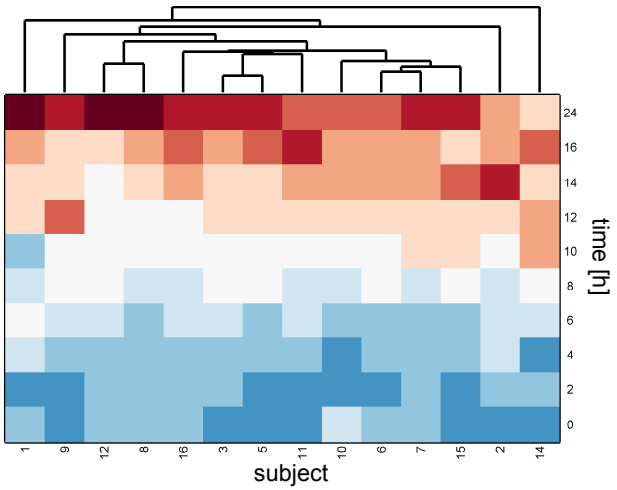

Figure 4.9: Clustergram of influx rate time-courses for HuMet probands. Clustering was done using Matlab clustergram algorithm with euclidean distance metric. We used euclidean distance since the same influx ratio was applied for all probands and outflux rate was set to 1. Proband 13 was not considered for the clustering analysis due to missing data points. For all probands, the influx rates increase during the fasting period. Probands 6, 7, 10 and 15, which fall into one cluster group, show low ratios of total fat in the body (15.6 - 17.8 %) and similar blood levels of triglycerides (62 - 75 mg/dl).

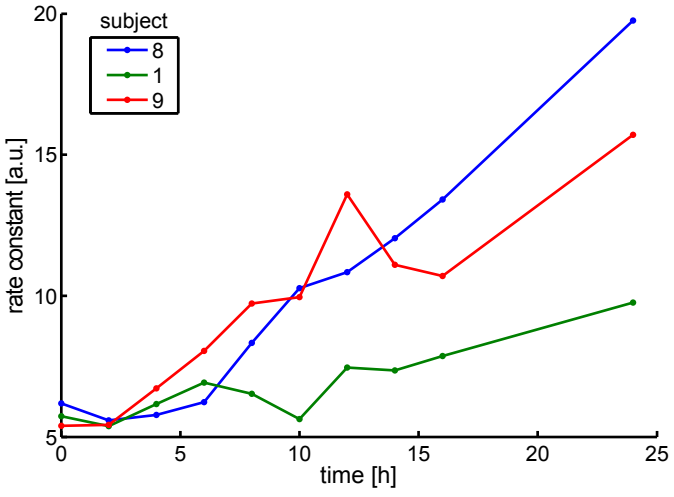

Figure 4.10: Time courses of influx rate constants for proband 8 (low), 1 (medium) and 9 (high BMI). Despite the difference in BMI values, proband 8 and 9 show similar rate constant profiles. Reaction rates for proband 1 are low compared to the other subjects.

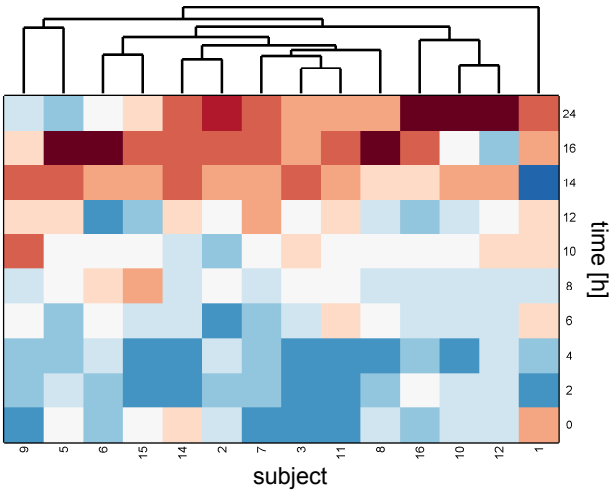

Figure 4.11: Clustergram of rate time-courses for the conversion from C12 to C10. Clustering was done using Matlab clustergram algorithm with euclidean distance metric. Proband 13 was not considered for the clustering analysis due to missing data points. For one group of subjects maximal reaction rates are attained at the end of the fasting period, while for others rates decline after 12 to 16 hours.

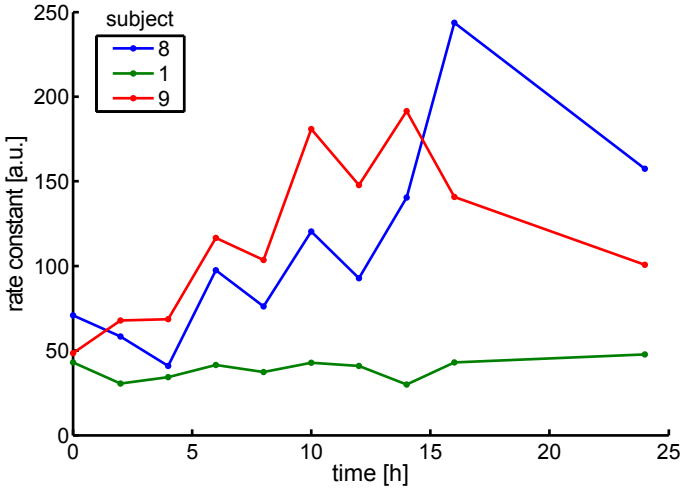

Figure 4.12: For the conversion reaction C12 to C10, rate constants are shown for proband 8 (low), 1 (medium) and 9 (high BMI). Reaction rates decrease for subjects 8 and 9 after 14 to 16 hours of fasting. Rate levels for subject 1 are very low compared to other probands and remain constant.

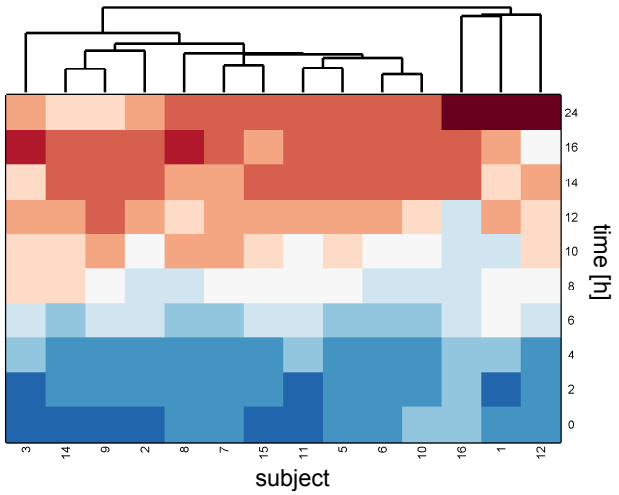

Figure 4.13: Clustergram of rate time-courses for the conversion from C4 to C2. Clustering was done using Matlab clutergram algorithm with euclidean distance metric. Proband 13 was not considered for the clustering analysis due to missing data points. Similar to the conversion from C12 to C10, one group of subjects shows maximal reaction rates at the end of the fasting period, for others rates decline after 14 to 16 hours.

interpretation would be that the proband has adapted more quickly to the fasting situation and has already attained a constant metabolic state. The increase of beta-oxidation activity took place before sampling has started, since probands received their last meal approximately 12 hours before the first blood sample was taken.

Rate constants for conversion from C4 to C2

Figures 4.13 and 4.14 illustrate the interindividual variations of rate constants for C4 fatty acid substrates. All rates increase at the beginning, representing activation of beta-oxidation reactions as a response to fasting conditions. Similar to the conversion reaction from C12 to C10, there is one group of probands (1, 12 and 16) which attains maximal rates at the end of the fasting period. For other probands rates already decline after 14 to 16 hours. Lacking supply of new, long-chain fatty acids can explain the dropping rates. New substrates for the conversion from C4 to C2 have first to be provided by influx and preceding catabolizing reactions. Intermediate molecules from other metabolic pathways, which enter the beta-oxidation cascade at this point, can also have an impact on the rate profiles. However, due to missing data of other metabolites, our model is not capable to capture these effects (see 4.2.1).
Subjects 6, 7, 10 and 15 that were in the same cluster group for influx reactions (see Figure 4.9) also show similar rate profiles for conversion from C4 to C2. This might indicate that influx reactions and steps which are at the end of the pathway are similarly regulated. If supply with long-chain substrates halts, also degradation of short-chain fatty acids is decreased.
Proband 12 and 16 fall into the same cluster for both the conversion from C12 to C10 and from C4 to C2. The time-courses show maximal rates at the end of the fasting period, which could indicate delayed mobilization of fat molecules from adipose tissue compared to other probands. Both subjects have very low levels of triglycerides in the blood (51 and 53 mg/dl), and low to

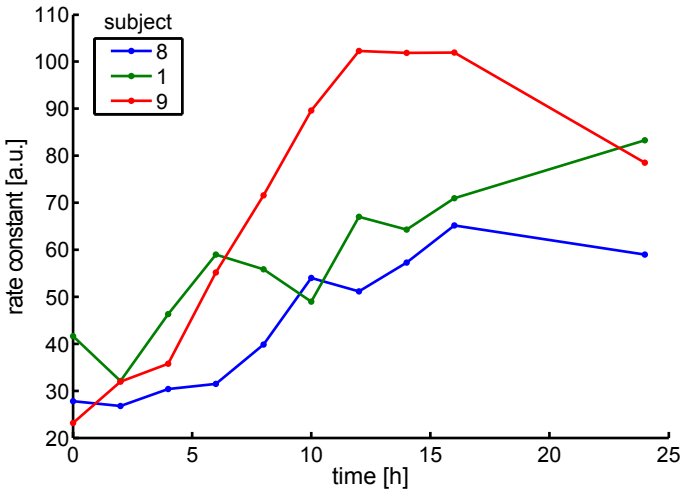

Figure 4.14: For the conversion reaction from C4 to C2, rate time-courses for proband 8 (low), 1 (medium) and 9 (high BMI) are shown. All rates increase at the beginning of the fasting period. For proband 9, rates decline after 16 hours of fasting. Compared to other reactions subject 1 now shows elevated rate constants.

medium ratios of total fat in the body (13.6 and 19.2 %). Potentially, under normal conditions the metabolism transports low levels of fatty acids and responds more slowly to the fasting conditions. For these probands, rate constants would possibly decline later.

To sum up, comparing time-courses for rate constants that were estimated using our beta-oxidation model revealed interindividual variations. Influx rates increased for all subjects during the fasting period, with differing strength of increase. For conversion reactions of long-chain and short-chain fatty acids, profiles show varying time points for maximal reaction rates. For one group, rates are high at the end of the fasting period, while for others rate constants decline after 10 to 16 hours. The drop of rates could be explained, for instance, by reduced supply of long-chain fatty acids from adipose tissue. Probands with related reaction rate profiles also showed similar levels of physiological parameters such as BMI, triglyceride blood levels or ratio of fat in the body. For further studies it will be interesting to compare more phenotypic parameters with reaction rate time-courses.

4.3 Non-negative factorization of reaction rate matrices

For the first reaction of the beta-oxidation cycle, the dehydrogenation of acyl-CoA to enoyl-CoA, four enzymes with varying chain-length specific activities are present in the mitochondrium: short-chain acyl-CoA dehydrogenase (SCAD), medium-chain acyl-CoA dehydrogenase (MCAD), long-chain acyl-CoA dehydrogenase (LCAD) and very-long-chain acyl-CoA dehydrogenase (VLCAD) [21]. Except for VLCAD, all enzymes catalyze reactions for substrates C_2 to C_{18}, acyl-CoA molecules which are incorporated into our model. The overlapping substrate specificity of enzymes SCAD, MCAD and LCAD is illustrated in Figure 4.15 (A). The first

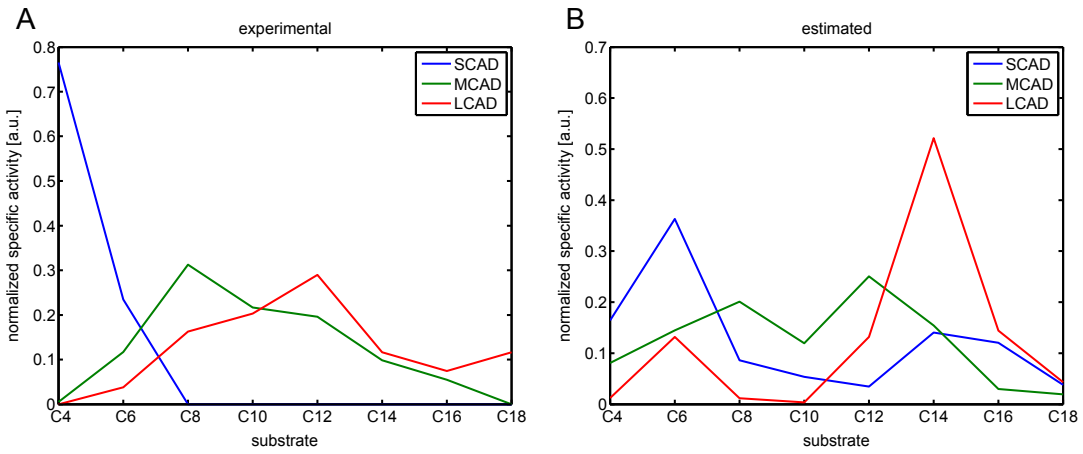

Figure 4.15: (A) Experimentally determined substrate specificity for acyl-CoA dehydrogenases SCAD, MCAD and LCAD. Catalytic activities have been taken from the literature [25, 27]. Values were normalized such that the total activity for each enzyme sums up to 1. (B) Enzyme activities estimated by non-negative factorization of a rate constant matrix based on blood concentration levels during the fasting period of the HuMet study. For the NMF algorithm, the number of components, i.e. the number of different enzymes, was set to 3.

reaction of a beta-oxidation cycle, the irreversible conversion of fatty acids to their respective enoyl-form, is the committed step of the whole beta-oxidation cycle. Our proposed model combines this step and all sequentially coupled reactions of a beta-oxidation round into one overall reaction (see Section 3.2.1). Therefore, we assume that estimated relative reaction rates for each step represent combined enzymatic activities of the three different dehydrogenase enzymes. For example, a rate constant for the conversion from palmitoylic (C16) to myristic (C14) fatty acid consists of mixed enzymatic activities of MCAD and LCAD, since C16 is a substrate for both dehydrogenases (see Figure 4.15 (A)). In the following sections, we will propose a mathematical model to describe overlapping substrate specific activities for dehydrogenases. We will also explain how we use this model to estimate enzyme activities and metabolic regulation.

4.3.1 Mathematical model for combined enzymatic activities

Fitting our model for fatty acid beta-oxidation to concentration data of the HuMet study yields rate constants for each time point t and proband p during the fasting period. For each reaction j the relationship between rate constant k_j of proband p at time point t, enzymatic specificity S and enzyme regulation α can be written as

$$k_j(p,t) = \sum_{i=1}^{n} S_{ij} \cdot \alpha_i(p,t) + error \tag{4.1}$$

where $i \in \{1, ..., n\}$ represents enzymes with varying chain length specificity and $j \in \{1, ..., 8\}$ represents conversion reactions for substrates C_{18} to C_2. For example, $k_1(2,3)$ is the rate constant for the conversion from C_{18} to C_{16}, which was estimated using concentration data for proband 2 at time point 3. This rate can be seen as a linear mix of the C_{18}-specific activity S_{i1} for all enzymes which catalyze this step. Regulation factor $\alpha_i(2,3)$ determines the weighting of specific

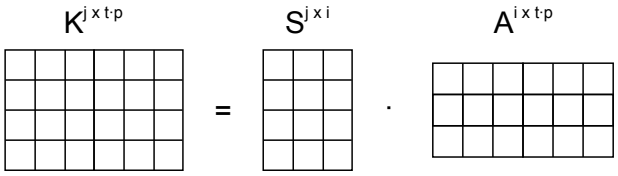

Figure 4.16: Rate constant matrix **K** is the product of a specific activity matrix **S** and a regulation matrix **A**. Using non-negative matrix factorization methods, given **K** is decomposed in **S** and **A**. This allows for the estimation of enzymatic parameters based on steady state metabolite concentrations.

enzymatic activities.
If we combine for each reaction step j all rate constants that were estimated for proband p at time point t, we get a $j \times (p \cdot t)$ matrix **K**. The linear mix of enzymatic activity of equation (4.1) can be written in matrix notation

$$\mathbf{K} \approx \mathbf{S} \cdot \mathbf{A} + \mathbf{error} \tag{4.2}$$

with specific activity matrix $\mathbf{S}^{\ j \times i}$ and regulation matrix $\mathbf{A}^{\ i \times (p \cdot t)}$ (see Figure 4.16). If only the rate constant matrix **K** is known, matrix decomposition techniques such as *non-negative matrix factorization* (NMF) [49] allow for the estimation of **S** and **A**. The NMF algorithm factorizes the matrix **K** into two non-negative matrices **S** and **A**, i.e. all entries have to be equal to or greater than zero. A matrix factorization in general is not unique, therefore non-negativity constraint and regularization of matrix **S** (i.e. the sum for each column is 1) are needed to obtain more uniqueness. Moreover, the non-negativity constraint ensures that only enzyme activities and regulation factors are derived which are greater than or equal to 0, since negative values do not make sense for the biological system. For the decomposition of rate constant matrix **K** we used an improved version of the NMF algorithm proposed by Lee *et al.* [49]. In iterative steps the cost function, which measures the Kullback-Leibler divergence between **K** and **SA**, is minimized. Each column of matrix **S** contains the normalized substrate specific activities for one enzyme, i.e. the chain length specificity. Each row of **A** contains the regulation of one enzyme for a specific proband at a specific time, that is how active the enzyme is at that point. In the following section we will now show results of our model based estimation of enzyme specificity and regulation effects.

4.3.2 Non-negative factorization applied on the HuMet dataset

Reaction rate matrix **K** was constructed using estimated rates of beta-oxidation reactions for substrates C_{18} to C_2. Rates for influx and outflux reactions were excluded, since they are catalyzed by other enzymes. According to the mathematical model that was described in equation (4.1), kinetic rate constants in matrix **K** can be seen as a linear mix between substrate-specific catalytic activities for enzymes SCAD, MCAD and LCAD and regulatory factors. Therefore non-negative factorization of matrix **K** allows for the estimation of the specificity matrix **S** and the regulation matrix **A**.

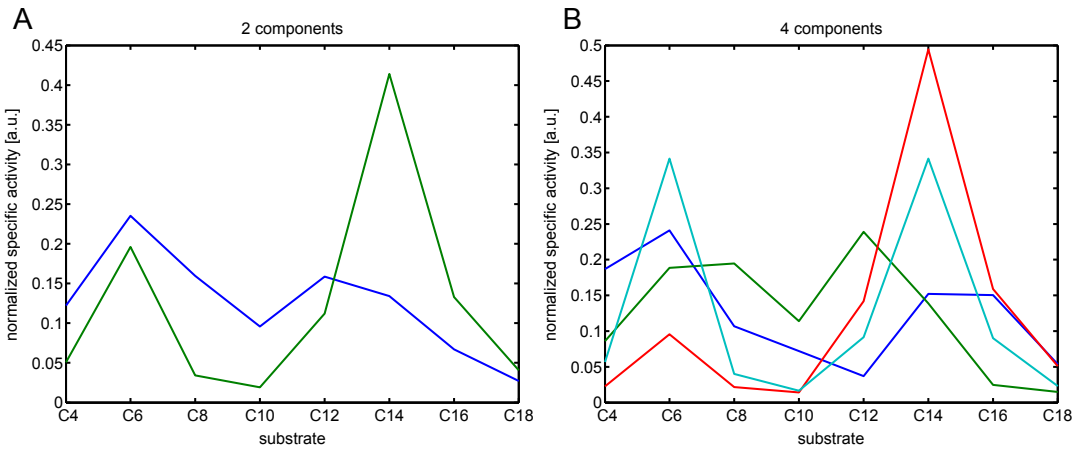

Figure 4.17: Estimation of enzymatic substrate specificities by non-negative factorization of the rate constant matrix. For the NMF algorithm, the number of components, i.e. the number of different enzymes, was set to 2 (A) and 4 (B). (A) The blue curve combines specificities for short and medium chains. (B) The red and the turquoise curve are similar except for different scaling and thus do not provide additional information.

Substrate specificity for enzymes SCAD, MCAD and LCAD (matrix S)

Figure 4.15 (B) illustrates the estimated substrate specificity of enzymes SCAD, MCAD and LCAD for fatty acid chain lengths. The factorization does not allow any assignment of enzyme names to the column numbers of matrix **S**. Therefore, a column with maximal activity for short-chain substrates corresponds to SCAD, a column with maximal activity for medium-chain substrates to MCAD and a column with maximal activity for long-chain substrates to LCAD. Short-chain acyl-dehydrogenase shows maximal activity for substrates with chain length 4 and 6, which matches experimental results shown in Figure 4.15 (A). Increased activity for long-chain substrates could be interpreted as artifacts of the factorization algorithm. MCAD enzyme shows maximal activity for C8 to C14 and LCAD for long-chain substrates C12 to C16. Moreover, all enzymes have overlapping specificities. Non-negative matrix factorization with two components does not separate specificities for short and medium fatty acid chains (see Figure 4.17 (A)). Choosing four components for the factorization method, and therefore incorporating also the impact of very long-chain acyl-CoA dehydrogenase VLCAD, does not result in a better separation of enzymatic activities. The red and the turquoise curve in Figure 4.17 (B) are similar except for differing scaling and thus do not provide additional information. A biological explanation for this is the substrate specificity of VLCAD for chain lengths of 20 and higher. However, these molecules have not been measured and are not part of our beta-oxidation model. Figure 4.18 illustrates estimated substrate specificity based on rate constants that were derived from randomly permuted concentration data. The figure does not show distinct patterns for the substrate specificity. This indicates that estimated substrate specificities of enzymes SCAD, MCAD and LCAD do not result from the NMF algorithm.

Comparing non-negative factorization and experimental results reveals that the NMF method is capable of separating enzyme specificities based on rate constants for different conversion reactions. Apart from minor artifacts, our proposed method allows for the estimation of substrate

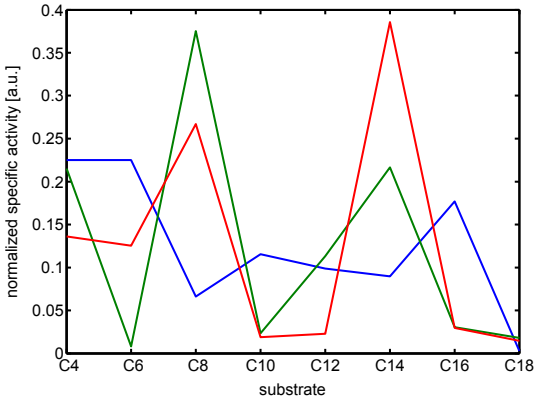

Figure 4.18: Estimation of enzymatic substrate specificities by non-negative factorization. Constants of the rate matrix were calculated using randomly permuted concentration profiles during the fasting period. For the NMF algorithm, the number of components, i.e. the number of different enzymes, was set to 3. For randomly permuted concentrations, no distinct pattern for the substrate specificity is visible.

specificities for all three enzymes SCAD, MCAD and LCAD. This estimation notably reflects the qualitative features of experimentally measured enzyme activities. Especially for short-chain acyl-CoA dehydrogenase, the estimated and experimental profile match to a great extent. It has to be noted that our model of beta-oxidation is based on steady-state blood metabolite concentrations. Nevertheless, the proposed linear mix model of substrate specificity and the factorization seems to provide results in the biological context.

Comparison of individual enzymatic regulation (matrix A)

The linear mix model of enzyme activity in equation (4.1) estimates for all probands the same substrate specificity. This assumption has biological relevance, since such typical enzyme features do not differ strongly. However, regulation of the distinct enzyme activities can vary between individuals, which can be seen as a response to changing conditions. For instance, the degradation of long-chain CoA molecules will start after the mobilization of fatty acids into the mitochondrium. This can be achieved for example by increased production and activation of LCAD enzymes. The estimated regulation matrix **A** probably reflects these regulatory effects.

Activation of LCAD Figure 4.19 illustrates the LCAD regulation for all probands of the HuMet study. For all subjects LCAD enzymes become more active with ongoing fasting conditions. Since long fatty acids are mobilized for providing energy to the body and since influx rates rise, LCAD activity increases as a response to the change in metabolism. For one group of probands (e.g. 2, 3, 7, 12, 15), the maximal activity is at the end of the fasting period. Interestingly, these probands show low to middle BMI values. Other probands (6, 9, 11) with high BMI already show increased regulation of LCAD after 10 to 12 hours. Potentially, the metabolism of probands with high BMI responds more quickly to the fasting conditions compared to individuals with low BMI. This could be the result of a faster mobilization of fatty acids from adipose tissue. Figure 4.20 shows the time-course of LCAD regulation for three subjects. Enzyme regulation of the proband with low BMI remains slow compared to the other subjects. For the proband with

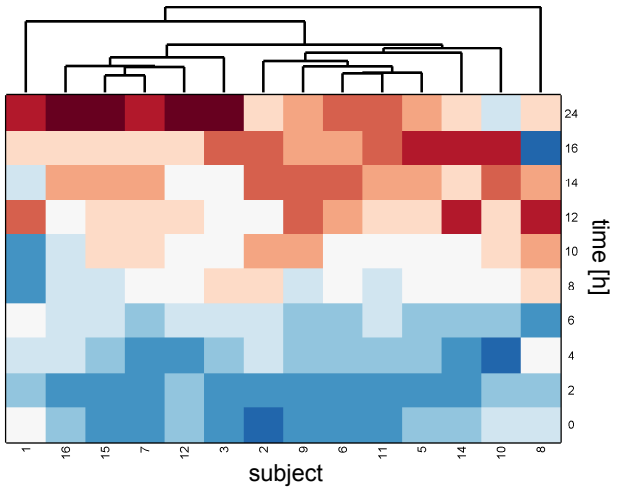

Figure 4.19: Clustergram of estimated regulation time-courses of LCAD during the fasting period. Clustering was done using Matlab clustergram algorithm with euclidean distance metric. Proband 13 was not considered for the clustering analysis due to missing data points. For all subjects LCAD enzymes become more active with ongoing fasting conditions.

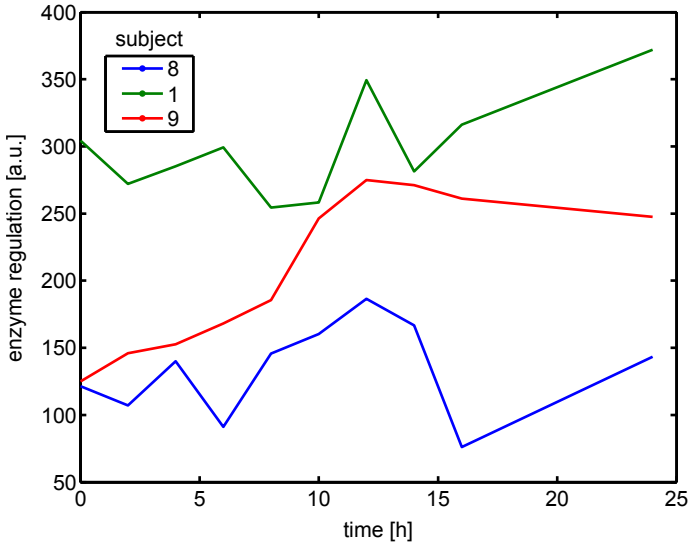

Figure 4.20: Time course of LCAD regulation for probands with low (proband 8), medium (1) and high BMI (9). Enzyme regulations of proband with low BMI remains slow compared to the other subjects. For the proband with high BMI, regulation strongly increases during the first 12 hours with a subsequent decline.

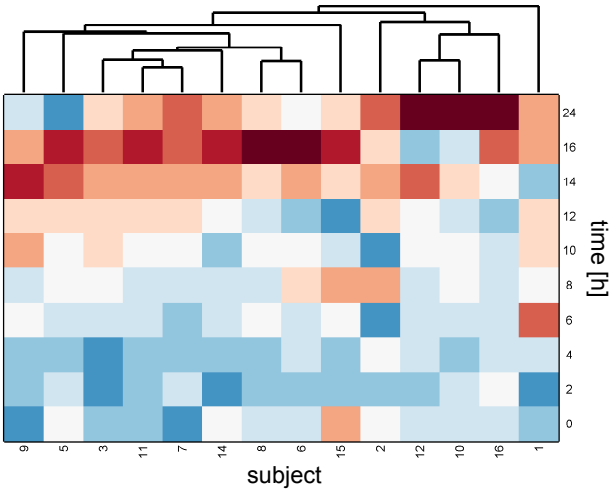

Figure 4.21: Clustergram of estimated regulation time-courses of MCAD during the fasting period. Clustering was done using Matlab clustergram algorithm with euclidean distance metric. Proband 13 was not considered for the clustering analysis due to missing data points. Similar to the profile of LCAD, MCAD activation generally increases for all subjects.

high BMI, regulation strongly increases during the first 12 hours with a subsequent decline. At the beginning, high LCAD activity is required due to the onset of the beta-oxidation pathway. Later on, the metabolism has adapted to the new conditions and no further increased activation of LCAD is needed.

Activation of MCAD The regulation profiles of the medium-chain acyl-CoA dehydrogenase MCAD are illustrated in Figure 4.21. Similar to the profile of LCAD, MCAD activation generally increases for all subjects. For probands 10, 12 and 16, the maximal activity is reached at the end of the fasting period, while for others the regulation declines after 14 to 16 hours. However, probands with similar regulation profiles of MCAD do not show similar profiles for LCAD. Similar regulation profiles would be expected for both enzymes, since products of LCAD reactions are subsequent substrates for MCAD. Possibly, the interval between sampling was too long in the study to provide detailed information. The time-course of enzyme regulation in Figure 4.22 shows the interindividual variation of MCAD regulation. For probands with low and high BMI, MCAD becomes strongly activated during the first 12 hours. Later on, the activation decreases. In contrast, the proband with medium BMI shows only a slight increase in MCAD activation. For this subject, conversion rates from C12 to C10 for example also remained stable during the whole fasting period (see Figure 4.12). As mentioned above, this proband shows the highest ratio of total fat in the body and total fat in the trunk, as well as the highest level of blood triglycerides. Beta-oxidation enzymes might be already activated under normal conditions, so no further activation is needed after starting the fasting period.

Activation of SCAD Figure 4.23 compares the individual regulation of SCAD activity during the fasting period. For some individuals (6, 11, 9), SCAD activity is high at the beginning and decreases later on. Interestingly, these probands all have a high BMI compared to other probands.

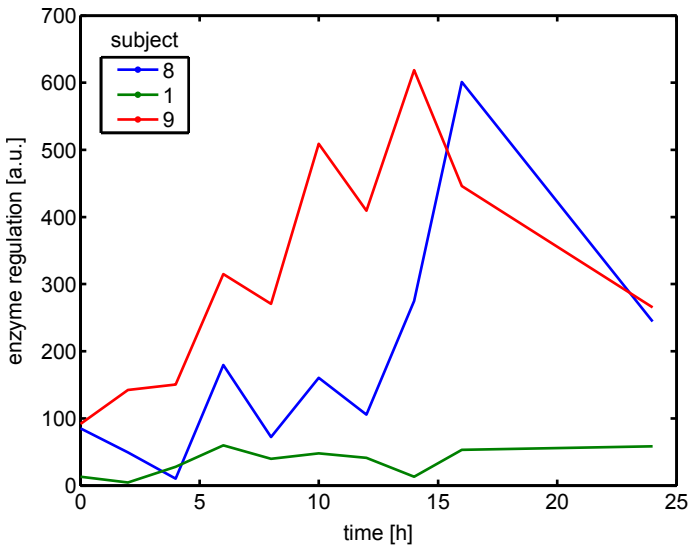

Figure 4.22: Time course of MCAD regulation for probands with low (proband 8), medium (1) and high BMI (9). For proband 8 and 9, MCAD becomes strongly activated during the first 12 hours. Later on, the activation decreases. In contrast, the proband with medium BMI shows only a slight increase in MCAD activation.

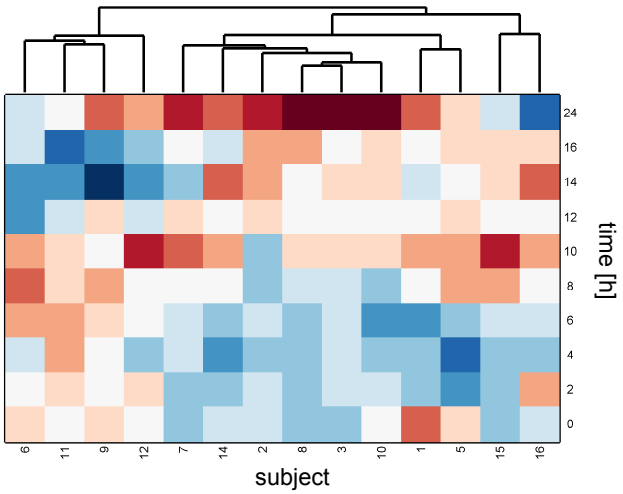

Figure 4.23: Clustergram of estimated regulation time-courses of SCAD during the fasting period. Clustering was done using Matlab clustergram algorithm with euclidean distance metric. Proband 13 was not considered for the clustering analysis due to missing data points. For some individuals (6, 11, 9), SCAD activity is high at the beginning and decreases later on. Interestingly, these probands all have a high BMI compared to other probands.

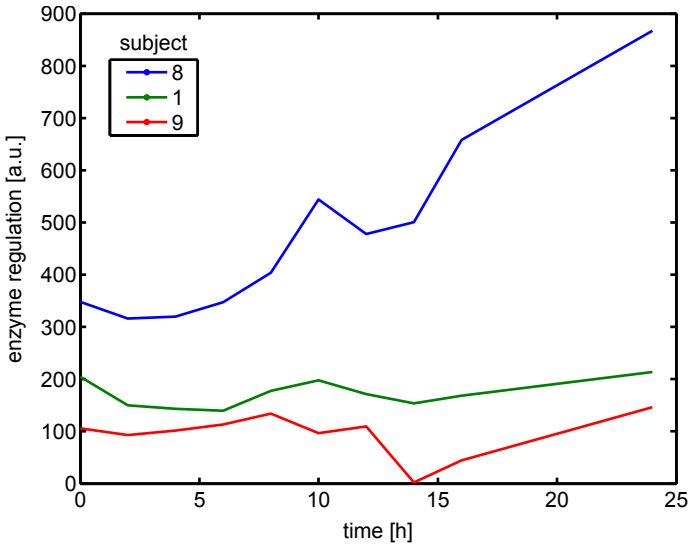

Figure 4.24: Time course of SCAD regulation for probands with low (proband 8), medium (1) and high BMI (9). Proband 1 with medium BMI shows no increased activation of SCAD, which was also the case for MCAD enzyme. For proband 8 with low BMI SCAD activity in turn increases during the whole fasting period.

Possibly, SCAD activity is reduced due to the lack of new fatty acids which are transported to the mitochondrium. Interestingly, probands with similar SCAD regulation also show similar LCAD activation (for instance proband 8 and 10, 6 and 9, or 15 and 16). This could indicate that LCAD and SCAD are concertedly activated, which is a known feature of enzymes of the same metabolic pathway [6]. This finding might be incorporated into a more refined model of the beta-oxidation pathway.
The regulation time-courses in Figure 4.24 show varying profiles. Proband 1 with medium BMI shows no increased activation of SCAD, which was also the case for MCAD enzyme. For proband 8 with low BMI SCAD activity in turn increases during the whole fasting period. It is interesting to note that for the proband with high BMI SCAD activation drops after 12 hours. This can be an artifact of the factorization method or possible influences from other metabolic pathways. A downregulation of SCAD and activation of MCAD and LCAD activity (as depicted in Figures 4.20 and 4.20) during fasting conditions is unlikely, since SCAD is downstream of the beta-oxidation pathway.

Figure 4.25 illustrates the distribution of individual regulation factors for enzymes LCAD and SCAD with respect to the subject's body mass index. For the enzyme SCAD there is a significant negative correlation between regulation factors and individual BMI values. Subjects with low BMI showed increased activation of SCAD. For these subjects, beta-oxidation activity might be very low under normal conditions and thus has to be activated more strongly during fasting conditions. For long-chain and medium-chain dehydrogenase no such relationship was obtained (correlation coefficients -0.05 and 0.07, respectively).

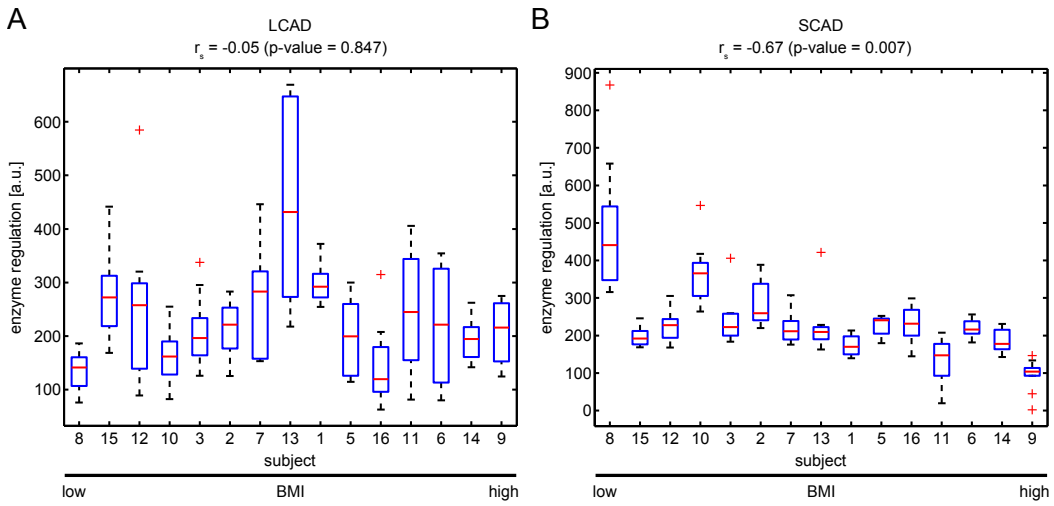

Figure 4.25: Boxplot of regulation factors for enzymes LCAD (A) and SCAD (B). Subjects are sorted with respect to the individual BMI. Spearman coefficient r_s shows significant negative correlation between the median of estimated regulation factors and individual BMI for enzyme SCAD.

4.4 Concluding discussion

The results presented above showed that our modeling approach provides insights into the beta-oxidation pathway that cannot be obtained by existing models. The model proposed by Modre-Osprian *et al.* [57] contains various enzymatic reactions for the degradation of fatty acids. However, many incorporated kinetic parameters have not been determined for specific human enzymes. In addition, *in-vitro* measurements of enzyme kinetics do not reflect the physiological *in-vivo* conditions and the variations between individuals. In contrast, estimated kinetic rates from our model are only based on metabolite concentrations. This allows for the determination of subject-specific rate constants for each individual reaction step. Since kinetic rates are not fixed, we can investigate the interindividual variability of metabolic reactions and compare substrate- and subject-specific rate profiles with the phenotypes of subjects. The comparison revealed correlations between specific reactions and physiological parameters which could not be obtained by investigating metabolite concentrations alone.
Our proposed modeling approach is related to the investigation of metabolite ratios by Gieger *et al.* [28] and Illig *et al.* [33]. In genome-wide association studies, single-nucleotide polymorphism of enzymes of the beta-oxidation pathway were associated with the ratio of substrate concentrations (see Section 3.2.2). The estimated rate constants from our model are also proportional to the ratio of metabolites and depend on the structure of the metabolic pathway (cf. Equation (3.6) in Section 3.3). Further studies could investigate the connections between findings of genome-wide association studies and results from our model. Associated metabolite ratios might provide evidence for other metabolic pathways which can be described by our modeling approach.

Chapter 5

Summary and Outlook

Mitochondrial beta-oxidation of fatty acid is an important physiological process which provides energy to the cell. The metabolic stages of this pathway have been investigated over the last 50 years and detailed biochemical information has been obtained. High-throughput methods in the field of metabolomics now allow for the quantification of multiple intermediate metabolites of beta-oxidation reactions. In this work, developed a model for the beta-oxidation pathway and investigated rate reaction profiles that were estimated based on steady state metabolite concentrations, that had been measured for 15 male subjects under varying physiological conditions, such as fasting and uptake of lipid rich diet.

In order to infer knowledge about the relationship between metabolite profiles and metabolic reactions we built a theoretical model of the beta-oxidation pathway. The model was developed by combining biochemical and physiological knowledge with mathematical modeling methods. For reducing the model complexity we introduced the following assumptions which are based on established biological knowledge about metabolic reactions. First, all cascade reactions are treated as irreversible, since the first reaction of the beta-oxidation pathway, the dehydrogenation of acyl-CoA, is assumed to be an irreversible reactions under physiological conditions. Moreover, outflux reactions of intermediate compounds were neglected, because experimental findings suggest that fatty acids are entirely metabolized and intermediate molecules stay within the mitochondrium. In addition, sequentially coupled reactions are combined into one reaction with only one effective parameter. The measured metabolite concentrations are very small compared to the Michaelis-Menten constants of catalyzing enzymes and lie within the linear range of the Michaelis-Menten curve which describes the relationship between reaction rate and substrate concentration. Therefore reaction kinetics are represented by mass action rate laws. Due to the fact that biochemical reactions are on a time scale of milliseconds to minutes while blood samples had been taken every two to four hours, we assumed that measurements reflect steady state metabolite concentrations. Finally we defined a fixed ratio of influx rates for specific main metabolites. The ratio reflects the experimentally determined composition of long-chain fatty acids in adipose tissue, which are mobilized during fasting conditions and therefore substrates for beta-oxidation reactions.

All assumptions were introduced to minimize parameter indeterminacies, which simplifies the investigation of the solution space of the mathematical model. As a result, the beta-oxidation cascade of n compounds can be described by $n+1$ parameters. Fixing one parameter then allows for the determination of the remaining rate constants. Contrary to other approaches, our model

does not rely on kinetic parameters that were derived from in-vitro measurements of purified enzymes. Instead, the estimation of rate constants is solely based on quantified blood metabolite concentrations. Therefore we can obtain individual reaction rate profiles that reflect subject- and metabolite-specific parameters for each time point during the fasting period.

As a first step of our analysis, we investigated metabolite concentration profiles in the HuMet study. Concentrations of acetylcarnitine (C2), the product of each beta-oxidation cycle, increase during the fasting period and rapidly decline after uptake of lipid and energy rich diet. For long chain fatty acids C14, C18 and especially C16, concentrations also increase during fasting conditions, which indicates higher mobilization of fatty acids from fat reservoirs.
Based on steady-state metabolite concentrations we estimated rate constants for the beta-oxidation pathway. Rate profiles differed significantly between subjects for several reactions. For one group of subjects, decreased overall rates indicated general low metabolic activity compared to other probands. Reactions with long- and medium-chain fatty acid substrates showed narrow ranges for the rate values compared to reaction with short-chain fatty acids as substrates. For the conversion of C16 to C14 and C14 to C12, rate profiles showed a significant negative correlation with individual body mass index (BMI). The reaction rates for substrate C16 also showed significant correlations with fat mass and fat fraction of the whole body. These relationships were not obtained by comparing metabolite concentrations with physiological parameters. Comparing reaction rate time-courses between subjects revealed that for one group of probands rates are maximal at the end of the fasting period, while for others rates decline after 12 to 14 hours of fasting. Four probands with low ratios of total fat in the body and similar levels of triglycerides (TG) showed similar influx rate profiles. Reaction rates for the conversion of C12 to C10 for one proband with high TG levels and high total fat ratio were distinct from other rate time courses. These findings might indicate furhter relationships between metabolic reactions and physiological parameters.
Based on reaction rate profiles we further estimated substrate specificities and regulatory effects for three enzymes which catalyze the first reaction of the beta-oxidation cascade. The results for enzymatic specificities notably reflect the qualitative features of experimentally measured enzyme activities. Especially for short-chain acyl-CoA dehydrogenase (SCAD), the estimated and experimental profile match to a great extent. Investigation of enzyme regulation time courses for all subjects revealed a concerted regulation of LCAD and MCAD, two beta-oxidation enzymes with differing substrate specificity.

Outlook

Our model was developed to investigate the degradation of fatty acids in the beta-oxidation pathway. Except for an initializing step, synthesis and degradation of fatty acids are reverse processes that use similar catalyzing enzymes [6]. We assumed that during the fasting period synthesis of fatty acids is inactivated, due to the antagonistic features of both pathways [1]. The HuMet study also contains data for the uptake of lipid rich diet and exercise conditions. For the investigation of the interplay between catabolism and anabolism of fatty acids we need to incorporate synthesis reactions into our model. Furthermore it will be interesting to compare oxidation rates during the fasting period with reaction rates during physical exercise, since both conditions induce the degradation of fatty acids [24].
For our investigation of beta-oxidation we considered only saturated and even-numbered fatty acids. For future studies we also want to include degradation steps of odd-numbered or unsaturated fatty acids. Especially the latter case is interesting, since oleic acid (C18:1) is the most

abundant fatty acid storage form [37, 48]. This can help to refine the fixed influx ratios of the proposed model, which then would reflect the composition of both saturated and unsaturated fatty acids in adipose tissue. In the HuMet study other methods of metabolite measurement were also applied, such as NMR-spectroscopy and liquid chromatography, which can detect free fatty acids in the blood. This allows for the investigation of the link between these data and our results, which are based on the concentrations of a transport form of fatty acids, and might provide more detailed knowledge about the physiological function of acylcarnitine in the blood.
Biochemical pathways of the human metabolism have been intensively studied and comprehensive information about involved metabolites and catalyzing enzymes is available [14, 38]. Our knowledge-based modeling approach thus can be used to describe other biochemical pathways, for example amino acid metabolism. However, many intermediate metabolites cannot be measured with up-to-date methods. For our beta-oxidation model we therefore combined subsequent steps into general reactions with effective parameters. For other metabolic pathways, further methods have to be developed in order to deal with missing observations and more complex pathway topologies including, for example, branched reactions. In addition, further metabolites from blood samples might be identified which are proportional to intracellular compound concentrations and hence reflect the metabolic state of a cell.
The estimation of specific enzymatic activity and regulatory effects for enzymes of the beta-oxidation pathway revealed interesting results. This approach can also be used for the description of other metabolic reactions that are catalyed by enzymes with overlapping substrate specificities. Further matrix factorization techniques can be applied for the estimation of enzymatic features, for instance non-negative tensor factorization. In addition, regulation factors could be estimated from rate constants using multiple linear regression with a non-negativity constraint and experimentally measured substrate specificities. These results can be compared to results of the matrix factorization.
Most metabolomics studies provide steady state data of compound concentrations. Based on these observations, our proposed model allows for the estimation of effective rate parameters, enzymatic substrate specificity and regulatory effects. This approach therefore seems capable of investigating metabolomics data consisting of samples for many individuals without time resolution. An example is the KORA F4 study, which provides metabolite profiles for more than 3000 subjects [33, 68, 69]. For the population of this study extensive data about physiological phenotypes and clinical records are available. Comparing estimated rate constants of HuMet data with physiological parameters such as BMI, triglyceride blood levels or ratios of total fat in the body revealed for some reactions a relationship between rate profiles and individual phenotype. Our proposed model can be used for both HuMet and KORA data to search for combinations of other physiological parameters as a classifier for individual phenotypes and diseases.

Malfunction of metabolism is a great contributor to the pathogenesis of human diseases. By the combination of knowledge of human physiology and pathology with the study of a collection of metabolites, further insights into the structure and regulation of metabolic pathways can be obtained. Understanding the complex interplay between individual genotype, metabolism, environment and nutrition is crucial for the identification of disease related biomarker molecules. The description of biochemical pathways with metabolic modeling techniques thus might provide insights which help to prevent systemic diseases like obesity and diabetes.

Appendix A

Metabolites measured using tandem mass spectrometry

The following list provides all metabolites that were measured in the HuMet study using electrospray ionization tandem mass spectrometry. Bold metabolites were used for the development of the proposed beta-oxidation model.

Abbreviation	Biochemical Name
Acylcarnitines	
C0	**Carnitine**
C2	**Acetylcarnitine**
C3	Propionylcarnitine
C3:1	Propenoylcarnitine
C3-OH	Hydroxypropionylcarnitine
C4	**Butyrylcarnitine**
C4:1	Butenylcarnitine
C4-OH (C3-DC)	Hydroxybutyrylcarnitine
C5	Valerylcarnitine
C5:1	Tiglylcarnitine
C5:1-DC	Glutaconylcarnitine
C5-DC (C6-OH)	Glutarylcarnitine (Hydroxyhexanoylcarnitine)
C5-M-DC	Methylglutarylcarnitine
C5-OH (C3-DC-M)	Hydroxyvalerylcarnitine
C6 (C4:1-DC)	**Hexanoylcarnitine**
C6:1	Hexenoylcarnitine
C7-DC	Pimelylcarnitine
C8	**Octanoylcarnitine**
C8:1	Octenoylcarnitine

C9	Nonaylcarnitine
C10	**Decanoylcarnitine**
C10:1	Decenoylcarnitine
C10:2	Decadienylcarnitine
C12	**Dodecanoylcarnitine**
C12:1	Dodecenoylcarnitine
C12-DC	Dodecanedioylcarnitine
C14	**Tetradecanoylcarnitine**
C14:1	Tetradecenoylcarnitine
C14:1-OH	Hydroxytetradecenoylcarnitine
C14:2	Tetradecadienylcarnitine
C14:2-OH	Hydroxytetradecadienylcarnitine
C16	**Hexadecanoylcarnitine**
C16:1	Hexadecenoylcarnitine
C16:1-OH	Hydroxyhexadecenoylcarnitine
C16:2	Hexadecadienylcarnitine
C16:2-OH	Hydroxyhexadecadienylcarnitine
C16-OH	Hydroxyhexadecanoylcarnitine
C18	**Octadecanoylcarnitine**
C18:1	Octadecenoylcarnitine
C18:1-OH	Hydroxyoctadecenoylcarnitine
C18:2	Octadecadienylcarnitine

Amino Acids	
Arg-PTC	Arginine
Gln-PTC	Glutamine
Gly-PTC	Glycine
His-PTC	Histidine
Met-PTC	Methionine
Orn-PTC	Ornithine
Phe-PTC	Phenylalanine
Pro-PTC	Proline
Ser-PTC	Serine
Thr-PTC	Threonine
Trp-PTC	Tryptophan
Tyr-PTC	Tyrosine
Val-PTC	Valine
xLeu-PTC	Leucine / Isoleucine

Sugars	
H1	Hexose

Glycerophospholipids	
lysoPC a C6:0	lysoPhosphatidylcholine acyl C6:0
lysoPC a C14:0	lysoPhosphatidylcholine acyl C14:0
lysoPC a C16:0	lysoPhosphatidylcholine acyl C16:0
lysoPC a C16:1	lysoPhosphatidylcholine acyl C16:1
lysoPC a C17:0	lysoPhosphatidylcholine acyl C17:0
lysoPC a C18:0	lysoPhosphatidylcholine acyl C18:0
lysoPC a C18:1	lysoPhosphatidylcholine acyl C18:1
lysoPC a C18:2	lysoPhosphatidylcholine acyl C18:2
lysoPC a C20:3	lysoPhosphatidylcholine acyl C20:3
lysoPC a C20:4	lysoPhosphatidylcholine acyl C20:4
lysoPC a C24:0	lysoPhosphatidylcholine acyl C24:0
lysoPC a C26:0	lysoPhosphatidylcholine acyl C26:0
lysoPC a C26:1	lysoPhosphatidylcholine acyl C26:1
lysoPC a C28:0	lysoPhosphatidylcholine acyl C28:0
lysoPC a C28:1	lysoPhosphatidylcholine acyl C28:1
PC aa C24:0	Phosphatidylcholine diacyl C24:0
PC aa C26:0	Phosphatidylcholine diacyl C26:0
PC aa C28:1	Phosphatidylcholine diacyl C28:1
PC aa C30:0	Phosphatidylcholine diacyl C30:0
PC aa C30:2	Phosphatidylcholine diacyl C30:2
PC aa C32:0	Phosphatidylcholine diacyl C32:0
PC aa C32:1	Phosphatidylcholine diacyl C32:1
PC aa C32:2	Phosphatidylcholine diacyl C32:2
PC aa C32:3	Phosphatidylcholine diacyl C32:3
PC aa C34:1	Phosphatidylcholine diacyl C34:1
PC aa C34:2	Phosphatidylcholine diacyl C34:2
PC aa C34:3	Phosphatidylcholine diacyl C34:3
PC aa C34:4	Phosphatidylcholine diacyl C34:4
PC aa C36:0	Phosphatidylcholine diacyl C36:0
PC aa C36:1	Phosphatidylcholine diacyl C36:1
PC aa C36:2	Phosphatidylcholine diacyl C36:2
PC aa C36:3	Phosphatidylcholine diacyl C36:3
PC aa C36:4	Phosphatidylcholine diacyl C36:4
PC aa C36:5	Phosphatidylcholine diacyl C36:5
PC aa C36:6	Phosphatidylcholine diacyl C36:6
PC aa C38:0	Phosphatidylcholine diacyl C38:0
PC aa C38:1	Phosphatidylcholine diacyl C38:1
PC aa C38:3	Phosphatidylcholine diacyl C38:3
PC aa C38:4	Phosphatidylcholine diacyl C38:4

PC aa C38:5	Phosphatidylcholine diacyl C38:5
PC aa C38:6	Phosphatidylcholine diacyl C38:6
PC aa C40:1	Phosphatidylcholine diacyl C40:1
PC aa C40:2	Phosphatidylcholine diacyl C40:2
PC aa C40:3	Phosphatidylcholine diacyl C40:3
PC aa C40:4	Phosphatidylcholine diacyl C40:4
PC aa C40:5	Phosphatidylcholine diacyl C40:5
PC aa C40:6	Phosphatidylcholine diacyl C40:6
PC aa C42:0	Phosphatidylcholine diacyl C42:0
PC aa C42:1	Phosphatidylcholine diacyl C42:1
PC aa C42:2	Phosphatidylcholine diacyl C42:2
PC aa C42:4	Phosphatidylcholine diacyl C42:4
PC aa C42:5	Phosphatidylcholine diacyl C42:5
PC aa C42:6	Phosphatidylcholine diacyl C42:6
PC ae C30:0	Phosphatidylcholine acyl-alkyl C30:0
PC ae C30:1	Phosphatidylcholine acyl-alkyl C30:1
PC ae C30:2	Phosphatidylcholine acyl-alkyl C30:2
PC ae C32:1	Phosphatidylcholine acyl-alkyl C32:1
PC ae C32:2	Phosphatidylcholine acyl-alkyl C32:2
PC ae C34:0	Phosphatidylcholine acyl-alkyl C34:0
PC ae C34:1	Phosphatidylcholine acyl-alkyl C34:1
PC ae C34:2	Phosphatidylcholine acyl-alkyl C34:2
PC ae C34:3	Phosphatidylcholine acyl-alkyl C34:3
PC ae C36:0	Phosphatidylcholine acyl-alkyl C36:0
PC ae C36:1	Phosphatidylcholine acyl-alkyl C36:1
PC ae C36:2	Phosphatidylcholine acyl-alkyl C36:2
PC ae C36:3	Phosphatidylcholine acyl-alkyl C36:3
PC ae C36:4	Phosphatidylcholine acyl-alkyl C36:4
PC ae C36:5	Phosphatidylcholine acyl-alkyl C36:5
PC ae C38:0	Phosphatidylcholine acyl-alkyl C38:0
PC ae C38:1	Phosphatidylcholine acyl-alkyl C38:1
PC ae C38:2	Phosphatidylcholine acyl-alkyl C38:2
PC ae C38:3	Phosphatidylcholine acyl-alkyl C38:3
PC ae C38:4	Phosphatidylcholine acyl-alkyl C38:4
PC ae C38:5	Phosphatidylcholine acyl-alkyl C38:5
PC ae C38:6	Phosphatidylcholine acyl-alkyl C38:6
PC ae C40:0	Phosphatidylcholine acyl-alkyl C40:0
PC ae C40:1	Phosphatidylcholine acyl-alkyl C40:1
PC ae C40:2	Phosphatidylcholine acyl-alkyl C40:2
PC ae C40:3	Phosphatidylcholine acyl-alkyl C40:3
PC ae C40:4	Phosphatidylcholine acyl-alkyl C40:4

PC ae C40:5	Phosphatidylcholine acyl-alkyl C40:5
PC ae C40:6	Phosphatidylcholine acyl-alkyl C40:6
PC ae C42:0	Phosphatidylcholine acyl-alkyl C42:0
PC ae C42:1	Phosphatidylcholine acyl-alkyl C42:1
PC ae C42:2	Phosphatidylcholine acyl-alkyl C42:2
PC ae C42:3	Phosphatidylcholine acyl-alkyl C42:3
PC ae C42:4	Phosphatidylcholine acyl-alkyl C42:4
PC ae C42:5	Phosphatidylcholine acyl-alkyl C42:5
PC ae C44:3	Phosphatidylcholine acyl-alkyl C44:3
PC ae C44:4	Phosphatidylcholine acyl-alkyl C44:4
PC ae C44:5	Phosphatidylcholine acyl-alkyl C44:5
PC ae C44:6	Phosphatidylcholine acyl-alkyl C44:6

Sphingolipids	
SM (OH) C14:1	Hydroxysphingomyeline C14:1
SM C16:0	Sphingomyeline C16:0
SM C16:1	Sphingomyeline C16:1
SM (OH) C16:1	Hydroxysphingomyeline C16:1
SM C18:0	Sphingomyeline C18:0
SM C18:1	Sphingomyeline C18:1
SM C20:2	Sphingomyeline C20:2
SM C22:3	Sphingomyeline C22:3
SM (OH) C22:1	Hydroxysphingomyeline C22:1
SM (OH) C22:2	Hydroxysphingomyeline C22:2
SM C24:0	Sphingomyeline C24:0
SM C24:1	Sphingomyeline C24:1
SM (OH) C24:1	Hydroxysphingomyeline C24:1
SM C26:0	Sphingomyeline C26:0
SM C26:1	Sphingomyeline C26:1

Appendix B

Phenotypic parameters

The following table provides selected phenotypic parameters for all subjects of the HuMet study.

Subject	Age	BMI [kg/m^2]	BMI group	Fat mass [kg]	Fat (body) [%]	Fat (trunk) [%]
1	26	23.46	middle	18.2	23.9	22.3
2	31	22.57	middle	11.4	18.6	18.4
3	32	22.45	middle	16.5	20.0	20.2
5	28	23.45	middle	15.2	18.7	17.8
6	27	25.12	high	13.8	17.4	15.9
7	28	22.52	middle	12.6	15.7	13.4
8	33	20.27	low	9.2	14.9	13.0
9	29	25.34	high	15.0	19.2	15.6
10	22	21.05	low	12.7	17.8	17.1
11	26	24.90	high	18.5	22.4	20.0
12	25	20.77	low	8.8	13.6	12.9
13	28	22.80	middle	16.4	20.9	19.6
14	24	24.96	high	19.0	21.9	21.4
15	30	20.75	low	11.4	15.6	14.4
16	28	24.78	high	17.5	19.2	16.1

Bibliography

[1] Alberts, B., Johnson, A., Lewis, J., Raff, M., Roberts, K., and Walter, P. *Molekularbiologie der Zelle*. Wiley-VCH, Weinheim, 2003.

[2] Allen, J., Davey, H.M., Broadhurst, D., Heald, J.K., Rowland, J.J., Oliver, S.G., and Kell, D.B. High-throughput classification of yeast mutants for functional genomics using metabolic footprinting. *Nat Biotechnol*, 21(6):692–696, 2003.

[3] Amarowicz, R., Sulik, M., Korczkowska, B., and Brykalska, A. Composition of fatty acids and triglycerides in human adipose tissue–results from north-east poland (short communication). *Nahrung*, 35(6):667–669, 1991.

[4] Atkins, P. *Physical Chemistry*. Oxford University Press, Oxford, Melbourne, Tokyo, 2006.

[5] Bartlett, K. and Eaton, S. Mitochondrial beta-oxidation. *Eur J Biochem*, 271(3):462–469, 2004.

[6] Berg, J.M., Tymoczko, J.L., Stryer, L., and Stryer, L. *Biochemistry*. W.H. Freeman, New York, 2007.

[7] Bloechl, F., W.D. and Theis, F. Effective parameters determining the information flow in hierarchical biological systems. *in revision*, 2010.

[8] Blow, N. Metabolomics: Biochemistry's new look. *Nature*, 455(7213):697–700, 2008.

[9] Bolton-Smith, C., Woodward, M., and Tavendale, R. Evidence for age-related differences in the fatty acid composition of human adipose tissue, independent of diet. *Eur J Clin Nutr*, 51(9):619–624, 1997.

[10] Briggs, G. and Haldane, J. A note on the kinetics of enzyme action. *Biochemical journal*, 19(2):338, 1925.

[11] Cakir, T., Hendriks, M.M.W.B., Westerhuis, J.A., and Smilde, A.K. Metabolic network discovery through reverse engineering of metabolome data. *Metabolomics*, 5(3):318–329, 2009.

[12] Calvetti, D., Kuceyeski, A., and Somersalo, E. A mathematical model of liver metabolism: from steady state to dynamic. *Journal of Physics: Conference Series*, 124:012012 (7pp), 2008.

[13] Carpenter, K., Pollitt, R.J., and Middleton, B. Human liver long-chain 3-hydroxyacyl-coenzyme a dehydrogenase is a multifunctional membrane-bound beta-oxidation enzyme of mitochondria. *Biochem Biophys Res Commun*, 183(2):443–448, 1992.

[14] Caspi, R., Foerster, H., Fulcher, C.A., Kaipa, P., Krummenacker, M., Latendresse, M., Paley, S., Rhee, S.Y., Shearer, A.G., Tissier, C., Walk, T.C., Zhang, P., and Karp, P.D. The metacyc database of metabolic pathways and enzymes and the biocyc collection of pathway/genome databases. *Nucleic Acids Res*, 36(Database issue):D623–D631, 2008.

[15] Chalhoub, E., Hanson, R.W., and Belovich, J.M. A computer model of gluconeogenesis and lipid metabolism in the perfused liver. *Am J Physiol Endocrinol Metab*, 293(6):E1676–E1686, 2007.

[16] Chang, A., Scheer, M., Grote, A., Schomburg, I., and Schomburg, D. Brenda, amenda and frenda the enzyme information system: new content and tools in 2009. *Nucleic Acids Res*, 37(Database issue):D588–D592, 2009.

[17] De Vries, G., Hillen, T., Lewis, M., Schõnfisch, B., and Muller, J. *A course in mathematical biology: quantitative modeling with mathematical and computational methods*. Society for Industrial Mathematics, 2006.

[18] Drger, A., Kronfeld, M., Ziller, M.J., Supper, J., Planatscher, H., Magnus, J.B., Oldiges, M., Kohlbacher, O., and Zell, A. Modeling metabolic networks in c. glutamicum: a comparison of rate laws in combination with various parameter optimization strategies. *BMC Syst Biol*, 3:5, 2009.

[19] Duarte, N.C., Becker, S.A., Jamshidi, N., Thiele, I., Mo, M.L., Vo, T.D., Srivas, R., and Palsson, B.. Global reconstruction of the human metabolic network based on genomic and bibliomic data. *Proc Natl Acad Sci U S A*, 104(6):1777–1782, 2007.

[20] Dunn, W.B., Bailey, N.J.C., and Johnson, H.E. Measuring the metabolome: current analytical technologies. *Analyst*, 130(5):606–625, 2005.

[21] Eaton, S., Bartlett, K., and Pourfarzam, M. Mammalian mitochondrial beta-oxidation. *Biochem J*, 320 (Pt 2):345–357, 1996.

[22] Eaton, S., Bhuiyan, A.K., Kler, R.S., Turnbull, D.M., and Bartlett, K. Intramitochondrial control of the oxidation of hexadecanoate in skeletal muscle. a study of the acyl-coa esters which accumulate during rat skeletal-muscle mitochondrial beta-oxidation of [u-14c]hexadecanoate and [u-14c]hexadecanoyl-carnitine. *Biochem J*, 289 (Pt 1):161–168, 1993.

[23] Eaton, S., Turnbull, D.M., and Bartlett, K. Redox control of beta-oxidation in rat liver mitochondria. *Eur J Biochem*, 220(3):671–681, 1994.

[24] Eaton, S. Control of mitochondrial beta-oxidation flux. *Prog Lipid Res*, 41(3):197–239, 2002.

[25] Eder, M., Krutle, F., Dong, Y., Vock, P., Kieweg, V., Kim, J.J., Strauss, A.W., and Ghisla, S. Characterization of human and pig kidney long-chain-acyl-coa dehydrogenases and their role in beta-oxidation. *Eur J Biochem*, 245(3):600–607, 1997.

[26] Famili, I., Mahadevan, R., and Palsson, B.O. k-cone analysis: determining all candidate values for kinetic parameters on a network scale. *Biophys J*, 88(3):1616–1625, 2005.

[27] Finocchiaro, G., Ito, M., and Tanaka, K. Purification and properties of short chain acyl-coa, medium chain acyl-coa, and isovaleryl-coa dehydrogenases from human liver. *J Biol Chem*, 262(17):7982–7989, 1987.

[28] Gieger, C., Geistlinger, L., Altmaier, E., de Angelis, M.H., Kronenberg, F., Meitinger, T., Mewes, H.W., Wichmann, H.E., Weinberger, K.M., Adamski, J., Illig, T., and Suhre, K. Genetics meets metabolomics: a genome-wide association study of metabolite profiles in human serum. *PLoS Genet*, 4(11):e1000282, 2008.

[29] Goodacre, R., Vaidyanathan, S., Dunn, W.B., Harrigan, G.G., and Kell, D.B. Metabolomics by numbers: acquiring and understanding global metabolite data. *Trends Biotechnol*, 22(5):245–252, 2004.

[30] Guldberg, C. and Waage, P. ber die chemische affinitt. *J. prakt. Chem*, 127:69–114, 1879.

[31] Hillenkamp, F., Karas, M., Beavis, R.C., and Chait, B.T. Matrix-assisted laser desorption/ionization mass spectrometry of biopolymers. *Anal Chem*, 63(24):1193A–1203A, 1991.

[32] Holmes, E., Wilson, I.D., and Nicholson, J.K. Metabolic phenotyping in health and disease. *Cell*, 134(5):714–717, 2008.

[33] Illig, T., Gieger, C., Zhai, G., Rmisch-Margl, W., Wang-Sattler, R., Prehn, C., Altmaier, E., Kastenmller, G., Kato, B.S., Mewes, H.W., Meitinger, T., de Angelis, M.H., Kronenberg, F., Soranzo, N., Wichmann, H.E., Spector, T.D., Adamski, J., and Suhre, K. A genome-wide perspective of genetic variation in human metabolism. *Nat Genet*, 2009.

[34] Insull, W. and Bartsch, G.E. Fatty acid composition of human adipose tissue related to age, sex, and race. *Am J Clin Nutr*, 20(1):13–23, 1967.

[35] Jackson, S., Bartlett, K., Land, J., Moxon, E.R., Pollitt, R.J., Leonard, J.V., and Turnbull, D.M. Long-chain 3-hydroxyacyl-coa dehydrogenase deficiency. *Pediatr Res*, 29(4 Pt 1):406–411, 1991.

[36] Jackson, S., Kler, R.S., Bartlett, K., Briggs, H., Bindoff, L.A., Pourfarzam, M., Gardner-Medwin, D., and Turnbull, D.M. Combined enzyme defect of mitochondrial fatty acid oxidation. *J Clin Invest*, 90(4):1219–1225, 1992.

[37] Jacobsson, L., Lindgrde, F., Manthorpe, R., and Akesson, B. Correlation of fatty acid composition of adipose tissue lipids and serum phosphatidylcholine and serum concentrations of micronutrients with disease duration in rheumatoid arthritis. *Ann Rheum Dis*, 49(11):901–905, 1990.

[38] Kanehisa, M., Araki, M., Goto, S., Hattori, M., Hirakawa, M., Itoh, M., Katayama, T., Kawashima, S., Okuda, S., Tokimatsu, T., and Yamanishi, Y. Kegg for linking genomes to life and the environment. *Nucleic Acids Res*, 36(Database issue):D480–D484, 2008.

[39] Kell, D.B., Brown, M., Davey, H.M., Dunn, W.B., Spasic, I., and Oliver, S.G. Metabolic footprinting and systems biology: the medium is the message. *Nat Rev Microbiol*, 3(7):557–565, 2005.

[40] Keseler, I.M., Bonavides-Martnez, C., Collado-Vides, J., Gama-Castro, S., Gunsalus, R.P., Johnson, D.A., Krummenacker, M., Nolan, L.M., Paley, S., Paulsen, I.T., Peralta-Gil, M., Santos-Zavaleta, A., Shearer, A.G., and Karp, P.D. Ecocyc: a comprehensive view of escherichia coli biology. *Nucleic Acids Res*, 37(Database issue):D464–D470, 2009.

[41] Kler, R.S., Jackson, S., Bartlett, K., Bindoff, L.A., Eaton, S., Pourfarzam, M., Frerman, F.E., Goodman, S.I., Watmough, N.J., and Turnbull, D.M. Quantitation of acyl-coa and acylcarnitine esters accumulated during abnormal mitochondrial fatty acid oxidation. *J Biol Chem*, 266(34):22932–22938, 1991.

[42] Klipp, E., Liebermeister, W., Wierling, C., Kowald, A., Lehrach, H., and Herwig, R. *Systems Biology: A Textbook*. Wiley-VCH, 1 edition, 2009. ISBN 3527318747.

[43] Kohn, M.C. Computer simulation of metabolism in palmitate-perfused rat heart. iii. sensitivity analysis. *Ann Biomed Eng*, 11(6):533–549, 1983.

[44] Kohn, M.C. and Garfinkel, D. Computer simulation of metabolism in palmitate-perfused rat heart. i. palmitate oxidation. *Ann Biomed Eng*, 11(5):361–384, 1983.

[45] Kohn, M.C. and Garfinkel, D. Computer simulation of metabolism in palmitate-perfused rat heart. ii. behavior of complete model. *Ann Biomed Eng*, 11(6):511–531, 1983.

[46] Kopelman, P.G. Obesity as a medical problem. *Nature*, 404(6778):635–643, 2000.

[47] Kunz, W.S. Application of the theory of steady-state flux control to mitochondrial beta-oxidation. *Biomed Biochim Acta*, 50(12):1143–1157, 1991.

[48] Lang, P.D., Degott, M., Heuck, C.C., Opherk, D., and Vollmar, J. Fatty acid composition of adipose tissue, blood, lipids, and glucose tolerance in patients with different degrees of angiographically documented coronary arteriosclerosis. *Res Exp Med (Berl)*, 180(2):161–168, 1982.

[49] Lee, D.D. and Seung, H.S. Learning the parts of objects by non-negative matrix factorization. *Nature*, 401(6755):788–791, 1999.

[50] Liebermeister, W. and Klipp, E. Bringing metabolic networks to life: convenience rate law and thermodynamic constraints. *Theor Biol Med Model*, 3:41, 2006.

[51] Lopes-Cardozo, M., Klazinga, W., and van den Bergh, S.G. Accumulation of carnitine esters of beta-oxidation intermediates during palmitate oxidation by rat-liver mitochondria. *Eur J Biochem*, 83(2):629–634, 1978.

[52] Lottspeich, F. *Bioanalytik*. Spektrum, Muenchen; Heidelberg, 2006.

[53] Luo, M.J., He, X.Y., Sprecher, H., and Schulz, H. Purification and characterization of the trifunctional beta-oxidation complex from pig heart mitochondria. *Arch Biochem Biophys*, 304(1):266–271, 1993.

[54] Melde, K., Jackson, S., Bartlett, K., Sherratt, H.S., and Ghisla, S. Metabolic consequences of methylenecyclopropylglycine poisoning in rats. *Biochem J*, 274 (Pt 2):395–400, 1991.

[55] Michaelis, L. and Menten, M. Die kinetik der invertinwirkung. *Biochemistry Zeitung*, 49:333–369, 1913.

[56] Michal, G. *Biochemical pathways: an atlas of biochemistry and molecular biology*. Wiley New York, 1999.

[57] Modre-Osprian, R., Osprian, I., Tilg, B., Schreier, G., Weinberger, K.M., and Graber, A. Dynamic simulations on the mitochondrial fatty acid beta-oxidation network. *BMC Syst Biol*, 3:2, 2009.

[58] Murray, J. *Mathematical biology*. Springer Verlag, 2003.

[59] Nada, M.A., Rhead, W.J., Sprecher, H., Schulz, H., and Roe, C.R. Evidence for intermediate channeling in mitochondrial beta-oxidation. *J Biol Chem*, 270(2):530–535, 1995.

[60] Nelson, D.L. and Cox, M.M. *Lehninger Principles of Biochemistry*. W. H. Freeman, 2004. ISBN 0716743396.

[61] Nicholson, J.K., Connelly, J., Lindon, J.C., and Holmes, E. Metabonomics: a platform for studying drug toxicity and gene function. *Nat Rev Drug Discov*, 1(2):153–161, 2002.

[62] Nicholson, J.K. and Lindon, J.C. Systems biology: Metabonomics. *Nature*, 455(7216):1054–1056, 2008.

[63] Nobeli, I. and Thornton, J.M. A bioinformatician's view of the metabolome. *Bioessays*, 28(5):534–545, 2006.

[64] Oldiges, M., Ltz, S., Pflug, S., Schroer, K., Stein, N., and Wiendahl, C. Metabolomics: current state and evolving methodologies and tools. *Appl Microbiol Biotechnol*, 76(3):495–511, 2007.

[65] Pacheco, Y.M., Prez-Camino, M.C., Cert, A., Montero, E., and Ruiz-Gutirrez, V. Determination of the molecular species composition of diacylglycerols in human adipose tissue by solid-phase extraction and gas chromatography on a polar phase. *J Chromatogr B Biomed Sci Appl*, 714(2):127–132, 1998.

[66] Pollitt, R.J. Disorders of mitochondrial long-chain fatty acid oxidation. *J Inherit Metab Dis*, 18(4):473–490, 1995.

[67] Rasmussen, B.B., Holmbck, U.C., Volpi, E., Morio-Liondore, B., Paddon-Jones, D., and Wolfe, R.R. Malonyl coenzyme a and the regulation of functional carnitine palmitoyltransferase-1 activity and fat oxidation in human skeletal muscle. *J Clin Invest*, 110(11):1687–1693, 2002.

[68] Rathmann, W., Haastert, B., Herder, C., Hauner, H., Koenig, W., Meisinger, C., Holle, R., and Giani, G. Differential association of adiponectin with cardiovascular risk markers in men and women? the kora survey 2000. *Int J Obes (Lond)*, 31(5):770–776, 2007.

[69] Rathmann, W., Haastert, B., Giani, G., Koenig, W., Imhof, A., Herder, C., Holle, R., and Mielck, A. Is inflammation a causal chain between low socioeconomic status and type 2 diabetes? results from the kora survey 2000. *Eur J Epidemiol*, 21(1):55–60, 2006.

[70] Ruderman, N.B., Saha, A.K., Vavvas, D., and Witters, L.A. Malonyl-coa, fuel sensing, and insulin resistance. *Am J Physiol*, 276(1 Pt 1):E1–E18, 1999.

[71] Schaefer, J. and Strimmer, K. Learning large-scale graphical gaussian models from genomic data. volume 776, pages 263–276. AIP, 2005.

[72] Schilling, C.H., Schuster, S., Palsson, B.O., and Heinrich, R. Metabolic pathway analysis: basic concepts and scientific applications in the post-genomic era. *Biotechnol Prog*, 15(3):296–303, 1999.

[73] Schuster, S., Dandekar, T., and Fell, D.A. Detection of elementary flux modes in biochemical networks: a promising tool for pathway analysis and metabolic engineering. *Trends Biotechnol*, 17(2):53–60, 1999.

[74] Shampine, L.F. and Reichelt, M.W. The matlab ode suite. *SIAM Journal on Scientific Computing*, 18:1–22, 1997.

[75] Sprecher, H. The roles of anabolic and catabolic reactions in the synthesis and recycling of polyunsaturated fatty acids. *Prostaglandins, Leukotrienes and Essential Fatty Acids*, 67(2-3):79 – 83, 2002. ISSN 0952-3278.

[76] Sprecher, H., Luthria, D.L., Mohammed, B.S., and Baykousheva, S.P. Reevaluation of the pathways for the biosynthesis of polyunsaturated fatty acids. *J Lipid Res*, 36(12):2471–2477, 1995.

[77] Stanley, K.K. and Tubbs, P.K. The occurrence of intermediates in mitochondrial fatty acid oxidation. *FEBS Lett*, 39(3):325–328, 1974.

[78] Stanley, K.K. and Tubbs, P.K. The role of intermediates in mitochondrial fatty acid oxidation. *Biochem J*, 150(1):77–88, 1975.

[79] Takahashi, K., Ishikawa, N., Sadamoto, Y., Sasamoto, H., Ohta, S., Shiozawa, A., Miyoshi, F., Naito, Y., Nakayama, Y., and Tomita, M. E-cell 2: multi-platform e-cell simulation system. *Bioinformatics*, 19(13):1727–1729, 2003.

[80] Tweeddale, H., Notley-McRobb, L., and Ferenci, T. Effect of slow growth on metabolism of escherichia coli, as revealed by global metabolite pool ("metabolome") analysis. *J Bacteriol*, 180(19):5109–5116, 1998.

[81] Uchida, Y., Izai, K., Orii, T., and Hashimoto, T. Novel fatty acid beta-oxidation enzymes in rat liver mitochondria. ii. purification and properties of enoyl-coenzyme a (coa) hydratase/3-hydroxyacyl-coa dehydrogenase/3-ketoacyl-coa thiolase trifunctional protein. *J Biol Chem*, 267(2):1034–1041, 1992.

[82] Wenk, M.R. The emerging field of lipidomics. *Nat Rev Drug Discov*, 4(7):594–610, 2005.

[83] Wilm, M. and Mann, M. Analytical properties of the nanoelectrospray ion source. *Anal Chem*, 68(1):1–8, 1996.

[84] Wishart, D.S., Knox, C., Guo, A.C., Eisner, R., Young, N., Gautam, B., Hau, D.D., Psychogios, N., Dong, E., Bouatra, S., Mandal, R., Sinelnikov, I., Xia, J., Jia, L., Cruz, J.A., Lim, E., Sobsey, C.A., Shrivastava, S., Huang, P., Liu, P., Fang, L., Peng, J., Fradette, R., Cheng, D., Tzur, D., Clements, M., Lewis, A., Souza, A.D., Zuniga, A., Dawe, M., Xiong, Y., Clive, D., Greiner, R., Nazyrova, A., Shaykhutdinov, R., Li, L., Vogel, H.J., and Forsythe, I. Hmdb: a knowledgebase for the human metabolome. *Nucleic Acids Res*, 37(Database issue):D603–D610, 2009.

[85] Wittig, U., Golebiewski, M., Kania, R., Krebs, O., Mir, S., Weidemann, A., Anstein, S., Saric, J., and Rojas, I. Sabio-rk: integration and curation of reaction kinetics data. *Lecture Notes in Computer Science*, 4075:94, 2006.

[86] Yamashita, M. and Fenn, J.B. Electrospray ion source. another variation on the free-jet theme. *The Journal of Physical Chemistry*, 88(20):4451–4459, 1984. ISSN 0022-3654.

[87] Yugi, K. and Tomita, M. A general computational model of mitochondrial metabolism in a whole organelle scale. *Bioinformatics*, 20(11):1795–1796, 2004.

Index

beta-oxidation, 1

differential equation, 19

fatty acid, 4

high performance liquid chromatography, 14

mass action rate-law, 20
mass spectrometry, 16
metabolome, 13
Metabolomics, 13
Michaelis constant, 22
Michaelis-Menten equation, 22

NMR-spectroscopy, 15
non-negative matrix factorization, 54
non-targeted metabolomics, 13

ordinary differential equations, 19

peroxisome, 10
production rate, 20

quasi-steady state, 22

stoichiometric coefficients, 20
stoichiometry matrix, 21

targeted metabolomics, 13